REPORTS ON PROGRESS IN PHYSICS

Volume 40, 1977

Edited by R J Blin-Stoyle MA DPhil FInstP FRS

A Europhysics Journal
published by
The Institute of Physics

Copyright © 1977 by The Institute of Physics.
All rights reserved. Multiple copying of the contents or parts thereof without permission is in breach of copyright, but permission is hereby given to copy titles and abstracts of articles and names of authors.

Published by The Institute of Physics
47 Belgrave Square, London SW1X 8QX

Printed in Great Britain by
Adlard and Son Ltd
Set in 11/12 pt Monotype Imprint

CONTENTS

Preface

R E Imhof and F H Read
1 The measurement of lifetimes of atoms, molecules and ions

R H Garstang
105 Atoms in high magnetic fields

H G Berry
155 Beam–foil spectroscopy

J Reinhardt and W Greiner
219 Quantum electrodynamics of strong fields

H W Kugel and D E Murnick
297 The Lamb shift in hydrogenic ions

W R Phillips
345 Heavy-ion transfer reactions

D H Perkins
409 Inelastic lepton–nucleon scattering

W B Somerville
483 Interstellar radio spectrum lines

J C Brice
567 The growth of insulating crystals

K H Ruddock
603 The organization of human vision for pattern detection and recognition

D E Cartwright
665 Oceanic tides

A Neveu
709 Quantization of non-linear systems

(*continued*)

R S Mackintosh
731 The shape of nuclei

G Grynberg and B Cagnac
791 Doppler-free multiphotonic spectroscopy

B L Moiseiwitsch
843 Recent progress in atomic collisions theory

A C Phillips
905 Three-body systems in nuclear physics

J Killingbeck
963 Quantum-mechanical perturbation theory

K J Whiteman
1033 Invariants and stability in classical mechanics

R W G Hunt
1071 Colour reproduction by photography

R C Young
1123 Fermi surface studies in pure crystalline materials

K H J Buschow
1179 Intermetallic compounds of rare-earth and 3d transition metals

S Feneuille
1257 Interaction of laser radiation with free atoms

J E Allen and A D R Phelps
1305 Waves and microinstabilities in plasmas—linear effects

R N Franklin
1369 Microinstabilities in plasmas—non-linear effects

H A B Bodin and B E Keen
1415 Experimental studies of plasma confinement in toroidal systems

The measurement of lifetimes in atoms, molecules and ions

ROBERT E IMHOF† and FRANK H READ

Department of Physics, Schuster Laboratory, University of Manchester, Manchester M13 9PL, UK

Abstract

The field of the direct measurement of atomic and molecular lifetimes has been characterized in the past few years by the development of several new and powerful techniques and by an improving ability to control and limit the measurement inaccuracies of older techniques. The establishment of a wide range of accurate values for atomic and molecular lifetimes is now possible. This review deals with the measurement of lifetimes of atoms and molecules in the gas phase, in the range 10^{-10}–10^{-5} s, and concentrates on the more accurate and promising techniques, which are grouped together according to whether their most prominent feature is the means of excitation or the interference between excited levels or the coincident detection of two decay events. Possible sources of systematic error are discussed at length and the theoretical background appropriate to the measurements is given when necessary. The techniques and their areas of applicability are compared and the likely future development of them is discussed.

This review was completed in February 1976.

† Present address: Department of Applied Physics, University of Strathclyde, Glasgow G4 0NG, UK.

Contents

	Page
1. Definitions	3
1.1. Introduction	3
1.2. Theoretical relationships	4
1.3. Radiation trapping	6
2. Methods using modulated optical excitation	8
2.1. Methods using pulsed light sources	9
2.2. Methods using externally modulated light sources	12
2.3. Methods using lasers	17
2.4. Synchrotron radiation sources	23
2.5. Experimental errors	24
3. Modulation techniques using electron-impact excitation	27
3.1. Methods using low-energy electrons	27
3.2. Methods using threshold-energy electrons	30
3.3. Methods using high-energy electrons	31
3.4. Methods using discharges	33
4. Foil excitation and related techniques	34
4.1. Experimental details	35
4.2. Lifetime measurement and systematic errors	40
4.3. Some recent measurements	44
5. Techniques using level crossing and double resonance	46
5.1. Résumé of hyperfine structures	46
5.2. Coherence	49
5.3. Level-crossing methods	52
5.4. The Hanle effect for atoms	54
5.5. The Hanle effect for molecules	61
5.6. Experimental details and systematic errors	64
5.7. Level crossing at non-zero fields	69
5.8. Double-resonance experiments	73
5.9. Quantum beat experiments	76
6. Coincidence methods	78
6.1. The photon–photon coincidence method	78
6.2. The electron–photon coincidence method	84
6.3. Experimental errors	87
Acknowledgments	88
Appendices	
1. The analysis of decay curves	89
2. Density matrices	93
References	97

1. Definitions

1.1. Introduction

The field of the direct measurement of atomic and molecular lifetimes has, in the past few years, experienced a vigorous growth, made possible by a marked widening in the range of experimental techniques and sustained by an increasing awareness of the measurement inaccuracies and an improving ability to control and limit them. These changes are reflected in the various reviews of the subject and in the compilations of measured lifetimes. In the early work of Mitchell and Zemansky (1934), for example, only a few rather crude experimental techniques were described with very little discussion or realization of their inherent errors and this position had changed very little even up to the time of the excellent review of Foster (1964). By the mid-1960s new techniques, such as the foil-excitation method, were being used to measure lifetimes, often rather uncritically, and also the systematic errors of older techniques, such as the Hanle effect, were beginning to be understood, but the overall quality of work in the field was still not high as evidenced, for example, by the lack of agreement in the results compiled by Anderson (1971). The beginnings of a new regime first became apparent in the review of Corney (1969) in which the experimental errors of established techniques were discussed at some length and a few new and potentially powerful techniques were briefly reviewed for the first time. In the short period since then some of these new methods have developed dramatically in accuracy and sophistication, to the stage at which their full description now requires a specialized review, as in the field of laser techniques (see, for example, Walther 1976). Further new techniques have also appeared in this period and the field now seems poised at a stage at which the available methods can start to be used to establish a wide range of atomic and molecular lifetimes with some confidence. It also seems that calculational methods may now have the accuracy to provide checks on experimental results and to fill in experimentally inaccessible gaps.

Clearly the present state of the subject of lifetime measurements is too diverse and detailed to be covered in its entirety by the present review and we have, of necessity, had to specialize in the more accurate and promising techniques, completely omitting some of the techniques covered in earlier comprehensive reviews, such as those involving the direct measurement of absorption oscillator strengths. Also we have dealt only with atoms, molecules and ions in the gas phase although lifetimes of condensed atoms or molecules can nearly always be measured by adaptations of some of the same techniques. More specialized techniques, such as those for measuring lifetimes of metastable species, of autoionizing states of atoms, or of atomic x-ray levels, have also been omitted. Although many recent works are cited and many measured lifetimes are quoted where this helps in the description and explanation of techniques, this review is in no sense a bibliography of lifetime work nor does it contain compilations of measured lifetimes.

We have attempted to cover all the relevant work published up to the middle of 1975 and in a few cases have also included some important new developments published in late 1975 and early 1976. SI units are used throughout the review except where they are unfamiliar (for example, we use Torr as a unit of pressure rather than the SI unit, the pascal, the relationship between these being 1 Torr $\approx$ 133 Pa).

The plan of the review is as follows. In the remainder of the present section we define what is meant by a radiative lifetime and present the relationships between lifetimes and transition probabilities, band strengths, oscillator strengths, etc, for both atoms and molecules. The section concludes with a discussion of radiative trapping. Many of the techniques can be chiefly characterized by the means of excitation (such as excitation by modulated photon beams, or by modulated electron beams, or foil excitation) and these techniques are dealt with in §§2, 3 and 4. Other techniques are chiefly characterized by interferences between excited levels, and these are grouped together and described in §5. The last range of techniques, dealt with in §6, are those in which two decay events are detected in coincidence.

1.2. Theoretical relationships

Free atoms, molecules and ions in excited states may have several possible concurrent modes of spontaneous decay, depending on the excitation energy. These modes include (i) decay to the ground state or to excited states of lower energy by emission of a photon, (ii) decay by emission of an electron if the excitation energy is sufficiently high, and (iii) decay, in the case of molecules, through dissociation. In the present review we treat excited states which have energies in the range from about 1 eV to about 20 eV above their respective ground states and are therefore mostly concerned with the photon decay mode, although the other two decay modes will occasionally be mentioned. We are concerned only with lifetimes lying in the range 10^{-10}–10^{-5} s which restricts our attention (at least in the energy range specified) to optically allowed (that is, electric dipole) transitions.

If a system contains $N_j(0)$ atoms in an excited state j at time zero and if A_{ji} is the probability per unit time for the spontaneous transition from j to a state i of lower energy, the rate of change of the population in state j is given by

$$\frac{\mathrm{d}N_j}{\mathrm{d}t} = -N_j \sum_i A_{ji} \tag{1.1}$$

assuming that no further states j are being created and ignoring de-excitations by collisions between atoms. The solution of this is

$$N_j(t) = N_j(0) \exp(-t/\tau_j) \tag{1.2}$$

where

$$1/\tau_j = \sum_i A_{ji}. \tag{1.3}$$

The time τ_j is the mean life, or the lifetime, of the state j. The sum in equations (1.1) and (1.3) is over all possible final states i and therefore also includes all the accessible modes of decay.

In the case of electric dipole transitions in atoms and atomic ions the transition probability (otherwise called the Einstein coefficient of spontaneous emission) is given by (see, for example, Condon and Shortley 1963, Kuhn 1969)

$$A_{ji} = \frac{16\pi^3}{3h\epsilon_0 \lambda_{ji}^3 g_j} S_{ji} \tag{1.4}$$

where S_{ji} is the line strength, defined by

$$S_{ji} = S_{ij} = e^2 \sum_{m_i, m_j} (|x_{jm_j im_i}|^2 + |y_{jm_j im_i}|^2 + |z_{jm_j im_i}|^2) \tag{1.5}$$

and where

$$x_{j m_j i m_i} = \int \psi_{j m_j}^{*}(\boldsymbol{r}_s) \left(\sum_s x_s\right) \psi_{i m_i}(\boldsymbol{r}_s)\, \mathrm{d}\boldsymbol{r}_s \tag{1.6}$$

where the subscript s labels the electrons of the atom. The label m_j refers to the degenerate sublevels of the state j, the total number of such sublevels being the degeneracy g_j. Other related quantities are (i) the absorption oscillator strength f_{ij}, given by

$$f_{ij} = \frac{\epsilon_0 mc \lambda_{ji}^2 g_j}{2\pi e^2 g_i} A_{ji} \tag{1.7}$$

(ii) the Einstein coefficient of absorption B_{ij} (defined as the probability per unit time for the upward transition $i \rightarrow j$ in a radiation field of unit energy density per unit wavelength interval centred at λ_{ji}), given by

$$B_{ij} = \frac{\lambda_{ji}^5 g_j}{8\pi hc g_i} A_{ji} \tag{1.8}$$

and (iii) the Einstein coefficient of stimulated emission B_{ji}, given by

$$B_{ji} = \frac{g_i}{g_j} B_{ij}. \tag{1.9}$$

These relationships also apply to neutral and ionic molecules but for these the development can be carried further to show the dependence of the line strength S on the electronic, vibrational and rotational motions of the molecule. We illustrate this by considering a transition in a diatomic molecule following Hund's case a. More complete treatments have been given by, for example, Tatum (1967) and Kuznetsova *et al* (1974). The non-degenerate levels of this type of molecule are characterized by the quantum numbers Λ and Σ for the components of the orbital and spin angular momenta of the electrons in the direction of the vector $\boldsymbol{r}$ joining the nuclei, the quantum numbers v, J and M for the vibrational and rotational motion and the symbol e to identify the individual state of the Λ-doubled pair. In the Born–Oppenheimer approximation the wavefunction of the molecule can be written as a product of electronic, vibrational and rotational wavefunctions (and also a nuclear spin wavefunction, which can be ignored in the present treatment), namely

$$\psi_{e\Lambda\Sigma v J M} = \frac{1}{r} \psi_{e\Lambda\Sigma}(\boldsymbol{r}_s, r) \psi_v(r) \psi_{JM}(\theta, \phi) \tag{1.10}$$

where θ and ϕ are the angular coordinates of the electric dipole moment of the molecule and $\boldsymbol{r}_s$ are the coordinates of the electrons relative to $\boldsymbol{r}$. The rotational part of the line strength S then separates out:

$$S_{e''\Lambda''\Sigma''v''J''}^{e'\Lambda'\Sigma'v'J'} = S_{J''}^{J'} S_{e''\Lambda''\Sigma''v''}^{e'\Lambda'\Sigma'v'} \tag{1.11}$$

where $S_{J''}^{J'}$ are the Hönl–London factors given by

$$S_{J''}^{J'} = \sum_{M'M''} \left| \int \psi_{J'M'}^{*} f(\theta, \phi) \psi_{J''M''} \sin\theta \, \mathrm{d}\theta \, \mathrm{d}\phi \right|^2 \tag{1.12}$$

and $f(\theta, \phi)$ gives the dependence of the dipole moment on the angular coordinates θ and ϕ (for example, in the simplest case the dipole moment is oriented along $\boldsymbol{r}$ and has a constant magnitude, so that θ and ϕ are the angular coordinates of $\boldsymbol{r}$ and $f = 1$). The

band strength $S^{\Lambda'v'}_{\Lambda''v''}$ is given by

$$S^{\Lambda'v'}_{\Lambda''v''}=\frac{1}{(2-\delta_{0,\Lambda'})(2S'+1)}\sum_{e''e''\Sigma'\Sigma''}S^{e'\Lambda'\Sigma'v'}_{e''\Lambda''\Sigma''v''}=\frac{1}{(2-\delta_{0,\Lambda'})(2S'+1)}\sum_{\substack{e''e''\\ \Sigma'\Sigma''}}\left|R^{e'\Lambda'\Sigma'v'}_{e''\Lambda''\Sigma''v''}\right|^2 \tag{1.13}$$

where

$$R^{e'\Lambda'\Sigma'v'}_{e''\Lambda''\Sigma''v''}=\int\psi_{v'}{}^{*}(r)R^{e'\Lambda'\Sigma'}_{e''\Lambda''\Sigma''}\psi_{v''}(r)\,\mathrm{d}r \tag{1.14}$$

and where the electronic transition moment $R^{e'\Lambda'\Sigma'}_{e''\Lambda''\Sigma''}$ is given by

$$R^{e'\Lambda'\Sigma'}_{e''\Lambda''\Sigma''}=\int\psi_{e'\Lambda'\Sigma'}{}^{*}(r_i,r)\,(\sum_i er_i)\psi_{e''\Lambda''\Sigma''}(r_i,r)\,\mathrm{d}r_i. \tag{1.15}$$

The summation over decay channels that appears in equation (1.3) is simplified by the existence of a sum rule for the Hönl–London factors, which leads to the following sum for all the branches in a $v'\rightarrow v''$ band:

$$\sum_{e''\Sigma''J''}S_{J''J'}=(2-\delta_{0,\Lambda'})(2S'+1)(2J'+1) \tag{1.16}$$

the three factors on the right-hand side representing the degeneracies of the Λ-doubling (namely, 1 for a Σ state and 2 for other states), the electron spin and the rotational motion respectively. The degeneracy g_f to be used in equation (1.4) for a single upper level $e'\Lambda'\Sigma'J'$ is $(2J'+1)$ and therefore the total transition probability for the decay of this level to any of the levels J'' of the $\Lambda''v''$ state is

$$A^{\Lambda'v'}_{\Lambda''v''}=\frac{16\pi^3}{3h\epsilon_0\lambda^3}S^{\Lambda'v'}_{\Lambda''v''} \tag{1.17}$$

with the approximation that λ is constant for all the lines of the band. Note that with the present assumptions and approximations the transition probability, and hence the radiative lifetime, is independent of the value of J'.

By making the usually rather poor approximation that the electronic transition moment $R^{e'\Lambda'\Sigma'}_{e''\Lambda''\Sigma''}$ is independent of the distance r between the nuclei, the vibrational and electronic transition strengths become separable and the lifetime of the state $\Lambda'v'$ is then independent of v'. An improvement can be made by expressing the electronic transition moment as a power series in the r centroid $\langle r_{v'v''}\rangle$, defined by

$$\langle r_{v'v''}\rangle=\int\psi_{v'}{}^{*}(r)r\psi_{v''}(r)\,\mathrm{d}r/\int\psi_{v'}{}^{*}(r)\psi_{v''}(r)\,\mathrm{d}r. \tag{1.18}$$

Values of the r centroid are tabulated for some molecules and the approach is then relatively easy to apply if the power series can be confined to the constant and linear terms. In this way measured variations of lifetime with the vibrational quantum number v' can lead to a knowledge of the approximate dependence of the electronic transition moment on the internuclear distance r.

1.3. Radiation trapping

So far we have dealt only with radiative decays. Competing decay modes, such as ionization and dissociation, simply contribute further terms to the summation in equation (1.3) as do de-excitation processes involving collisions between atoms (see §5.6.1).

A process which can reduce the value of one of the terms in equation (1.3) is that of 'radiation trapping'. This occurs when the pressure in the gas cell is high enough for a

photon emitted by an excited atom to have an appreciable probability of being successively absorbed and re-emitted by other atoms in the gas cell before eventually finding its way to the detector. If this happens the photon is effectively delayed and the measured lifetime τ_0 appears to be longer than the natural lifetime τ of an isolated atom. This process was first studied in detail by Holstein (1947) who treated the decay of excitation in a slab of finite thickness, the other two dimensions being infinite. The problem was studied again by Barrat (1959a, b, c) who also considered the related process of coherent trapping (see §5.6.1), and by D'yakonov and Perel (1965a) who improved upon the approximation made by Barrat of treating all the atoms as having the same velocity.

Assuming that nearly all the atoms in the gas cell are in their ground state 0, the process of radiation trapping affects only the term A_{J0} in equation (1.3). D'yakonov and Perel (1965a) found theoretically that the effective value of this transition probability becomes

$$A_{J0}' = (1 - xa)A_{J0} \tag{1.19}$$

where $a = 1$ (other values of a, corresponding to coherent trapping, will be given in §5.6.1) and where

$$x \approx 1 - \frac{1}{\sqrt{\pi}} \int_{-\infty}^{+\infty} \exp\left(-t^2 - \frac{L}{l_0} e^{-t^2}\right) dt. \tag{1.20}$$

Numerical values of this integral can be derived from tabulations of Mitchell and Zemansky (1934). The length L is a characteristic dimension of the scattering cell and l_0 is the mean free path of a photon in the centre of the Doppler-broadened line and is given by

$$l_0 = \frac{2J_0 + 1}{2J_J + 1} \frac{8\pi}{n_0 \lambda_{J0}^3 A_{J0}} \left(\frac{2\pi kT}{m}\right)^{1/2} \tag{1.21}$$

where m is the mass of the atom and n_0 is the number density of ground-state atoms in the scattering cell. In the limit at which $l_0 \ll L$,

$$x \approx 1 - \frac{l_0}{L}\left(\pi \ln \frac{L}{l_0}\right)^{-1/2} \tag{1.22}$$

and for sufficiently small values of l_0/L the decay route to the ground state becomes almost completely blocked. The measured lifetime then gives the sum of the transition probabilities of the competing (unblocked) decay modes.

Experimental tests (for example, Omont 1965a, Nussbaum and Pipkin 1967) confirm the theoretical results of D'yakonov and Perel and show that with typical gas cell dimensions the radiation trapping process can in some cases cause changes of a few per cent in measured lifetimes at pressures as low as a few times 10^{-5} Torr. The importance of radiation trapping is reduced if the lower state is not the ground state of the atom or if the upper-state decay has only a small branching ratio to the ground state (Saloman and Happer 1966). The effect is also much less important for molecules, even when the lower level is a rotational level of the ground vibrational–electronic state, both because the probability that a molecule is in one particular rotational level is usually of the order of 0·1 or less (except in the case of the lightest and simplest molecules such as H_2) and because the upper-state decay will in general have branch routes to many lower rotational–vibrational levels.

2. Methods using modulated optical excitation

In this and the next section we describe methods of measuring lifetimes using modulated excitation. Methods using optical excitation are described in this section and those using electron-impact excitation in §3. The reasons for this division are that the ranges of application, the experimental difficulties and the technologies involved differ for the two methods of excitation. The fundamental principles on which modulation techniques are based are the same, irrespective of the method of excitation, however, and these are described below.

Consider the population $N_j(t)$ of a level j of an isolated atom or molecule which is subjected to some time-dependent excitation $E(t)$. If we neglect all other sources of population, such as cascading from higher excited states, then we can write

$$\frac{dN_j}{dt} = -\frac{N_j}{\tau_k} + E \tag{2.1}$$

where τ_j is the lifetime of the level. Generally speaking, only two types of modulation have been used for measuring lifetimes: pulsed and sinusoidally modulated excitation.

(*a*) *Pulsed excitation.* If the excitation $E(t)$ is suddenly removed at time $t=0$ then equation (2.1) can be solved to give

$$N_j(t) = N_j(0) \exp(-t/\tau_j) \tag{2.2}$$

where $N_j(0)$ is the initial population at time $t=0$. It is this exponential decay of population which is measured in pulsed excitation experiments. The expression can be applied directly in practice if the lifetime of interest is much larger than the excitation cut-off time and if the time between excitation pulses (most experiments use a pulse train rather than an isolated excitation pulse) is much larger than the lifetime. The effects of cascading and the detailed shape of the excitation pulses on the measured decay curves are discussed in appendix 1.

(*b*) *Sinusoidally modulated excitation.* If the excitation $E(t)$ is a periodic function of time with a fundamental frequency ν, then it may be expressed as a Fourier series:

$$E(t) = \sum_{-\infty}^{\infty} a_n \exp(2\pi i n \nu t). \tag{2.3}$$

Substituting this into equation (2.1) gives for the steady-state solution

$$N_j(t) = \sum_{-\infty}^{\infty} \frac{a_n \exp(2\pi i n \nu t)}{(1/\tau_j) + 2\pi i n \nu}.$$

The amplitude of the nth harmonic component can be written in the form $A_n \exp(-i\phi_n)$, where

$$A_n = \left(\frac{a_n^2}{(1/\tau_j^2) + 4\pi^2 n^2 \nu^2} \right)^{1/2} \tag{2.4}$$

and

$$\tan \phi_n = 2\pi n \nu \tau_j. \tag{2.5}$$

In practice, the excitation function is often approximately sinusoidal and the detected fluorescence signal is electronically filtered to attenuate the higher harmonic components so that a measurement of the phase difference between the fundamental components of the excitation and fluorescence waveforms often suffices to determine

the lifetime ($n=1$ in equation (2.5)). Maximum sensitivity is achieved if the modulation frequency is chosen to give a phase difference of 45°. With optical excitation the phase of $E(t)$ can be measured directly by observing the excitation light with identical optical paths and with the same detector under the same experimental conditions as are used for observing the fluorescence. With electron-impact excitation this is not possible and known transitions have to be used for calibration.

The techniques described in this section use modulated optical excitation. This is a selective method of excitation: only allowed transitions in resonance with the photon energies in the excitation beam are strongly excited. With traditional light sources such as hollow-cathode lamps and arc and spark discharges (see §§2.1 and 2.2) relatively few transitions could be studied. Presently available laser sources (see §2.3) already have a much wider range of application. Another promising new light source for lifetime measurements, particularly in the vacuum ultraviolet spectral region, is the synchrotron, described in §2.4.

2.1. Methods using pulsed light sources

Pulsed light sources (flashlamps) have been used for many years for studying fluorescence decay times in condensed media but it is not until recently that they have also been used for measuring single vibronic level lifetimes in isolated molecules at moderately high temporal and spectral resolutions. The design and adjustment of flashlamps is empirical and opinions often differ as to how to achieve the best results. Hess (1975 and references therein) has recently reported a theory of spark plasmas in nanosecond light sources that could be very useful for designers. Ware (1971) and Knight and Selinger (1973a) discuss many practical details of flashlamp design and use.

Lewis and Ware (1973) reported a gated lamp which exemplifies what can be achieved with this technique. It used an electrode separation of 3 mm, a pressure of 0·5 atm of nitrogen, air, deuterium or hydrogen, an applied voltage of 7 kV and a pulse repetition frequency of 30 kHz. They measured an absolute intensity in the wavelength region 250–500 nm of 2×10^9 and 4×10^7 photons per flash with pulse widths of 3 and 2 ns, respectively, for nitrogen and deuterium. The pulse widths quoted are not corrected for the finite response time of the photomultiplier, which is likely to dominate the measurement in deuterium. Emission in nitrogen is mainly from the $c\,^3\Pi_u$ state, with several intense bands superimposed on a quasi-continuum. In deuterium the continuum from the a $^3\Sigma^+$ state predominates—it is relatively weak in the spectral region measured but is likely to be quite intense at shorter wavelengths, well into the vacuum ultraviolet.

Flashlamps are ideal sources for use with the multichannel delayed-coincidence technique (see below) and for this reason the various experimental arrangements reported superficially resemble each other and only one is described in any detail below.

Spears and Rice (1971) reported fluorescence lifetime and relative quantum yield measurements of a large number of single vibronic levels of benzene. These studies are of particular interest because benzene is expected to show radiationless decay behaviour, characteristic of a large molecule in the statistical limit, with an excited-state structure that still allows excitation of single vibronic levels. A block diagram of their apparatus is shown in figure 1. A thyratron-gated, deuterium-filled flashlamp with a pulse width of 6 ns FWHM and a repetition frequency of 5 kHz was used for excitation. The pulse shape is shown in figure 2(*a*). The light was filtered by means of a grating

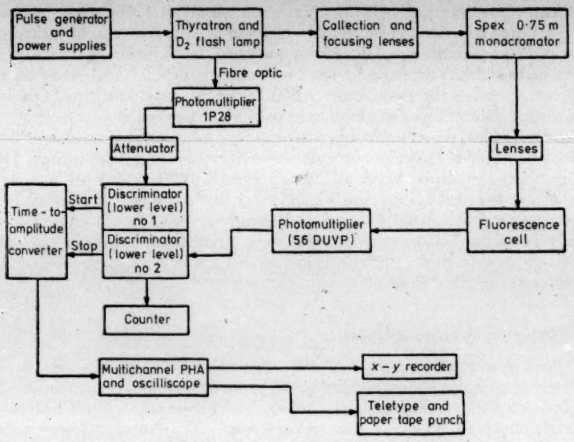

Figure 1. Block schematic diagram of the instrument used by Spears and Rice (1971) to measure single vibronic level lifetimes in benzene using flashlamp excitation and the delayed-coincidence measurement technique.

monochromator set for resolutions between 68 and 135 pm and focused into a sample cell equipped with a Rayleigh horn, used with vapour pressures of 6×10^{-3} Torr and higher. Fluorescence was observed at right angles to the direction of excitation by means of a cooled, focused photomultiplier used as a single-photon detector and no dispersive elements or filters were used to discriminate against scattered excitation light.

Fluorescence decay curves were measured with the *delayed-coincidence* or *single-photon correlation* technique which is used very widely in pulsed excitation measurements and which is described below. In this technique the 'start' gate of a time to

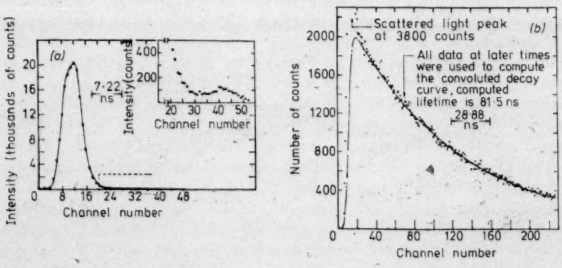

Figure 2. Performance of the flashlamp. (*a*) Excitation pulse shape. (*b*) A typical decay curve in benzene (from Spears and Rice 1971).

pulse height converter (most modern converters use a constant current source to charge a capacitor, the current being turned on by a signal applied to the 'start' input and turned off by a subsequent signal applied to the 'stop' input) is triggered by pulses that are accurately synchronized with the excitation pulses. This was achieved in the work of Spears and Rice by means of a small photomultiplier viewing the excitation flashes through a light guide. Single fluorescence photons from the main photomultiplier are used to stop the converter. The output pulse heights are then proportional to the differences in times of arrival between the start pulses and the first subsequent stop pulses. They are analysed in a multichannel pulse height analyser where the data are evaluated and stored in such a way as to accumulate a histogram of the number of events recorded as a function of pulse height. It is important to note that only the first stop event in each excitation cycle is recorded and that the accumulated histogram is not an accurate representation of the decay of fluorescence intensity unless the probability of detecting more than one stop event per excitation cycle is negligibly small.

This can be seen by considering the probability $P(i)$ of registering an event in the ith channel of the analyser, which is

$$P(i)=q[1\rightarrow(i-1)]p(i) \tag{2.6}$$

where $q[1\rightarrow(i-1)]$ is the probability of recording no events in channels $1\rightarrow(i-1)$ and $p(i)$ is the probability of recording an event in channel i. These probabilities depend on the shape of the decay curve being measured and we consider only a very simple case here in which the stop pulses are completely random and are not correlated with the start pulses. We can then use the Poisson formula for the probability p_n of observing n events in a given time

$$p_n=\frac{\mu^n\,\mathrm{e}^{-\mu}}{n!} \tag{2.7}$$

where μ is the mean number of events in this time. Combining this with equation (2.6) we can write for the probability of registering an event in channel i

$$P(i)=\bar{N}\Delta t\exp(-\bar{N}i\Delta t) \tag{2.8}$$

where $\bar{N}$ is the mean counting rate of stop pulses and Δt is the width of each channel. The histogram accumulated for such randomly distributed stop pulses therefore is an exponential function of decay constant, $\bar{N}\Delta t$. At low stop counting rates $\bar{N}i\Delta t\ll 1$, $P(i)\approx\bar{N}\Delta t$ and all delay times are recorded with equal probability because the probability of more than one stop pulse occurring after each start pulse is then negligibly small. In cases when the stop pulses are not randomly distributed a similar loss of data at large delay times occurs unless $\bar{N}\Delta t\ll 1$. In practice, one would arrange for the stop counting rate to be at least two orders of magnitude smaller than the start counting rate if the accumulated histograms are to be accurate representations of the fluorescence decay curves. This places a severe restriction on the speed with which decay curves can be measured, especially with excitation sources that are restricted in their pulse repetition frequencies. Methods of overcoming this restriction either by using an electronic pile-up rejection circuit or by numerically correcting the measured histograms have been proposed (see Coates 1972, Davis and King 1972 and references therein).

The instrument of Spears and Rice was used to investigate the dependence of the radiative and non-radiative lifetimes† in benzene on excess vibrational energy and

† What are meant here are the reciprocals of the radiative and non-radiative transition probabilities.

vibrational symmetry class. The non-radiative lifetime was found to decrease as the number of vibrational quanta in the prepared state increased. The theory of radiationless transitions was further tested with extensive studies of partially deuterated and fluorinated derivatives of benzene (Abramson *et al* 1972, Guttman and Rice 1974a, b).

Other measurements using this technique have been reported by Selinger and Ware (1970) and Loper and Lee (1972) on benzene and derivatives, Laor and Ludwig (1971) and Knight *et al* (1973) on naphthalene, Halpern and Ware (1971) on acetone and some derivatives, Hui and Rice (1972) on the higher excited states of SO_2, Knight and Selinger (1973b) on phenanthrene, Hui and Rice (1974) on cis–trans isomerization of styrene and derivatives, and Scheps *et al* (1974) on aniline and derivatives.

2.2. *Methods using externally modulated light sources*

There are several methods of modulating light at frequencies sufficiently high to be useful for measuring lifetimes. These include Kerr and Pockels cells, ultrasonic diffraction gratings and even mechanical modulators. They have been mainly used for studying resonance transitions in metal vapours where the corresponding resonance lamps provide intense and highly selective excitation light. They have also been used recently for modulating CW laser light (see §2.3.2) and this may often be a convenient alternative to using pulsed lasers, especially for studies requiring high spectral or temporal resolution. Thanks to the intensive development of modulators for laser communications, high-quality materials as well as complete systems are now commercially available, further increasing the ease of application of the technique.

Methods of modulating light at high frequencies have been reviewed by Jones (1964) and more recently by Graf (1972).

2.2.1. Mechanical modulators. Mechanical modulators are likely to be only of historical interest in lifetime work except possibly for their use in the vacuum ultraviolet spectral region. Brewer *et al* (1962) reported an ambitious modulator, using a rotating diffraction grating, which was designed to give modulation frequencies in the megahertz region. Because of vibrations it only worked at 60 kHz but nevertheless proved useful for measuring lifetimes and quenching cross sections of the B $^3\Pi$ state of I_2 for groups of unresolved vibronic levels in the range $v' = 10$–100 (Chutjian *et al* 1967) using the phase-shift technique. Their data agree reasonably with more recent data.

Schwartz and Johnston (1969) reported measurements of lifetimes in NO_2 over the range of excitation wavelengths 398–600 nm. A 1·6 kW high-pressure xenon arc lamp was used for excitation, a bandwidth of approximately 2·5 nm being selected by means of two grating monochromators in tandem. The light was chopped by a wheel with 60 blades driven at 60 Hz. At this frequency, a phase shift of 45° corresponds to a lifetime of 44 μs, which is close to the expected values in NO_2. A steady increase in the lifetime, from 60 to 90 μs, with increasing excitation wavelength was observed. A similar arrangement was used by Keyser *et al* (1971) in an extensive study of quenching of NO_2 fluorescence. Most of their work was concerned with spectroscopic measurements, but they did report some lifetime measurements, and of particular interest here is their method of measuring phase shifts using a photon-counting multichannel technique. Fluorescence photons were detected (see figure 3(*a*)) by means of a cooled photomultiplier and correlated with a signal bearing a constant relationship with the phase of the excitation light using a time to pulse height converter and a multichannel pulse height analyser. If the probability of detecting more than one fluorescence

photon per excitation cycle is negligibly small then the counts accumulated in the channels correspond accurately to the intensity of fluorescence at the corresponding delay with respect to the reference signal. A typical waveform measured by this technique is shown in figure 3(*b*). Phase shifts were measured between this and a reference waveform, measured under identical conditions but with scattered excitation light replacing the fluorescence. Both waveforms were expanded in a Fourier series (up to the fifth harmonic) and the resultant coefficients of the fundamental were used to determine the phase difference by computer analysis.

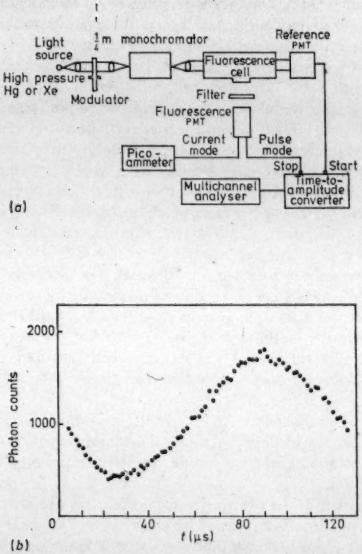

Figure 3. (*a*) Arrangement used by Keyser *et al* (1971) for measuring lifetimes with the phase-shift technique, but using the delayed-coincidence technique of measurement. (*b*) A typical fluorescence signal waveform.

2.2.2. Electro-optical modulators. The use of Kerr cell shutters in lifetime measurements can be traced back to the 1920s (see Mitchell and Zemansky (1934) for a description of early work). Osberghaus and Ziock (1956) and Ziock (1957) reported the measurement of the oscillator strength of the 372 nm resonance line of Fe I. They used a hollow-cathode iron source modulated by means of a Kerr cell. The Kerr active medium was o-dichlorobenzene, which is transparent in the visible and near-ultraviolet spectral region down to approximately 300 nm. The electrodes were 50 mm long × 15 mm wide and were separated by 8 mm. The cell was placed between crossed Nicol prisms, oriented so that no light was transmitted in the absence of an electric field. With this arrangement, 100% modulation at 1 MHz was achieved with a 15 kV

alternating signal superimposed on a DC level of the same magnitude. The modulated beam was focused onto a beam of atomic iron and the fluorescence emitted at 90° to the direction of excitation was dispersed with a quartz prism spectrometer and detected with a photomultiplier. The phase of the fluorescence signal was measured by gating the photomultiplier on and off with pulses derived, after a variable delay, from the main oscillator. Their measured value of $0{\cdot}046 \pm 30\%$ for the oscillator strength of this line ($\tau = 55$ ns) resolved the disagreement by more than a factor of three between the two previous determinations. With further improvements in their technique, Ottinger and Ziock (1961) obtained a more accurate value of $0{\cdot}035 \pm 10\%$ ($\tau = 72$ ns). In the same paper they also reported measurements on two transitions in gallium.

Kibble *et al* (1967a, b), Copley *et al* (1967) and Habib *et al* (1968) used a Kerr cell in a pulsed mode to investigate the lifetime, resonance trapping and quenching of the sodium 3^2P resonance state. The Kerr cell, filled with nitrobenzene, was excited at 60 Hz with pulses of approximately 15 kV amplitude and 20 ns width. The light source was a commercial sodium spectral lamp. The measurements were performed using the single-photon correlation technique, each decay curve being accumulated for several hours in a multichannel pulse height analyser.

Kerr cells have many disadvantages and have now been virtually abandoned for lifetime work. They have a very low étendue, require large driving voltages and have a restricted range of transmission. Pockels cells require lower driving voltages and their useful transmission extends further into the ultraviolet (125 nm for ADP). They normally have a narrow angular aperture but Enemark and Gallagher (1969) describe a field-widened design which gives two orders of magnitude more modulated light than the ultrasonic diffraction grating of Brewer *et al* (1962). Dodd *et al* (1969) used this modulator to measure the lifetimes of the $6^2P_{1/2}$ and $6^2P_{3/2}$ states of Cs, which were found to be $30{\cdot}8 \pm 1{\cdot}5$ ns and $35{\cdot}2 \pm 1{\cdot}5$ ns respectively. Quenching by helium was also studied, a velocity-averaged cross section less than 10^{-23} m^2 being found.

2.2.3. Acousto-optical modulators. Acousto-optical modulators have been actively developed recently because of their potential value in optical communications systems. The principles of operation of the various devices have been described in an excellent review by Adler (1967).

The first application of such a device for measuring lifetimes was reported by Brehm *et al* (1961) and described in detail by Demtröder (1962). Their arrangement is shown in figure 4(*a*). Light from the hollow-cathode lamp was passed through the modulator (described below) and focused onto an atomic beam emanating from a heated ceramic crucible. Fluorescence was collected in a direction perpendicular to the incident light and directed with mirror M_2 onto the photomultiplier. Transmitted excitation light was directed onto the photomultiplier with mirrors M_1 and M_3. Mirror M_3 was mounted on a pivot so that it could be moved out of the way to measure the fluorescence signal. The two light paths were made as nearly equal as possible so that the lifetime could be directly calculated from the phase difference between the two beams.

In the ultrasonic modulator (see figure 4(*b*)), a standing wave is set up between the piezoelectric quartz transducer Q and the reflector R. This modulates the refractive index of the medium in the cell in both space and time. A 19% volumetric mixture of alcohol in water, which has a zero temperature coefficient for the velocity of sound, was used. The spatial modulation produces a diffraction grating with a spacing equal to one-half the wavelength of the ultrasonic wave and the temporal variation causes this

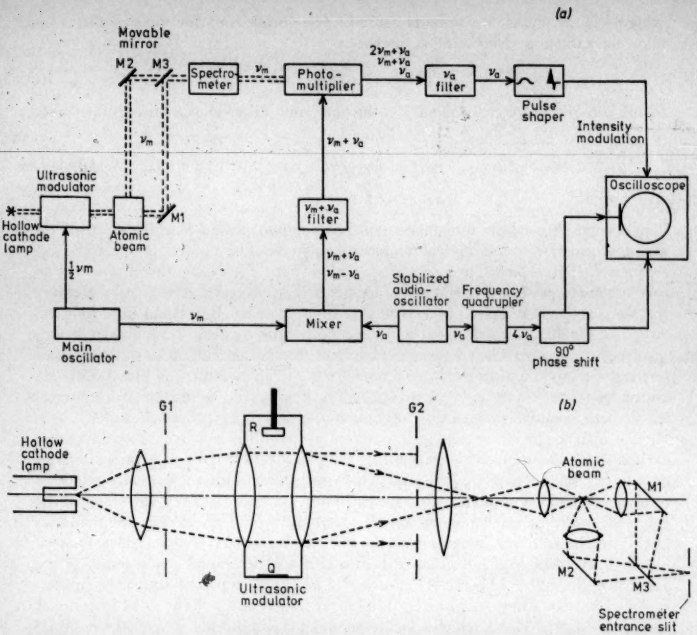

Figure 4. Phase-shift instrument of Demtröder (1962). (*a*) Schematic diagram of the instrument. = = =, light path; ——, electrical connections. (*b*) Detailed design of the acousto-optical modulator, which used grids instead of single slits at the entrance and exit to increase the étendue.

grating to disappear twice in every period of oscillation. The modulator was used in conjunction with two external coarse gratings G_1 and G_2 and an optical system which imaged the transparent lines of G_1 onto the opaque lines of G_2. No light is therefore transmitted when the modulator is turned off. When it is turned on the zeroth order of diffraction is still stopped by G_2 but the diffraction orders 1–3 are transmitted. This arrangement produces a modulation degree of 100% and an étendue that is very high compared with the more usual single-slit arrangements. Modulation frequencies ν_m of 2, 6 and 18 MHz were used to span a measuring range 100–1 ns.

The method of phase measurement used a heterodyne technique which has since been widely adopted by other workers in the field. For excitation at a modulation frequency ν_m the main oscillator of figure 4(*a*) is set to produce a signal of frequency $\frac{1}{2}\nu_m$ for exciting the ultrasonic modulator and one of frequency ν_m for mixing with a stable audio-frequency ν_a (20 kHz in this experiment). The fluorescence signal F detected by the photomultiplier can be described by

$$F = F_0[1+\cos(2\pi\nu_m t-\phi)] \qquad (2.9)$$

where ϕ is the phase shift to be measured. The output from the mixer is filtered to allow only the upper sideband S, where

$$S = S_0 \cos 2\pi(\nu_m + \nu_a)t \tag{2.10}$$

to mix with the fluorescence signal F at the photomultiplier, whose output is then given by

$$FS = F_0 S_0 \{\cos [2\pi(\nu_m + \nu_a)t] + \tfrac{1}{2} \cos [2\pi(2\nu_m + \nu_a)t - \phi] + \tfrac{1}{2} \cos (2\pi\nu_a t - \phi)\}. \tag{2.11}$$

The output filter selects the audio-frequency component of FS which contains the phase information of the original fluorescence signal but at a much more manageable frequency. This is passed to a pulse shaper whose output is applied to the z input of an oscilloscope to produce a bright spot once per oscillation cycle. The x and y plates of the oscilloscope were driven by two 80 kHz sinusoidal signals of equal amplitude but 90° phase difference, which were derived from the audio-oscillator through a frequency quadrupling circuit. The arrangement confines the spot on the screen to the circumference of a circle which is traversed once for a 90° phase shift. As phase shifts are always less than 90°, no ambiguity results. The phase could be read to an accuracy of 0·2°, which is equivalent to a time resolution $\delta\tau/\tau$ of 0·07 at a phase shift of 45°.

The instrument was used to measure lifetimes and quenching cross sections of first excited states of a number of metal atoms. Hulpke *et al* (1964) reported measurements on Ca, Sr, Ba, In and Na using the same instrument with some modifications to minimize variations in phase across the excitation light beam. They also changed the geometry of the interaction region to facilitate studies of self-absorption. Bästlein *et al* (1969) developed a new apparatus on the same lines but used a digital phase-meter.

An instrument similar to that of Demtröder was developed concurrently at the Lawrence Radiation Laboratory. Brewer *et al* (1962) reported measurements on organic solutions using an ultrasonic modulator driven at 2·6 MHz. The instrument used single entrance and exit slits for the modulator and did not achieve the required sensitivity for studying low-density vapours. Link (1966) improved the apparatus and measured the lifetimes of the first resonant states of Na, K, Rb and Cs. Cunningham and Link (1967) and Cunningham (1968) extended the work to include many other metal vapours.

Schlag and von Weyssenhoff (1969) reported an instrument for measuring lifetimes of selected vibronic levels in organic molecular vapours. For this they required a tunable light source covering the visible and near-ultraviolet spectral regions. Their design incorporated a high-intensity (1 kW) xenon arc lamp, a grating monochromator and an acousto-optical modulator. The signal processing electronics were similar to those of Demtröder except that they used a phase-null indicator in place of the oscilloscope display. The sensitivity was low: vapour pressures in the range 0·5–1 Torr and excitation bandwidths of 2·5–3 nm were used in the study of the first excited state of β-naphthylamine. Schlag *et al* (1974) improved the sensitivity considerably with a photon-counting phase-meter. Their design was basically a fast phase-sensitive detector with an adjustable delay in the reference channel. For the case of a single exponential decay with no scattered excitation light entering the detectors the lifetime could be determined by measuring the output of the detector with two different delays in the reference channel. The authors also discussed measurements of more complex decays where more than two measurements are required to determine the parameters.

With this instrument, Schlag *et al* (1971) studied fluorescence lifetimes of vibronic levels of naphthalene vapour at low density, with a spectral resolution of 170 pm.

2.3. Methods using lasers

Lasers are now beginning to make a major impact in atomic and molecular physics and several excellent reviews have recently been published on their technology and applications. For lifetime work one is mainly interested in tunable dye lasers emitting in the visible and ultraviolet spectral regions and these have been reviewed by New (1972) and Schäfer (1973). Hänsch (1972) described one particular design of tunable dye laser pumped by a pulsed nitrogen laser which has found wide application in lifetime work. The uses of lasers in spectroscopy, lifetime measurement and photochemistry have been reviewed by Moore (1971), Hänsch (1973) and Walther (1974, 1976).

In this subsection we review lifetime work using modulated laser excitation. Methods using laser beams with ion beam targets are described in §4.2.1, those using lasers in level-crossing and double-resonance work in §5.

2.3.1. Pulsed lasers. Pulsed lasers have an obvious potential for lifetime work and a large number of measurements using several different configurations have already been reported. The most widely used laser system to date is the nitrogen-laser-pumped tunable dye laser as used, for example, by Sakurai *et al* (1971) and Capelle and Broida (1973) for studying vibronic level lifetimes of the $B\ ^3\Pi_{0u}{}^+$ state of I_2 and by Capelle *et al* (1971) for studying the same state of Br_2. The nitrogen laser (see figure 5) produced pulses of 100–200 kW peak power, 337·1 nm wavelength, 6 ns width (FWHM) and up to several hundred hertz repetition frequency, and these were used to pump the various dyes. These lased in a direction perpendicular to the excitation beam in a cavity formed by a partially reflecting mirror at one end and a reflection grating in the Littrow mounting at the other end. The grating, with 2160 lines mm^{-1}, gave selective

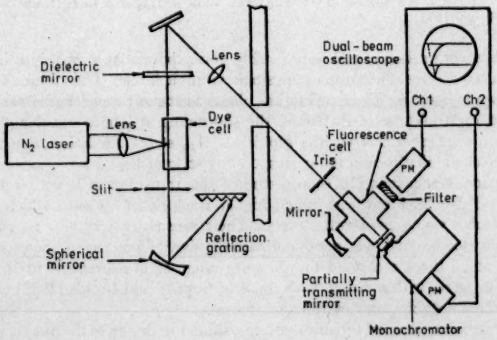

Figure 5. Schematic diagram (not to scale) of the instrument of Sakurai *et al* (1971), which used a tunable pulsed dye laser pumped with a nitrogen laser.

feedback to the cavity and allowed tuning of the output wavelength over the fluorescence range of the dye with bandwidths in the range 100–800 pm and powers in the range 1–5 kW. As indicated in the figure, the nitrogen laser was kept in a separate electrically shielded room because of the large amount of electrical interference it emitted. The excitation beam was passed through the fluorescence cell to a semi-reflecting mirror where most of it was reflected back in order to increase the effective path length of excitation. The transmitted light went to a monochromator which was used to monitor the wavelength and pulse shape of the beam. The fluorescence was observed with a bi-alkali photomultiplier using glass filters to block off stray excitation light. Decay curves were displayed on an oscilloscope. The observed decay rates were

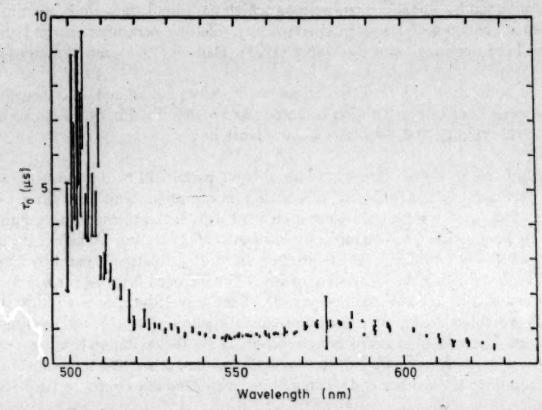

Figure 6. Variation of the lifetime of vibronic levels of the B $^3\Pi_{0u}^+$ state of I_2 (from Capelle and Broida 1973).

found to vary with pressure and were usually non-exponential, probably because the resolution used was insufficient to excite single vibronic levels. The lifetime spectrum in I_2 is shown in figure 6. The long lifetime observed at short wavelengths was thought to be the natural lifetime of this state, the shortening at longer wavelengths being attributed to predissociation via the repulsive $^1\Pi_{1u}$ state. Predissociation was also found to affect the lifetimes in the corresponding state of Br_2.

Paisner and Wallenstein (1974) also studied this transition in I_2 with a nitrogen-laser-pumped dye laser but with much higher resolution (~1 pm), which allowed them to resolve single rovibronic levels. Their sensitivity was also much higher because they used a signal averager to enhance the signal from a sampling oscilloscope and this enabled them to extend the pressure range of measurement to 10^{-3} Torr. Their results agree, within errors, with those of Capelle and Broida (1973) except in one case, where a discrepancy of 18% was found.

A nitrogen-laser-pumped tunable dye laser, similar in design to the one reported by Hänsch (1972), was used by Figger *et al* (1974, 1975) and Heldt *et al* (1975) in a series of measurements of lifetimes in Fe I, Ni I and Co I. Their dye laser (see figure 7) used

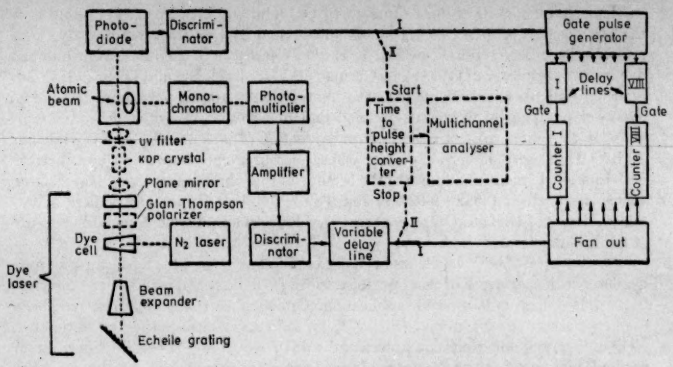

Figure 7. Schematic diagram of an apparatus for measuring lifetimes in metal vapours using pulsed, tunable dye laser excitation (from Figger *et al* 1974).

a beam-expanding telescope and an echelle grating of 79 grooves mm^{-1} to produce an excitation bandwidth of approximately 10 pm, sufficient to resolve the fine structure of the multiplets studied. For some experiments frequency-doubled radiation was required and this was produced by means of a KDP crystal mounted outside the laser cavity. The atoms were evaporated into an atomic beam of approximately 5 mm diameter and 10^{16} m^{-3} density. Fluorescence was observed at right angles to the direction of excitation through a grating monochromator which served both to suppress the intense thermal radiation from the oven and to discriminate against cascading via lower levels. The longer lifetimes were measured by means of eight gated scalers whose inputs were derived from the single-photon pulses via eight calibrated delays. Short lifetimes were measured with the delayed-coincidence method (see §2.1) which required long data collection times because of the low ($\sim$200 Hz) pulse repetition frequency of the laser.

Many other measurements in atoms, molecules and radicals using a similar excitation technique have also been reported. Pace and Atkinson (1975) measured the lifetimes of the $7^2P_{1/2}$ and $7^2P_{3/2}$ states of Cs and found good agreement with recent level-crossing measurements. McClelland and Yardley (1973) and Van der Werf *et al* (1974) reported lifetime and quenching measurements in biacetyl, Yardley *et al* (1971), Beyer and Lineberger (1973, 1975) and Beyer *et al* (1975) in glyoxal and Thayer and Yardley (1972) and Thayer *et al* (1975) in propynal. Several experiments where the molecules of interest were produced by chemical reaction *in situ* have also been reported. In particular, Dagdigian *et al* (1974) studied several alkaline earth monohalides MX, where M = Ca, Sr or Ba and X = F, Cl, Br or I, produced by chemical reaction of an atomic beam of M with a reagent gas (SF_6, HCl, HBr, CH_3I or CH_2I_2) at pressures between 10^{-3} and 10^{-5} Torr. Similar studies of Al 0 (Johnson *et al* 1972, Dagdigian *et al* 1975), Ba 0 (Johnson 1972) and Be 0 (Capelle *et al* 1972) were also reported. Jourdan *et al* (1976) studied CdH and CdD produced by direct chemical reaction of Cd vapour with H_2 or D_2. Jackson (1974) measured the lifetime of the B $^2\Sigma^+$ state of CN using pulsed UV dissociation of cyanogen prior to dye laser excitation. Lifetime measurements of

single rovibronic levels of the A $^2\Sigma^+$ state of OH (and OD in some cases) produced by the fast reaction of NO_2 with H atoms and excited by frequency-doubled dye laser radiation have been reported by Becker *et al* (1974a, b) (both used flashlamp-pumped dye lasers), Brophy *et al* (1974) and German (1975a, b). Hogan and Davis (1974) also reported similar measurements but used the reaction of atomic oxygen with H_2 and a dye laser pumped by frequency-doubled radiation from a Q-switched neodymium-glass laser. The narrowest bandwidth of excitation (4 pm) and the lowest pressures ($< 10^{-3}$ Torr) were used by German, whose measurements showed a slight increase with rotational quantum number of the lifetime of the vibrationless level. His absolute values (respectively $0{\cdot}688 \pm 0{\cdot}021$ μs and $0{\cdot}692 \pm 0{\cdot}021$ μs for the rotationless, vibrationless levels of OH and OD) were somewhat lower than the others, possibly because of the lower pressures used.

Another type of laser which has been used in lifetime work is the flashlamp-pumped dye laser which, because of its large pulse width ($\sim 0{\cdot}5$ μs) and inability to be repetitively pulsed, has not found wide application. One such instrument has, however, been used by Sackett and Yardley (1970, 1971, 1972) in an extensive study of lifetimes in NO_2 in the range of excitation wavelengths 451·5–460·5 nm. These lifetimes are of particular interest because the energy level structure of this molecule is very irregular and has not yet been analysed in terms of separable electronic, vibrational and rotational motions. This apparent breakdown of the Born–Oppenheimer approximation also implies that the individual levels are likely to have differing lifetimes and a knowledge of these could clearly help in identifying the interactions responsible for these irregularities. Early measurements (see Sackett and Yardley (1972) and references therein for a summary of early work) which were unable to excite individual levels indicated that the 'lifetime' was more than two orders of magnitude longer than that calculated from absorption measurements. The theoretical basis for understanding such anomalously long lifetimes was laid by Douglas (1966) but detailed measurements to quantify our understanding have been lacking.

The measurements of Sackett and Yardley, some of which are presented in figure 8, only partly fulfil this need because their resolution was still insufficient to resolve individual levels and they observed non-exponential decays from clusters of levels with possibly widely differing lifetimes. Further work with ultra-high resolution (~ 1 fm) was later reported by Paech *et al* (1975) and is described in §2.3.2.

A similar flashlamp-pumped tunable dye laser was used by Holleman and Steinfeld (1971) in a study of time-resolved fluorescence of ICl. Boesl *et al* (1975a, b) used a frequency-doubled flashlamp-pumped dye laser to measure single vibronic level lifetimes in naphthalene and deuterated naphthalene.

The laser used by Brus and McDonald (1974) produced tunable ultraviolet radiation in the range 260–325 nm by using a Q-switched frequency-doubled Nd : YAG laser to pump a dye laser which itself was intracavity frequency-doubled. The excitation pulses had a duration of 50–150 ns, a spectral width of approximately 30 pm, a peak power of 50–200 W and a repetition frequency of 75 Hz. They studied unresolved groups of rovibronic levels in the crowded first-excited-state manifold of SO_2 which, like NO_2, has a complicated structure that is not yet understood. Fluorescence was excited in the centre of a large gas cell and observed with uniform efficiency over a large volume to minimize non-linearities caused by the diffusion of long-lived excited molecules out of the field of view. Glass and liquid filters were used to absorb scattered excitation light and the fluorescence signals were either displayed and photographed on an oscilloscope screen or averaged in a waveform eductor (PAR model

THD-9). This is a multipoint signal averager that captures the waveform sequentially in 100 independent analog memories. Two different groups of rovibronic states with different lifetimes and quenching rates were observed, the major group having exceptionally long lifetimes (80–600 μs), the minor group which had not been observed by previous workers having lifetimes ~50 μs.

A different laser excitation technique was used by Yeung and Moore (1971, 1973a, b) in their study of radiative and radiationless processes in formaldehyde and its deuterated variants excited to single vibronic levels of the $^1A_2$ state. This state absorbs in the

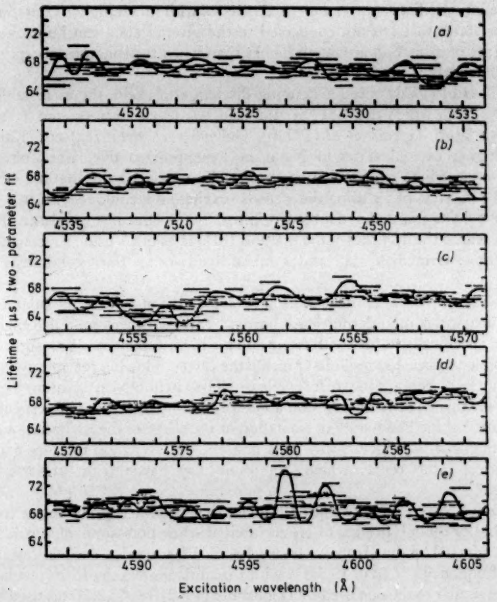

Figure 8. Lifetime spectrum of unresolved rovibronic levels of NO_2 measured by Sackett and Yardley (1972).

range 255–400 nm and two different arrangements were used to cover this range. The first produced tunable radiation in the range 255–335 nm of approximately 100 kW peak power, 7 ns duration and 100 pm bandwidth. It used frequency addition of a ruby laser fundamental (694·3 nm) and the output from a tunable dye laser, the dye itself being pumped by frequency-doubled radiation from the ruby laser. The second arrangement produced tunable radiation in the range 300–400 nm and was similar to the first except that the dye was pumped directly by the fundamental of the ruby laser. Additionally, some of the rovibronic lines were excited by two-photon absorption of

the frequency-doubled output at 669 and 679 nm of a Nd : YAG laser. In all cases an oscilloscope was used to display the fluorescence decays and photographs were taken for further analysis. Their measurements showed a decreasing trend in the natural lifetime and an increase in the quenching cross section with vibrational excess energy which was attributed to a competing predissociation.

Several experiments have recently been reported in which the state of interest was excited in two steps via an intermediate excited state. These techniques clearly extend the range of application of selective optical excitation enormously, especially as only one step needs to be selective and discharges, electron beams or other means of populating the intermediate state can be used. States with much higher excitation energies as well as states that are not connected to the ground state can be excited and the probabilities of excitation are much higher than when two-photon absorption with no intermediate state is used.

Gornik *et al* (1973a) used a Penning discharge to excite the metastable $4s4p\ ^3P_2$ level of Ca from which the $4s5s\ ^3S_1$ and $4s4d\ ^3D_1$ levels were excited by means of a pulsed dye laser. Gornik *et al* (1973b), Gallagher *et al* (1975a) and Kaiser (1975) studied higher excited states of Na using synchronized dye laser pulses and the $3p\ ^2P_{3/2}$ intermediate state. Siomos *et al* (1975) measured the lifetime of the $3d^64s$ (a ^{3}D) 4d e ^{5}G state of Fe using the stepwise excitation technique with two dye lasers, one of them being frequency-doubled, pumped by the same nitrogen laser. Deech *et al* (1975) measured the lifetimes of the 8, 9 and 10D states of Cs using a resonance lamp to populate the intermediate state and a pulsed dye laser for the second step.

2.3.2. Modulated CW laser sources. The low étendue of optical modulators is of no consequence when modulating laser beams. Indeed, many modulators have been developed specifically for use with lasers and are highly efficient. With some lasers it is even possible to place the modulator inside the cavity, allowing the energy to be stored within the laser for a time before release (Q-switching, cavity-dumping). These factors make this an attractive combination for lifetime measurement, especially when better control of the bandwidth of excitation or the shape of the excitation waveform is required than can be achieved with pulsed lasers. CW lasers also produce considerably less electrical interference, which can often play havoc with sensitive detection electronics.

Tango and Zare (1970) exploited the fact that several vibronic levels (principally $v' = 7$ and 8) of the B $^1\Pi_u$ state of K_2 are excited when potassium vapour is irradiated with red light (632·8 nm) from a He–Ne laser. They used a Pockels cell modulator driven at frequencies of 10 or 13 MHz with a modulation depth of 20%. A heterodyne technique, similar to the one used by Demtröder (1962) (see §2.2.3) was used to convert the phase-shifted fluorescence signal to a frequency of 800 Hz. The phase was then measured with a phase-sensitive detector and a phase-meter.

Baumgartner *et al* (1970) report the use of a He–Ne laser or an argon ion laser for studying alkali molecules excited to different rovibronic states that happen to coincide with the available laser lines. The apparatus was similar in concept to the one described by Demtröder (1962) except that single entrance and exit pinholes were used in the ultrasonic modulator. The alkali metal was contained in a sidearm of the absorption cell and the vapour pressure was controlled by varying the temperature of this sidearm while maintaining the rest of the cell at a higher temperature to avoid condensation. Vapour pressures in the range 10^{-3}–10^{-4} Torr were used where the fraction of diatomic molecules in thermal equilibrium is about 1%. Typically, 0·1% of these are in the

particular rovibronic state from which a particular laser line was absorbed. The lifetime of the B $^1\Pi_u$ state of Na_2 was found to increase slightly with increasing excitation energy, the average value for the state with six vibrational quanta being $6{\cdot}50 \pm 0{\cdot}20$ ns. This could be due to the $1/\lambda^3$ dependence in the transition probability formula or to a slight increase in the transition moment with internuclear separation (see §1.2). Such an increase is consistent with the fact that the corresponding state in the separated-atom limit is the 3^2P state whose lifetime is longer (16·3 ns). The information obtained from the other molecules was less specific and further work seems desirable. This is particularly true of Rb_2 and Cs_2 where large changes in the lifetime were observed and where the electronic structure is not understood.

A high spectral resolution ($\lesssim 1$ pm FWHM) was achieved by Erdmann *et al* (1972) by using an intracavity Lyot birefringent filter (Walther and Hall 1970) in a flashlamp-pumped dye laser. The laser output was tunable over a range of 400 pm by means of an applied voltage to the filter—coarse tuning was achieved by means of a grating end reflector. The Lyot filter was also used to extinguish the laser beam in less than 1·5 ns by shifting the transmission maximum outside the band selected by the grating. The instrument was used for measuring the decay of the $3^2P_{1/2}$ state of Na at densities as low as 10^{16} m^{-3}.

An ultra-high resolution instrument was developed by Paech *et al* (1975) using a single-mode argon ion laser whose output frequency was servo-stabilized to a spectral width of approximately 1 MHz (≈ 1 fm). They used a well collimated molecular beam of NO_2 to reduce the Doppler spreading to approximately 1% of its value in a gas cell and were thus able to excite single hyperfine levels. Because of the long lifetimes of this molecule they had to take great care in the design of the light-collecting optics to ensure that the excited molecules remained within the field of view during their lifetimes. Decays were observed with the delayed-coincidence method using an external electro-optical modulator to pulse the excitation. The experimental results proved that several directly excited states have short lifetimes (1–3 μs) which are determined mainly by fast internal conversion to neighbouring excited states and only weakly by fluorescence to the ground state. They also observed two vibronic states which are populated indirectly by non-radiative transitions from the primary excited state and which decay by fluorescence with lifetimes of approximately 30 μs and 100 μs.

2.4. Synchrotron radiation sources

Synchrotron sources exploit the radiation emitted by relativistic electrons confined to circular orbits in synchrotron accelerators and storage rings (see Codling (1974) for a general review of synchrotron sources and applications). Storage rings are generally preferred for synchrotron radiation work because their mean intensity varies only slowly with time (typical decay rates of beam current vary between 2 and 20 h). They can also carry as much as two orders of magnitude more current than typical synchrotron accelerators. The following are the main characteristics of synchrotrons and storage rings as light sources.

(*a*) They are highly intense continuum sources in the spectral range from infrared to soft x-rays. The emission is highly directional, the light spreading in the plane of the orbit, parallel to the instantaneous velocity vector of the electrons.

(*b*) The radiation is highly polarized with the electric vector in the plane of the orbit. This is particularly important for wavelengths less than about 100 nm where no efficient polarizers exist.

(*c*) The intensity of the light is modulated, typically at many megahertz. The exact form of the modulation depends on the characteristics of the machine and on the way it is operated. It can be ideal for measuring short lifetimes, especially with storage ring sources.

(*d*) The radiation is emitted in a high or ultra-high vacuum environment.

(*e*) The machines are very expensive to build, maintain and run.

(*f*) Synchrotron accelerators are prolific sources of biologically harmful radiation and radio-frequency interference. Sensitive detectors are difficult to operate in their vicinity and all experiments have to be remotely controlled. Storage rings are electrically quiet and biologically safer and access to the experiment is possible once the beam is stored. The x-ray emission can be a considerable nuisance for lifetime work, however, because it can damage optical components as well as contribute to the stray excitation background.

Heaps *et al* (1973) report the observation of the decay of fluorescence from a doped glass excited by pulses of radiation from the storage ring of Wisconsin Physical Science Laboratory. This is a 240 MeV ring with an orbital radius of 0·54 m. The ring operates at approximately 32 MHz, producing pulses of approximately 4 ns width. Widths as small as 1 ns could be produced by 'bunching' the electrons in the ring but only at the expense of greatly increasing the decay rate of beam current. The mean time between pulses was approximately 31 ns. This value could be increased for measuring longer lifetimes by 'wobbling' the beam so that only a subharmonic of the ring frequency is transmitted to the experiment. The sample was irradiated with undispersed radiation, the fluorescence being passed through a small monochromator to a photomultiplier. A sampling oscilloscope was used for display.

Lopez-Delgado *et al* (1974) and Lindqvist *et al* (1974) reported a range of fluorescence measurements conducted at the ACO storage ring at Orsay. This ring has a radius of 1·1 m and an energy of 550 MeV and was designed as an electron–positron collision ring. The ring orbital frequency is 13·7 MHz, giving a fundamental orbital period of approximately 73 ns. The electron bunch is approximately 0·3 m long and produces pulses of radiation of approximately 1 ns duration. The multichannel delayed-coincidence technique was used to measure fluorescence lifetimes and time-resolved spectra of several solutions contained in quartz cuvettes.

The experiments reported to date are clearly only preliminary feasibility studies. Over one dozen synchrotron radiation laboratories exist or are being built the world over. Most of these use existing high-energy physics installations, but some purpose-designed machines are planned. Their main applications are likely to be in areas other than lifetime measurement, such as biological and medical x-ray studies (photography, microscopy, diffraction and scattering), atomic, molecular and solid-state photoionization and photodissociation work (photoelectron spectroscopy, ESCA, mass spectrometry and absorption spectrometry) and photochemical studies, where no other sources can seriously compete. Conventional fluorescence lifetime work using the single-photon correlation technique is nevertheless part of the research programme at several laboratories.

2.5. Experimental errors

The attraction of modulated optical excitation methods is the high accuracy of which they are intrinsically capable. The selective nature of optical excitation precludes any possibility of cascading from higher excited states and cascading to lower

states can be discriminated against by suitably filtering the fluorescence light. In the past, however, these advantages have often been negated by the lack of suitably intense or monochromatic excitation sources or sufficiently sensitive detection electronics and measurements have often proved to be no more reliable than others obtained by intrinsically less accurate methods. Tunable lasers have surpassed traditional sources in brightness and spectral purity and they are now opening up many new areas of application both with direct and with two-stage excitation. Synchrotron radiation (and possibly Čerenkov sources—see Piestrup *et al* (1976) for example) promise to extend high-resolution measurements into the vacuum ultraviolet spectral region and with these new light sources a very wide range of highly accurate lifetime measurements now seems possible. For these reasons we consider it important to discuss the limitations and further possible sources of error in these techniques.

The selectiveness of the excitation depends on the spectral width of the exciting light, the Doppler width of the absorption lines and, especially in the case of molecules, the possible thermal population of states close to the ground state. Several recent experiments with lasers have used excitation bandwidths as low as 1 pm but narrower bandwidths require servo-stabilization of the output frequency. Ultimately, of course, the spectral width $\Delta\lambda_u$ achievable in modulated excitation experiments is limited by the uncertainty principle

$$\Delta E \Delta t \geqslant \hbar \tag{2.12}$$

where $\Delta E (= hc\Delta\lambda_u/\lambda_0^2)$ is the uncertainty in the photon energy and Δt is the uncertainty in the time of excitation. The resolution of approximately 1 fm attained with the servo-stabilized argon ion laser of Paech *et al* (1975, see §2.3.2) is close to this limit.

The Doppler width $\Delta\lambda_D$ of absorption lines in static gas cells is given by

$$\frac{\Delta\lambda_D}{\lambda_0} \approx 7 \times 10^{-7} \left(\frac{T}{A}\right)^{1/2} \tag{2.13}$$

where T is the absolute temperature and A is the mass number of the atoms or molecules. In NO_2 at room temperature and 500 nm, for example, $\Delta\lambda_D \approx 1$ pm, more than three orders of magnitude larger than the ultimate resolution that could be used with this transition. Doppler broadening can be reduced by a factor $\sin\theta$ by using a collimated molecular beam of divergence semi-angle θ crossed perpendicularly with the laser beam, as was done by Paech *et al*, for example.

The third difficulty in the way of achieving single-level excitation is the thermal population of states lying close to the ground state, especially ground vibrational and rotational levels in molecules. This can, in cases where there is a high density of excited states, lead to absorption of light by several upper levels within an energy band of approximately kT. Ordinary cooling does little to improve the situation before condensation sets in but Smalley *et al* (1974) have shown that, for example, NO_2 can be supercooled in a supersonic molecular beam to temperatures as low as 3 K and that a very substantial simplification in the absorption spectrum can be achieved by this means.

Sufficient resolution in the detection of fluorescence is also required if possible cascading transitions via lower excited states and scattered excitation light are to be discriminated against. In pulsed experiments, scattered excitation light manifests itself as a sharp peak superimposed on the decay curve, as shown for example in figure 2(*b*), which is undesirable because it makes it more difficult to analyse the full fluorescence decay curve, as described in appendix 1. In phase-shift work an error is introduced into the measured phase angle which requires measurements with at least

two different modulation frequencies to correct. Scattered excitation light can also cause saturation of the photomultiplier and detection electronics which may introduce non-linearities into their responses or cause time-dependent enhancement of the dark current (see Pettifer and Healey 1974 for example). Glass absorption or interference filters are often used to suppress scattered excitation light, but care needs to be exercized because many types have been found to fluoresce weakly (Turner 1973).

Many early laser experiments used oscilloscope displays or other real-time means of measuring the decay curves and have consequently been insensitive, requiring high target vapour densities to be used. Signal averaging techniques can increase the sensitivity by several orders of magnitude and mostly provide digital data in a suitable form for computer analysis, thus further improving the accuracy and helping to uncover possible systematic errors. Methods of signal averaging that have been used in pulsed excitation work include the multichannel delayed-coincidence technique, boxcar integrator, sampling oscilloscope, parallel-gated scalers, waveform eductors and transient recorders coupled to on-line averaging computers. The delayed-coincidence technique is unattractive with some lasers because of their low pulse repetition frequencies. Boxcar integrators and sampling oscilloscopes are sequential in operation and therefore wasteful of signal. The parallel-gated scalers used by Figger *et al* (1974, see §2.3.1) is a promising new approach which attempts to overcome these disadvantages. The instrument reported used eight channels and was suitable for lifetimes longer than 120 ns, but considerable improvements seem possible. Transient recorders and waveform eductors, their analog counterparts, are also becoming increasingly useful as their speed and resolution are improved. One very fast transient digitizer using a special cathode-ray storage tube is the Tektronix model R7112 where transients as short as 5 ns can be captured, digitized and transmitted to an averaging computer in approximately 65 ms. Another possible averager for longer lifetimes is the digital correlator which is presently available with channel widths as low as a few tens of nanoseconds. In phase-shift work long time signal averaging has been achieved by Keyser *et al* (1971, see §2.2.1 and figure 3) using the multichannel delayed-coincidence technique and by Schlag *et al* (1974, see §2.2.3) using a photon-counting phase-meter.

A systematic error with long lifetimes which is not confined to optical-excitation techniques is the movement of excited atoms or molecules from the field of view. The importance of the effect depends on the lifetime, the fluorescence-light-collecting geometry and the mean thermal velocity $\bar{v}$ of the atom or molecule, which is approximately given by

$$\bar{v} \approx 145 \left(\frac{T}{A}\right)^{1/2} \text{m s}^{-1} \tag{2.14}$$

where A is the mass number. An NO_2 molecule in a room-temperature gas cell, for example, moves approximately 30 mm during an 80 μs lifetime. The effect can also become important with much shorter lifetimes if a highly focused light collection system is used or if the excitation involves a discharge. A related problem is the possibility of quenching collisions with the walls of the sample cell.

The determination of the phase of the excitation light in phase-shift measurements is not without its difficulties. In some experiments the phase of the modulation is not uniform across the excitation beam and this can lead to an error if the scattering geometry used in the determination of the average phase of the excitation light does not correspond accurately to the excitation geometry used in measuring the lifetime. This is particularly difficult to achieve with molecular beam targets because of their ill

defined density profiles. Another difficulty arises (which can also be important in pulsed excitation experiments when the instrumental response function is to be measured) if the wavelengths of excitation and fluorescence are not the same because photomultipliers have wavelength-dependent transit times. The effect on the rise time is quite small (approximately 0·3 ns difference with wavelengths of 350 and 500 nm (see Sipp *et al* 1976)) if care is taken to always illuminate the same area of photocathode and to have as large an electric field in the vicinity of the photocathode as possible. Wahl *et al* (1974), however, report a much larger effect (nearly 2 ns difference in transit time with wavelengths of 317 and 568 nm), possibly partly caused by their low electric field in the vicinity of the photocathode.

3. Modulation techniques using electron-impact excitation

In this section we describe pulsed and sinusoidally modulated electron beam or discharge excitation experiments. Particles other than electrons (e.g. Nichols and Wilson (1968) used a pulsed proton beam) have also been used but they appear to offer no advantages over electron excitation. The fundamental principles behind modulation techniques are described in the introduction to §2 and the principles of the delayed-coincidence or single-photon correlation technique, which is used widely in pulsed electron-excitation experiments, are described in §2.1.

Electronic excitation has two main advantages when compared with optical excitation. Firstly, electrons are ubiquitous exciters: their energies can easily be varied over a wide range; they can excite optically allowed as well as forbidden states in atoms and molecules; and they can simultaneously dissociate and excite, ionize and excite, and even produce highly ionized excited atoms by knocking out an inner atomic electron. Secondly, electron beams are much easier to modulate at high frequencies than photon beams. Their main disadvantage is their lack of selectivity which is limited only by the conservation of energy. This leads to two major systematic errors in lifetime work, namely cascading and an increased probability of observing line blending. The first can, in principle, be eliminated by using a low enough excitation energy so that none of the higher lying states, which can repopulate the state of interest, are excited. This 'threshold-excitation technique' is discussed further in §3.2. Blending possibilities can be reduced by using very high spectral resolution which requires a very high sensitivity to be practical. This has been achieved in the 'high-frequency deflection technique' of Erman (1972) described in §3.3.

3.1. Methods using low-energy electrons

A large number of instruments using modulated low-energy ($\lesssim 200$ eV) electron-impact excitation, mostly pulsed and using the delayed-coincidence technique of measurement, have been reported. Heron *et al* (1954, 1956) were the first to report such an instrument which they used to study lifetimes and resonance trapping in helium. A more modern version was reported by Campos (1971) and is shown in figure 9(*a*). Their electron gun was a conventional gridded structure with a coiled tungsten filament cathode which could supply currents as high as 400 μA, with impact energies in the range 30–120 eV, to the collision volume. The control grid in front of the cathode was maintained at a sufficiently negative potential to cut off the beam completely except when recurrent positive pulses were applied. Light from the collision volume was dispersed in a monochromator with a mean resolution of 1·5 nm and

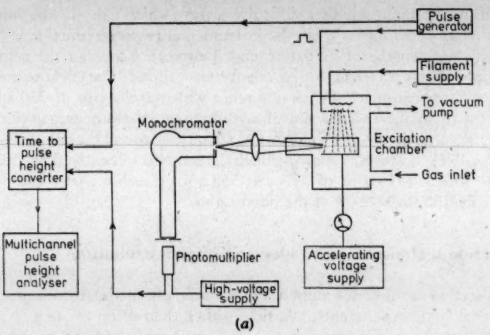

(*a*)

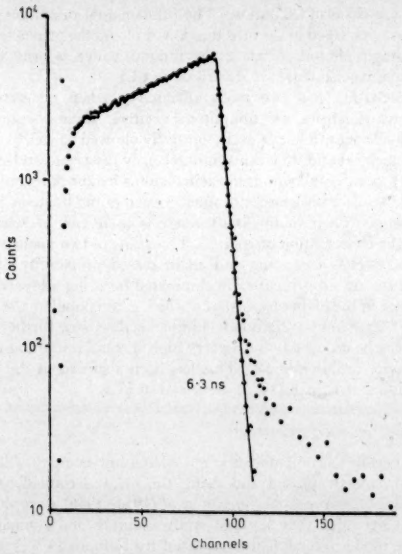

(*b*)

Figure 9. (*a*) Schematic diagram of the instrument used by Campos and co-workers to measure lifetimes by the delayed-coincidence technique using pulsed low-energy electron-impact excitation (after Campos 1971). (*b*) Decay curve of the (^{1}D) 5p $^2P_{3/2}$ state of Kr II measured with this instrument. The raw data (circles) show a low intensity tail at long delay times caused by cascading, which was subtracted in the analysis (triangles). Excitation energy 30 eV at 1 mTorr, 2·08 ns per channel (from Delgado *et al* 1972).

detected with a fast photomultiplier used as a single-photon detector whose output pulses were passed to the stop gate of the time to pulse height converter. The start pulses at 75 kHz were supplied by the same pulse generator as was used to modulate the excitation and the output of the time to pulse height converter was analysed and stored in a multichannel pulse height analyser. The instrument has been used to measure lifetimes in Kr I and II (Delgado *et al* 1972), Ar I (Campos and Zurro 1973) and Xe I and II (Jiménez *et al* 1974). A decay curve of the (^{1}D) 5p $^2P_{3/2}$ state of Kr II is shown in figure 9(*b*). Cascading from higher excited states manifests itself here as a low-intensity tail to the decay curve, which was subtracted out in the analysis.

Similar instruments have been reported by Verolainen and Osherovich (1966) and by Lawrence (1969), the latter instrument being capable of measurements in the vacuum ultraviolet spectral region. The instruments of Klose (1966) and Kurzweg *et al* (1973) are also similar in principle but use multistage guns based on the designs of Simpson and Kuyatt (1963). These guns afford a better control of the electron beam in the target region at the expense of intensity.

A somewhat different design of excitation source, capable of producing very high excitation currents, is the 'invertron' of Holzberlein (1964) in which a cylindrical cathode 50 mm long and 20 mm in diameter and heated externally by means of an induction coil surrounded the excitation volume. Two cylindrical coaxial grids were used to control the intensity and energy of the electrons in the central region. Several amperes of peak current could be produced with impact energies in the range 40–100 eV. It was developed as a high-intensity source for measuring lifetimes by directly viewing the decay on the screen of a fast oscilloscope (see Fowler *et al* 1964) but later experiments, such as those of Johnson and Fowler (1970), used the delayed-coincidence technique.

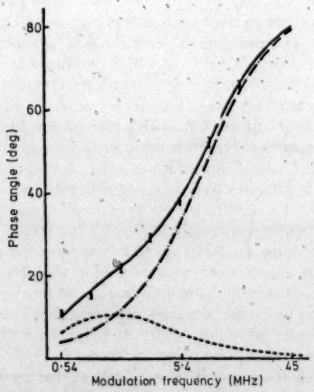

Figure 10. Phase-shift analysis for the A $^2\Sigma^+$–X $^2\Pi$ transition in CF excited by collisions of 200 eV electrons with perfluorobutadiene. The points are the data, the solid curve is the fit obtained by combining the phase shifts produced by a lifetime of 19 ns (chain curve) with those of a cascade component of 120 ns lifetime (broken curve) (from Hesser 1968).

Sinusoidal modulation and phase-shift measurements have also been used with low-energy electron excitation. In particular, the instrument originally developed by Lawrence (1965, 1966) and improved by Hesser (1968) and Smith (1970) has been used for a large number of lifetime measurements of astrophysical interest. The effects of cascading on the observed phase shifts have been discussed by Lawrence (1965) and in more detail by Curtis and Smith (1974). An example ($A\,^2\Sigma^+$–$X\,^2\Pi$ transition in CF as reported by Hesser (1968)) of a phase–frequency plot where cascading was found to cause the measured phase shifts to deviate from the ideal relationship (chain curve) of equation (2.5) is shown in figure 10. A fit to the data (full curve) was obtained when a cascading component (broken curve) of 120 ns lifetime was assumed to be present. A disadvantage of the phase-shift technique with electron excitation is that absolute lifetimes cannot be measured: the phase shifts have to be determined relative to those of known transitions.

Methods using low-energy electron excitation can conveniently be applied to a wide variety of measurements in atoms, molecules and ions. They suffer, however, from the one major systematic error of cascading. Also, the sensitivities that have been achieved have not been sufficient to work both with the very high spectral resolution needed to resolve blended lines and with the low pressures needed to eliminate collisional de-excitation or resonance trapping.

3.2. Methods using threshold-energy electrons

One possible way of eliminating cascading is to use excitation energies that are high enough for the state of interest but too low to excite the higher states that might repopulate it. Instruments designed to use this 'threshold-excitation technique' have been reported by Bennett (1961), Bennett *et al* (1965), Bridgett and King (1967) and Allen *et al* (1969). As excitation cross sections are very small and threshold energies are low, the design of the electron gun presents formidable problems. The design of Bennett *et al* (1965), for example, achieved a high perveance by using an oxide-coated cathode of very large area (200 mm long × 10 mm wide) and a control grid of large transparency very close to it (1·5 mm). The anode was placed 7 mm from this grid and electrically connected to it to form a field-free excitation volume. The cathode was operated at low temperatures to minimize optical emission and thermal energy spread of the emitted electrons ($\sim 2{\cdot}5kT$ full width at half-maximum). Space-charge limited currents in the range 100–200 mA were achieved with this design. The pulses applied to the gun were 100 ns wide, cutting off the excitation in less than 2 ns, but the time resolution of the instrument was mainly limited by the transit time of the electrons across the excitation volume ($\sim 2{\cdot}7$ ns at 20 eV) and by the response time of the photomultiplier. Decay curves were measured using the delayed-coincidence technique with a phase-locked vernier chronotron in place of the more usual time to pulse height converter–analog to digital converter combination. This instrument consists basically of two oscillators of slightly different frequencies that are triggered into oscillation by a start and a stop pulse whose difference in time of arrival is to be measured. The stop pulse is fed to the faster oscillator so that its pulse train output can catch up in phase with the output from the start oscillator. Phase equality is detected with a coincidence circuit whose output is used to stop the oscillators. The number of oscillations of the start or stop oscillators are counted and this number is proportional to the time difference. The instrument used in the experiments (see Kindlmann and Sunderland 1966) achieved a time resolution of 2 ns, a differential non-linearity less

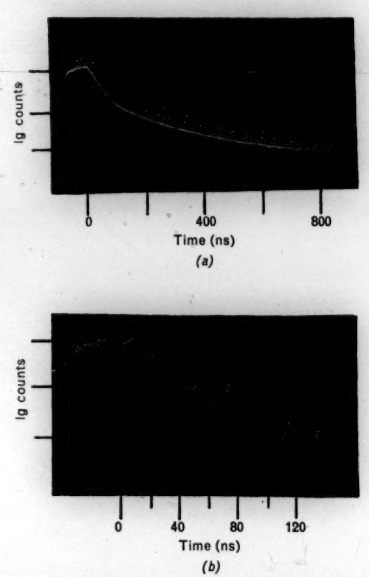

Figure 11. Decay curves of the $2p_8$ state of Ne measured with electron-impact energies of (*a*) 11 eV above the threshold of the state and (*b*) approximately 0·1 eV above the threshold. No cascades were excited in the latter experiment and these data were well fitted with a single exponential decay with a lifetime of $19{\cdot}7 \pm 0{\cdot}2$ ns. In case (*a*) the decay curve is clearly affected by cascading (approximately one dozen strong transitions from levels in the $2p^54s$ and $2p^53d$ configurations can be identified) and least-squares analyses with one, two and three superimposed exponential decay components yielded estimates of the $2p_8$ lifetime of respectively 52, 29 and 27 ns (from Bennett and Kindlmann 1966).

than 0·1% and a very high stability because its start and stop oscillators were phase-locked to a stable quartz oscillator. Barton and King (1971) described two instruments, one using standard NIM modules with a time resolution of approximately 200 ps and one using fast logic integrated circuits with a time resolution as low as 10 ps. The main advantage of vernier chronotrons is their low differential non-linearity.

In a series of measurements on the $2p^53p$ configuration in neon, Bennett and Kindlmann (1966) convincingly demonstrated the effects of cascading. The decay curve of figure 11(*a*) (plate) was measured with an impact energy 11 eV above the threshold of the state and that of figure 11(*b*) (plate) with an impact energy 0·1 eV above the threshold. The threshold excitation data were well represented by a single exponential decay curve with a lifetime of $19{\cdot}7 \pm 0{\cdot}2$ ns ($2p_8$ state). Attempts were then made to extract this lifetime from the cascaded decay curve by fitting superpositions of exponentially decaying terms. The details are summarized in the caption of figure 11. The method fails even when three decay components were assumed.

The threshold excitation technique has not found wide application, however, because of its inherently low sensitivity. Oxide-coated cathodes also tend to poison easily and only a very limited number of atoms and molecules can be studied. This has been partially overcome by Bridgett and King (1967) who used a more rugged, though much smaller, dispenser cathode.

3.3. Methods using high-energy electrons

The use of high impact energies (several keV) for exciting atomic, molecular or ionic states has several advantages over low impact energy or discharge excitation. Although the excitation cross sections of atomic and molecular states have their maximum values at low energies (typically from near threshold to a few 100 eV above), the product of cross section and available excitation current peaks at much higher energies because of space-charge limitations in electron guns (Erman 1972). A further advantage is that highly ionized atoms can be studied by using sufficiently high energies to knock out an inner atomic electron. The resultant shake-off of outer electrons ('vacancy cascade') yields an excited ion with a wide range of possible charge states (Erman and Berry 1971).

One such instrument was described by Erman *et al* (1972) and is shown in figure 12. A magnetic lens focused the beam from a water-cooled electron gun to a small spot. A double-focusing sector magnet converted this spot to a line, focused 600 mm away, on the axis of the molecular beam. A slit and electrostatic deflection plates were placed close to the magnet and a further slit, situated 100 mm from the molecular beam, served as beam-stop, except for electrons directed at the molecular beam. Modulated excitation was achieved by electrostatically deflecting the electron beam across this aperture at high frequencies. An electron collection plate behind the molecular beam served as a signal pick-up for synchronizing the time to pulse height converter for delayed-coincidence lifetime measurements. The electron beam intensity was typically 10 mA at 7 keV, the deflection frequency being chosen to optimize the yield for the decay time being measured. A 2 m Czerny–Turner spectrometer was used to disperse the emission with a resolution in the range 1–10 pm.

With this high resolution and sensitivity, the systematic errors of line blending, collisional quenching and resonance trapping have been greatly reduced or eliminated. Cascading is still present because of the non-selective nature of the excitation. It has been found, however, that cascading is not as important in many cases as had previ-

ously been thought. Indeed, in molecules, cascade effects are generally negligible, partly because there are often very few electronic states and partly because of the Franck–Condon factors and rotational selection rules which restrict the number of possible intercombinations. The situation is more complicated in atoms. In hydrogen-like atoms, Erman (1975) argued that lifetimes could be measured to 15–20% accuracy if decays could be followed for 20–30 lifetimes. It would be difficult to maintain a uniform detection probability for such long observation times in most practical cases, however. Spectral line blending is often the dominant systematic error and has

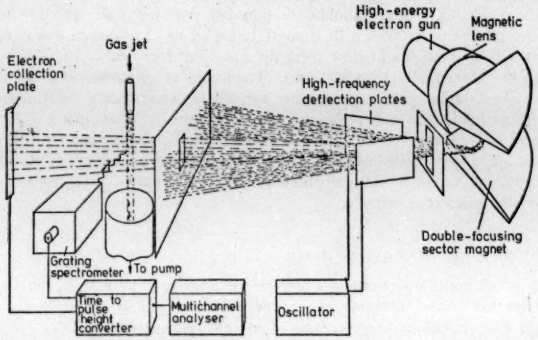

Figure 12. Schematic diagram of the instrument used in 'high-frequency deflection' measurements of lifetimes (from Erman *et al* 1972).

often been misinterpreted as cascading in other measurements. For example, the lifetime of the 5p $[2\frac{1}{2}]_2$ level of Ar I was found by this technique to be 303 ± 15 ns (Erman and Martinson 1973), longer by a factor of 2 than previously measured values, which had presumably been falsified by two neighbouring lines of Ar II which were discriminated against in the work of Erman and Martinson. Another example where high resolution is necessary is in the study of lifetimes of individual rovibronic levels of molecules. In a particularly elegant series of experiments Smith *et al* (1976) discovered weak predissociations in the higher rovibronic levels of the A $^3\Pi$ and C $^1\Pi$ states of NH and were able to deduce the ground-state dissociation energy and the singlet–triplet manifold separation energy from their data. The measurements on the A state are reproduced in figure 13.

Other measurements by this technique include studies of lifetimes in neutral iron (Erman *et al* 1974), of low-lying excited states of NO (Brzozowski *et al* 1974a), and of the ion molecules H_2O^+ (Erman and Brzozowski 1973) and NH^+, OH^+ and SH^+ (Brzozowski *et al* 1974b)†.

† The recent measurements of Möhlmann *et al* (1976) show that these data on long-lived ionic states may be seriously in error because of a rapid drift due to Coulomb repulsion of the excited ions out of the field of view. For several vibronic levels of the $\tilde{A}\ ^3A_1$ state of H_2O^+, for example, they measured a value of $10{\cdot}5 \pm 1$ μs, more than an order of magnitude larger than the value measured by Erman and Brzozowski (1973). The effect may sometimes be difficult to detect because it does not always lead to non-exponential decay curves.

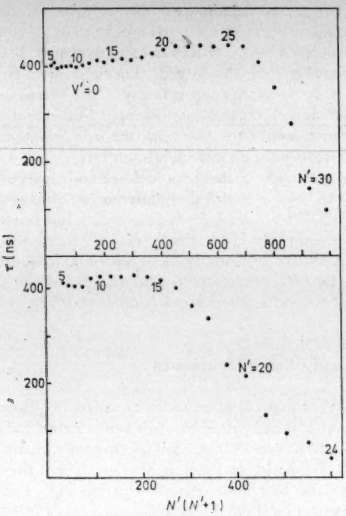

Figure 13. Lifetimes of the various rotational levels N' of the A $^3\Pi$ state of NH plotted against rotational energy. The strong variations in τ indicate that the A state predissociates in both ($v' = 0$, 1) sequences (from Smith *et al* 1976).

3.4. Methods using discharges

Apart from the various electron-impact sources described above, two basic designs of discharge source have also been used for lifetime measurement: the radio-frequency electrodeless discharge and the pulsed hollow-cathode discharge. Their advantage over electron-impact sources is in not requiring a heated cathode which might react with the atoms or molecules being studied. They have three main disadvantages. Firstly, they produce very hot plasmas with wide distributions of electron and ion velocities which restricts their application to short lifetimes, both because of the increased rate of collisions and because of the increased speed with which the excited species move out of the field of view. Secondly, the plasma characteristics (energy distributions of electrons and ions, relative populations of excited states and charge states, distribution of velocities among quenching partners, etc) strongly depend upon gas density and Stern–Volmer kinetics (linear dependence of decay rate on density) cannot be assumed to apply. The accuracies of lifetimes deduced from extrapolations to zero density from measurements at high densities must therefore be questioned. Thirdly, these discharges do not work at low densities.

Donovan and Duncan (1961) and Jeunehomme and Duncan (1964) developed an instrument using a radio-frequency discharge source. The circuit used a Tesla transformer, the primary low-induction side being connected to a capacitor bank, charging

resistor and switch (air gap or vacuum gap), the secondary winding being coupled to the quartz sample cell by means of a wire wrapped around the outside. The ringing frequency of the secondary was ~10 MHz and approximately 20 cycles were observed each time the capacitor bank was discharged. The light intensity from the cell was in the form of a single pulse, rising in approximately 10 ns. It was sufficiently intense for decays to be displayed directly on a fast oscilloscope. Sutherland and Anderson (1973) used a similar excitation source together with the delayed-coincidence technique to study lifetimes and predissociation probabilities in OH.

The pulsed hollow-cathode discharge or 'cold-cathode invertron' of Copeland and Fowler (1970) consisted of a cylindrical aluminium cathode, approximately 150 mm long and 50 mm in diameter, together with an axial stainless steel anode. An axial magnetic field of approximately 150 G was applied to reduce the breakdown voltage. It was operated with pulses of 2 kV amplitude at repetition frequencies up to 1 kHz and was used to measure the lifetimes of several vibronic levels of the A $^2\Sigma^+$ state of NO by means of the delayed-coincidence technique (Copeland 1972).

4. Foil excitation and related techniques

Since the first observations of optical radiation emanating from the beam of a Van de Graaff accelerator after it had passed through a thin carbon foil (Kay 1963, Bashkin and Meinel 1964), the technique of beam–foil spectroscopy has developed rapidly into an important branch of experimental atomic physics. The main properties that have made such foil-excited ion beams attractive for spectroscopic studies are:

(*a*) Most elements can be studied.

(*b*) Very high stages of ionization can be achieved with an appreciable fraction of each species in excited states. Doubly excited levels also appear with appreciable intensities.

(*c*) High chemical and isotopic purities can usually be achieved by mass-analysing the ion beam before it interacts with the foil.

(*d*) The excited states decay spontaneously in a high vacuum and the effects of collisions and resonance trapping are therefore negligible.

(*e*) The high vacuum environment facilitates observations in the vacuum ultraviolet spectral region.

(*f*) Because of the very short ($\lesssim 10^{-13}$ s) interaction time within the foil, the states are coherently excited. They also appear to be aligned (the populations are functions of the modulus of the magnetic quantum number $|M_J|$). Quantum beat experiments to measure Landé g factors, fine- and hyperfine-structure separations can therefore be attempted (see §5.9).

(*g*) Lifetimes of excited states can be measured because the decay probability in time becomes a decay probability in (x/v) where x is the distance between the foil and the point of observation and v is the velocity of the ions.

In this section we limit ourselves to those aspects of foil-excitation spectroscopy that are relevant to the measurement of lifetimes. Variants of the method, such as excitation by means of a gas target or a laser beam, are also described. Our treatment will necessarily be sketchy considering the vast amount of published information. The three proceedings of the international beam–foil spectroscopy conferences† are particularly

† Bashkin S (ed) 1968 *Beam-foil Spectroscopy* vol 1 and 2 (New York: Gordon and Breach), 1970 *Nucl. Instrum. Meth.* **90** and 1973 *Nucl. Instrum. Meth.* **110**.

copious sources for further reading. Bashkin (1974) and Martinson (1974) have also recently published reviews on the subject.

4.1. Experimental details

The principle of the foil-excitation method is illustrated in figure 14. An accelerator (usually a Van de Graaff accelerator) is used to produce an energetic beam of ions which are mass-analysed in a magnetic field, the mass fraction of interest being passed through a thin carbon foil. Interaction of the primary ions with the foil causes further ionization and excitation and the beam emerges into the observation chamber where it is viewed, usually in a direction perpendicular to the direction of motion, by means of a

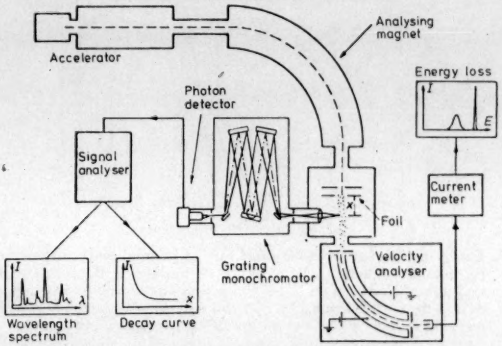

Figure 14. Experimental arrangement for studying atomic and ionic spectra and lifetimes in foil-excitation spectroscopy (from Martinson 1974).

grating monochromator and a photomultiplier. Because of the high velocity of the beam, the particles move a considerable distance before decaying. A decay curve is measured by tuning the monochromator to the emission line of interest and measuring its intensity $I(x)$ as a function of the distance x between the foil and the point of observation. As the time t between excitation and decay is proportional to x, the temporal decay curve $I(t)$ can be determined and this forms the basis of the method of measuring lifetimes by the beam–foil technique. The main characteristics of the technique are described in more detail below.

4.1.1. Beam properties. Ion beam energies in the range 20 keV to over 400 MeV have been used in foil-excitation studies. The choice of beam energy depends mainly on the mass and charge state of the ions to be studied, high-energy beams being necessary for studying highly charged heavy elements. Low-energy beams ($\lesssim 500$ keV) are usually generated in electromagnetic isotope separators, medium-energy beams ($\lesssim 5$ MeV) in Van de Graaff accelerators and high-energy beams in tandem Van de Graaf accelerators, linear accelerators or cyclotrons. Beam currents of the mass fraction of interest are usually less than 1 μA in intensity and their diameters are of the order of 2 mm.

The foil-excited source can therefore be seen to be very tenuous, of the order of 10^{10} particles m^{-3}. Re-absorption of resonance radiation, perturbations of excited states by interionic fields and collisions among beam particles are very improbable, as are collisions with residual gas in the observation chamber with the usually low ($\lesssim 10^{-5}$ Torr) background pressures used.

4.1.2. Foils and other exciters. Ideal foils should be of low-Z material and strong enough to be self-supporting with very low thicknesses to minimize the energy loss, energy spreading and angular scattering of the beam. They should also be able to withstand heavy-ion bombardment without damage for long periods of time. Beryllium would be an attractive choice if it were not for its toxicity. Boron foils are

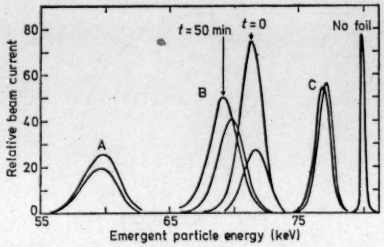

Figure 15. Energy distribution curves measured with a Li^+ ionic beam of 80 keV initial energy penetrating A, thick (~ 18 μg cm^{-2}), B, medium (~ 9 μg cm^{-2}) and C, thin (~ 3 μg cm^{-2}) carbon foils. The profiles labelled $t = 0$ and $t = 50$ min were measured with the same foil immediately after insertion and after 50 min of bombardment respectively (from Bickel and Buchta 1974).

difficult to prepare and have little mechanical strength, but carbon foils are in common use. Thicknesses above 5 μg cm^{-2} can be used without a supporting grid. Their lifetimes vary from several minutes to several hours, depending upon thickness, ion mass, energy and current. Their characteristics change continually during bombardment, either increasing or decreasing in thickness, depending on the respective rates of contamination build-up and sputtering. Bickel and Buchta (1974) have recently made a study of these effects. Figure 15, taken from their publication, shows the velocity distributions observed when a beam of 80 keV Li^+ ions penetrates foils of various thicknesses. Both the energy loss and the energy spread increase with increasing foil thickness. Also shown is the change in foil characteristics after it has been bombarded for 50 min. They measured a deposition rate of 2·7 μg cm^{-2} h^{-1} for this foil under these conditions, leading to a decrease in the mean ion velocity of 2·4% over its 80 min life.

Static gas cells in differentially pumped chambers have also been used as exciters. They have the advantages of longevity and much reduced angular scattering of the beam but they are unable to produce high states of ionization or short interaction times.

4.1.3. Spectrometers. Most experimental arrangements use commercial grating spectrometers, together with photoelectric detectors. The design of the viewing

geometry and input optics for observing foil-excited beams is of crucial importance if the often very large line broadening due to the Doppler effect is to be reduced. The wavelength λ observed when a source moves with velocity v in a direction subtending an angle θ with the direction of observation is given by

$$\frac{\lambda}{\lambda_0}=\left(1-\frac{v}{c}\cos\theta\right)\left(1-\frac{v^2}{c^2}\right)^{-1/2} \tag{4.1}$$

where c is the speed of light and λ_0 is the wavelength observed from a source at rest. Figure 16 shows the usual lateral viewing geometry ($\theta=90°$), which is the only arrangement we discuss because other viewing geometries are unsuitable for measuring lifetimes. Four contributions to the line broadening, all caused by the Doppler effect, can be identified.

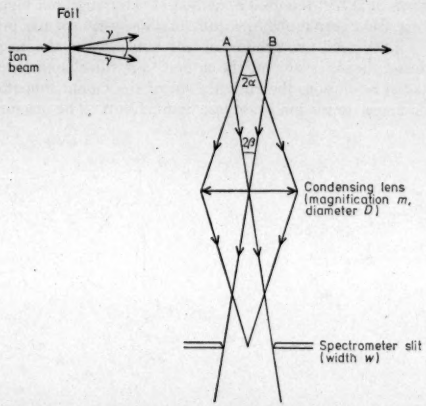

Figure 16. Arrangement for observing the foil-excited ion beam in the lateral viewing geometry, which is used for measuring lifetimes.

(*a*) A finite element AB of the beam is imaged by the condensing lens onto the entrance slit of the spectrometer. Light from A and B is respectively blue- and red-shifted by an amount $(\lambda_0 v/c)(1-v^2/c^2)^{-1/2}\sin\beta$. The line broadening (basewidth) caused by this effect is therefore approximately given by

$$\frac{\Delta\lambda_a}{\lambda_0}\approx\frac{vw}{cf(1+m)} \tag{4.2}$$

where w is the slit width of the spectrometer, f is the focal length of the lens and m is the linear magnification with which the beam segment AB is imaged onto the slit.

(*b*) The finite acceptance angle of the condensing system similarly leads to a line broadening which, at the centre of the beam segment, is given by

$$\frac{\Delta\lambda_b}{\lambda_0}\approx\frac{vmD}{cf(1+m)} \tag{4.3}$$

where D is the active diameter of the condensing lens.

(*c*) The velocity spread Δv of ions, caused mainly by scattering within the foil, leads to a contribution to the line broadening given approximately by

$$\frac{\Delta\lambda_c}{\lambda_0} \approx \frac{\Delta v}{c}\left(\frac{v}{c} - \cos\theta\right) \tag{4.4}$$

which is of second order and therefore unimportant in the lateral viewing geometry.

(*d*) The range of inclinations ($\pm\gamma$) of the trajectories of the excited ions, caused mainly by small-angle scattering within the foil, leads to a contribution given approximately by

$$\frac{\Delta\lambda_d}{\lambda_0} \approx \frac{v\gamma}{c}\sin\theta. \tag{4.5}$$

Kay and Lightfoot (1970) reported a method of achieving both high spectral and spatial resolutions while exploiting the full luminosity-resolvance product of the monochromator. They used two cylindrical lenses in place of the usual single condensing lens to image the ion beam onto the entrance slit with changed aspect ratio. To achieve good spatial resolution, the entrance slit of the monochromator was placed vertically at right angles to the ion beam (see figure 17(*a*)). The magnification in the

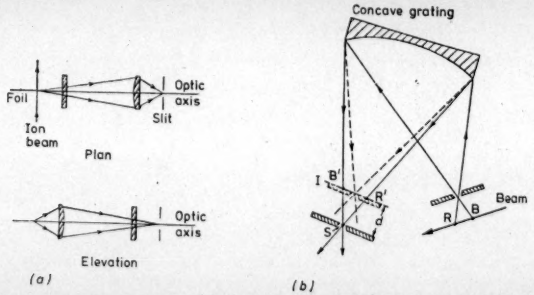

Figure 17. Two efficient methods of observing the foil-excited beam in the lateral viewing geometry. (*a*) An anamorphotic condensing system (from Kay and Lightfoot 1970). (*b*) The re-focusing method, in which red and blue Doppler-shifted light, indicated by R and B respectively, are brought to a common focus at the re-positioned exit slit S (from Stoner and Leavitt 1971a).

vertical plane can then be made large enough to fill the length of the slit with light without sacrificing spectral resolution. The magnification in the horizontal plane needs to be made small enough to ensure that the acceptance angle of the condensing system remains low to keep line broadening due to mechanism (*b*) to a minimum. In practice, there is no point in making the acceptance angle (α) much smaller than the angular spread (γ) within the beam. From equations (4.2) and (4.3), line broadening due to mechanism (*a*) can be neglected as long as $w < mD$, which is always true in practice (m is the magnification in the horizontal plane in this case).

An alternative method of achieving high spectral resolution exploits the fact that the observed wavelength varies monotonically with θ. With the spectrometer arranged without coupling optics, as shown in figure 17(*b*), the spectral width observed in the

normal image plane of the spectrometer is $\Delta\lambda/\lambda_0=(2v/c)\sin\beta$. A much reduced spectral width is observed if the exit slit is moved a distance $d\approx v\lambda_0/ck$, where k is the reciprocal dispersion of the instrument (Stoner and Leavitt 1971a). Furthermore, a field lens of appropriate strength can be placed in front of the entrance slit, so that the effect of a non-zero entrance slit width is largely compensated for by the Doppler shift of the light. This greatly increases the signal strength with only a slight increase in the observed linewidths (Stoner and Leavitt 1971b). These, and some further aspects of the line-broadening problem with fast ion beams, were discussed by Stoner and Leavitt (1973).

These methods do not, however, compensate for the finite angular spread of the foil-excited beam (broadening mechanism (*d*)). Scattering within the foil, therefore, places a fundamental limitation on the observable linewidths. With thin carbon foils, the observed linewidths are limited to $\gtrsim 0{\cdot}1$ nm for visible light. The use of beryllium foils would reduce this by a factor of about 2. With gas targets, linewidths $\lesssim 10$ pm can be achieved (Stoner and Radziemski 1972) but with the disadvantage that only low stages of ionization are observable.

4.1.4. Charge-state identification. With the large number of charge states and the many previously unidentified lines prominent in foil-excited spectra, the problem of line identification is a formidable one. Part of the problem is solved if a line can be ascribed to a particular charge state. Three methods of charge-state analysis are in use.

(*a*) Kay (1963, 1965) found that the dependence of the relative intensities of spectral lines on beam velocity could be used to identify the charge state of the emitting ion. This is illustrated for several well identified transitions in C, N and O in figure 18 where the mean charge can be seen to increase with increasing velocity, the excitation function of any particular charge state showing a peak at a particular energy. No quantitative theory exists for this.

(*b*) An electric field applied perpendicularly to the direction of observation and the direction of the beam causes the latter to be deflected. The beam splits into a number of parabolic trajectories, depending on the charge state, which can then be observed separately (Bashkin *et al* 1964, Malmberg *et al* 1965).

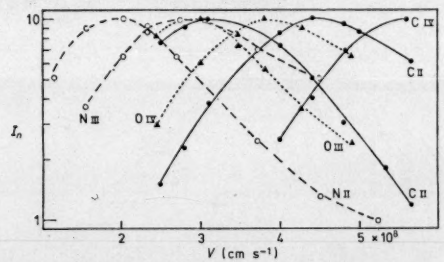

Figure 18. Normalized excitation functions for several transitions in C, N and O, from which the charge state of the emitter can be determined. (●) C II 3d ^{4}F–4f ^{4}G, C III 4d ^{3}D–5f ^{3}F, C IV 5s ^{2}S–6p ^{2}P; (○) N II 3p ^{1}D°–3s ^{1}D, N III 4f ^{2}F°–5g ^{2}G; (▲) O III 3d ^{5}P–3p ^{5}D°, O IV 3p ^{4}D–3d ^{4}F (from Dufay (1970), who gives references to the original sources of the data).

(*c*) The electric field is now applied in the direction of observation. This causes the ions to accelerate towards or away from the spectrometer, their sideways velocity components being proportional to their charge (for an isotopically pure beam). A study of the Doppler shifts of spectral lines as a function of the applied field then gives information about the charge states of the emitters (Fink 1968).

Method (*a*) is easy to apply and nearly universal in application. It can also be used to study the composition of a blended line where transitions from different charge states are involved but often gives ambiguous results, however. Method (*b*) is difficult to apply because the parabolic beam paths reduce the spectral resolution achievable. The Doppler shifts achievable in method (*c*) tend to be small, especially in the ultraviolet spectral region, and it is often difficult to interpret the observed pattern when the spectrum is crowded or when Stark broadening is appreciable. Neither method (*b*) nor (*c*) can be used for assigning short-lived states.

4.2. Lifetime measurement and systematic errors

The decay curve of a selected spectral line can be measured by recording the intensity $I(x)$ as a function of the distance x between the foil and the point of observation. As the time t between excitation and decay is proportional to x, $I(x)$ can be scaled to give $I(t)$, the temporal decay curve. Theoretically, the range of decay times (τ) that can be measured is limited by (Bromander 1973):

(*a*) The maximum ionic velocity attainable, $v_{max}=c$.
(*b*) The minimum ionic velocity required to penetrate a foil, $v_{min}\sim 10^5$ m s^{-1}.
(*c*) The spatial resolution attainable (AB of figure 16), $AB_{min}=v\tau\sim 5\times 10^{-4}$ m.
(*d*) The maximum attainable observation distance, $x_{max}\sim 1$ m.

These limits are indicated in figure 19. In practice, however, the accessible range of lifetimes is more restricted. Ionic velocities are at least one order of magnitude lower, spatial resolutions usually an order of magnitude larger and observation lengths a factor of about 5 smaller than indicated. Furthermore, decay curves should be measured over several lifetimes if there is to be any chance at all of assessing the various systematic errors of measurement.

Decay curves measured with the foil-excitation technique are almost invariably

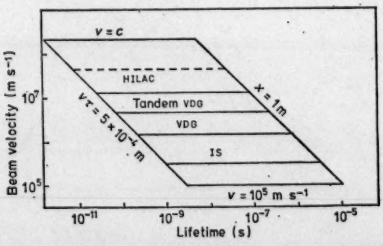

Figure 19. Limitations in the range of lifetimes that can be measured with the foil-excitation technique. The useful ranges of the most commonly used accelerators (isotope separator, Van de Graaf, tandem Van de Graaf and heavy-ion linear accelerator) are shown (from Bromander 1973).

non-exponential. The main systematic effects that could, alone or in combination, be responsible for this are described below.

4.2.1. Cascading. As with other non-selectively excited sources, cascading is a major problem in foil-excitation spectroscopy. General methods of treating cascade-affected decay curves are discussed briefly in appendix 1. Here we concentrate on those methods of cascade suppression or elimination that apply specifically to the foil-excited source.

Berry *et al* (1972) reported a method of eliminating cascading by measuring and subtracting separate decay curves for light polarized parallel and perpendicular to the ion beam. The change of polarization with time is determined, in the absence of external fields and quantum beat effects (see §5.9), by cascading from higher excited states. The authors argued that, in many cases, these contributions are isotropic and only introduce an unpolarized component which is subtracted out in this method.

Liu and Church (1972) reported a method which exploits the initial alignment and the coherent excitation property of the foil-excited source. Their method consists of measuring and subtracting two decay curves, one for field-free decay and one with a magnetic field applied perpendicularly both to the direction of observation and the direction of the ion beam. The magnetic field strength B is chosen so that the Larmor precession frequency ω_L ($=g_J\mu_B B/\hbar$) gives an easily resolvable modulation on the decay curve (see also §5.9). In both cases only radiation polarized with the electric vector parallel to the ion beam is observed. The observed intensity $I(t)$ in the absence of the magnetic field is

$$I(t)=a\exp(-t/\tau)+c(t,0)+d \tag{4.6}$$

where d is the background and c is the contribution due to cascading. When the magnetic field is turned on,

$$I'(t)=\exp(-t/\tau)(a+b\cos 2\omega_L t)+c(t,B)+d \tag{4.7}$$

and

$$I'-I=b\exp(-t/\tau)(\cos 2\omega_L t-1)+c(t,B)-c(t,0).$$

In many cases, they argued $c(t,B)\approx c(t,0)$ and the effect of cascading cancels in the subtraction. Such a difference spectrum is shown in figure 20 where the damped oscillation is clearly resolved. This can be analysed to determine both the g factor and the lifetime. The method has been applied to several levels known to be subject to strong cascading (see Church and Liu 1973, for example) and seems to work.

Both the above methods suffer from two main weaknesses, apart from the fact that they cannot be applied to all transitions. Firstly, the reduction or elimination of cascading cannot be positively demonstrated. Rather, it depends on assumptions about the

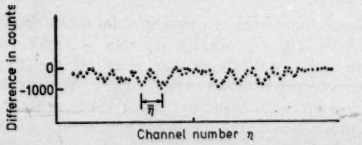

Figure 20. Quantum beat signal of the $3p'\ ^2F^o_{7/2}$ level of O II from which the lifetime and the g factor can be determined without the influence of cascading (from Church and Liu 1973).

nature of the cascading levels and their effectiveness in transferring their alignment to the level of interest. Secondly, both methods are insensitive because the required signal is the difference between two nearly equal signals. This is particularly true with heavy ions, high charge states and high beam velocities as the fraction of ions that are initially aligned decreases rapidly with these parameters.

Masterson and Stoner (1973) reported an experiment in which the lifetime of an intermediate state was measured by counting correlated photons from decays into and out of this level (such 'photon–photon' coincidence experiments are discussed more fully in §6.1). Because of the high velocity of the emitters, the experiment had to be repeated for several distances between the two detectors. Ten days of run time were required for an initial measurement of the lifetime of the unresolved $3d'\ ^2G_{7/2,\ 9/2}$ levels of O II. It seems unlikely that high accuracies will be achieved with this method because of the difficulty of keeping the experimental parameters, especially the ion beam velocity, constant for such long periods of time.

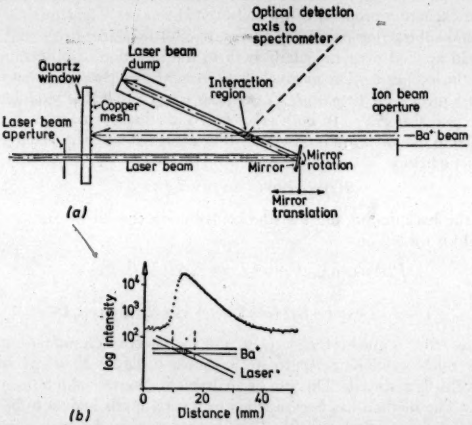

Figure 21. Laser beam excitation of an ionic beam. (*a*) The experimental arrangement. (*b*) A decay curve of the $6^2P_{3/2}$ state of Ba^+. The intensity of the 455·4 nm line was measured at a fixed point, while the laser deflecting mirror was moved (from Andrä *et al* 1973a).

A different and very promising new technique for measuring lifetimes, using well collimated crossed ion and laser beams, was reported by Andrä *et al* (1973a, b). Their experimental arrangement, with which they measured the lifetime of the $6^2P_{3/2}$ ($\lambda_0 = 455{\cdot}4$ nm) state of Ba^+, is shown in figure 21(*a*). They exploited the accidental near-coincidence between this line and the line at 454·5 nm from an argon ion laser. Resonance excitation was achieved by means of Doppler tuning using a small rotatable mirror mounted on the linear displacement mechanism which was normally used for foils. An angle of 23° was used in the experiment. The difference in wavelength of 0·9 nm between the excitation light and the fluorescence, viewed with a resolution of

0·6 nm in a direction perpendicular to the plane containing the ion and laser beams, ensured complete suppression of scattered excitation light. A peak signal strength of 13 kHz (photon counting rate) was observed with ion and laser beam intensities of 100 nA and 50 mW, respectively. The decay of intensity downstream of the excitation region was measured (see figure 21(*b*)) from which the lifetime was determined. Several such measurements yielded an average of $6{\cdot}21 \pm 0{\cdot}06$ ns for the lifetime of this state which agrees well with an earlier precision measurement by Gallagher (1967). The uncertainty was mainly due to uncertainties in the velocity of the ions which was measured by calibrating the accelerator voltage with several well known nuclear reactions. A direct calibration by means of a velocity analyser would, according to the authors, reduce the uncertainties considerably. They also point to high-power pulsed dye lasers with and without frequency doubling and to the preparation of ions in metastable states, using beam–gas excitation prior to laser excitation, as ways in which the applicability of the technique could be extended. Further, as the ion beam could be saturated with laser powers of approximately 1 kW, non-resonant higher states could be excited efficiently via an intermediate state with two lasers. In these ways hundreds of levels could usefully be studied with a precision as high as 0·1%.

Harde and Guthöhrlein (1974) reported a similar experiment in which they excited, by means of a dye laser, an ion beam which had previously been excited by means of a foil or gas cell. In this way they could measure decay curves with and without the selective laser re-population and eliminate cascades in the difference curve. The lower level from which laser radiation is absorbed need not be metastable, although it is generally easier to use long-lived lower levels. The advantage of using a foil for initial excitation lies in the large number of charge states and excited levels that can be generated. The principal disadvantage is the large angular scattering in the foil which leads to a large reduction in selectivity and in the number of ions that can be excited with a monochromatic laser beam. They reported measurements on the $6p\ ^2P_{3/2}$ state of Ba^+ and the $3p'\ [\frac{3}{2}]_2$ state of neon.

4.2.2. Spectral line blending. As already discussed in §4.1.3, the spectral resolution achievable in foil-excitation spectroscopy is limited by the angular scattering in the foil and linewidths of $\sim 0{\cdot}1$ nm in the visible are only rarely achieved. This, together with the large number of excited ionic species that are produced, make line blending possibly the most serious limitation of the beam–foil technique. The problem is less severe by more than an order of magnitude in beam–gas experiments at the expense of reduced time resolution and a more restricted range of charge states. No general methods of eliminating this systematic error exist. However, the methods used for charge-state analysis (§4.1.4) can give information about the degree of blending if spectral lines from different charge states are involved. Further, the methods of cascade reduction and elimination, especially those involving selective excitation, are also effective in reducing or eliminating blending errors.

4.2.3. Normalization of decay curves. In measuring decay curves in the foil-excitation technique, the intensities at the several positions downstream from the point of excitation have to be normalized to take account of variations in beam current and foil characteristics with time. The usual practice is to use the current collected in a Faraday cup as the common denominator, but this has several disadvantages. It is difficult to collect all the current, especially at low beam energies, without making the cup so large that it obstructs the view of the spectrometer. Moving the cup with the foil to

collect a constant fraction of the beam is equally difficult in practice. Another disadvantage is that the collected current is not an accurate indicator of the initial population of the level being studied because, as the foil ages, perhaps developing pinholes, the excited-state distributions and the scattering characteristics change. An alternative technique, which goes some way to overcoming these limitations, is to use a photomultiplier and filter or monochromator combination to monitor the intensity of a selected spectral line, preferably the line whose lifetime is being measured at a fixed distance from the foil. This method is not in common use, however. Neither method corrects for the changing collection efficiency of the spectrometer with distance from the point of excitation or with time as the foil characteristics change. These factors may or may not be important in any one measurement and a quality judgment is ultimately necessary when assessing the relative merits of different measurements (Bashkin 1974).

4.2.4. Methods of calibration. The time calibration of a decay curve requires a measurement of the mean velocity of the emitting ions. Direct measurements with a velocity analyser (e.g. Bickel *et al* 1969) or a time-of-flight technique (e.g. Schlectman *et al* 1970) are not common. Generally, the mean velocity is estimated from the known velocity of the primary ion beam and a correction for the energy lost in the foil. This calculated correction can be appreciably in error, especially for heavy ions at low energies (see Andersen 1973, for example). Also, the correction requires a knowledge of the thickness of the foil, which is difficult to measure accurately. The change in foil thickness during an experiment can also have an appreciable effect on the mean energy loss. Bickel and Buchta (1974), for example, reported a decrease in the mean velocity of 1·8% in one hour with a Li II beam of 80 keV primary energy and a carbon foil of initial thickness 9 $\mu g\ cm^{-2}$.

4.2.5. Other systematic errors. Other systematic errors, which have been discussed in the literature and which may sometimes be important, include effects due to the non-isotropic nature of the beam (Dufay 1973), contamination of the ion beam and changes in the decay curves as the beam current is increased (Oona and Bickel 1970). Andersen *et al* (1970) also pointed out that a systematic shortening of measured lifetimes could occur if the primary ion beam was focused in the vicinity of the foil.

4.3. Some recent measurements

Foil-excitation work has yielded an enormous amount of data on atomic and ionic spectra, energy levels and lifetimes. The accuracy of the measured lifetimes has often tended to be poor, however, and the data have been shown to be systematically too large when compared with reliable data (Wiese 1970). This is usually attributed to cascading although other systematic errors can have the same effect. Indeed, cascading has often been invoked as the ubiquitous systematic error to explain all deviations of a decay curve from exponentiality, even in cases where it is most unlikely to be significant. The repeatability has also been shown to be poor in many cases with large discrepancies between data from different research groups, from the same research group at different times and even between data measured with different transitions from the same upper state. The assessment of the relative merits of several conflicting measurements is often made difficult by a lack of critical discussion and experimental detail in many published papers. However, the greater attention paid to reducing systematic errors

and to the more careful analysis of the primary data has led to an improvement in the consistency of recent data. This is particularly to be welcomed as the foil-excitation method is often the only one that can be used in several fields of great interest.

One such field is the exploration of systematic trends in oscillator strengths (see Smith *et al* 1973, for example). Such trends tie many independently measured or calculated data together and help to establish a reliable framework of values. They are also of fundamental interest in atomic physics. Foil-excitation spectroscopy is uniquely suited to the exploration of such trends, especially along isoelectronic sequences,

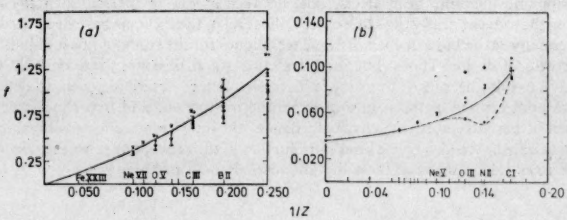

Figure 22. Oscillator strength variation with $1/Z$ along isoelectronic sequences. (*a*) The $2s^2\ {}^1S$–$2s2p\ {}^1P^o$ transition of the beryllium isoelectronic sequence. (*b*) The $2s^22p^2\ {}^1D$–$2s^22p3s\ {}^1P^o$ transition of the carbon isoelectronic sequence (from Smith *et al* (1973b), who give references to the original sources of the data).

because of the large number of charge states that can be studied. One well established trend is the Be $2s^2\ {}^1S$–$2s2p\ {}^1P^o$ isoelectronic sequence, which is shown in figure 22(*a*). From perturbation theory oscillator strengths, f, can be expressed as a power series in inverse powers of the nuclear charge Z:

$$f=f_0+f_1Z^{-1}+f_2Z^{-2}+\ldots.$$

In the limit as $Z\rightarrow\infty$, all terms but the first vanish and this is equal to the value calculated from a hydrogenic model. $f_0=0$, therefore, if there is no change in the principal quantum number as in the case illustrated above. Also noteworthy in such figures is that the theoretical points tend to lie above, while the beam–foil data lie below, the lines of best fit. It is, of course, not possible to pin down the relative magnitudes of the various systematic errors responsible for this, but cascading has usually been invoked as the chief experimental error while also recognizing that the theoretical values could be too large because of interference effects.

Another interesting sequence is the C $2p^2\ {}^1D$–$2p3s\ {}^1P^o$ because the upper state can mix with the $2p^3\ {}^1P^o$ state with a crossing of energy levels between N II and O III which could affect the regularity of the trend. The available data are shown in figure 22(*b*) where the scatter is too large, unfortunately, to establish a possible dip in the trend line.

There is also great astrophysical interest in lifetime data obtained from foil-excitation experiments because elemental abundances in stars are determined from known oscillator strengths of transitions observed in stellar spectra. Iron is of outstanding significance because there appears to be a strong local maximum in the abundance of elements in the immediate neighbourhood of iron. Several foil-excitation and other measurements of lifetimes in Fe I and Fe II have shown there to be errors

in the earlier oscillator strength values and the previously accepted value for the solar iron abundance has had to be increased by a factor of about 6 (see Smith (1973) and Bashkin (1974) for recent reviews).

5. Techniques using level crossing and double resonance

Various interference and resonance effects, such as the double-resonance, level-crossing and quantum beat effects, exist between atomic or molecular energy levels having the same or nearly the same energy. Several of these effects have been used very successfully as the basis of spectroscopic techniques for the study of fine and hyperfine structures of excited states, but in this section we shall concentrate on only those which have also been used to measure lifetimes. Before describing them in detail we give a brief résumé of the nature of hyperfine interactions and hyperfine structures since it is these structures which usually display the interference effects with which we are concerned. We also give a brief introduction to the concept of coherence since this plays a key role in many of these lifetime measurement techniques.

5.1. Résumé of hyperfine structures

As a specific example of hyperfine structure we consider the $7^2P_{3/2}$ level of the caesium atom (which we have chosen only for the diversity of level-crossing and double-resonance techniques which have been used and not for any intrinsic importance of the atom or the lifetime). The [Xe] 7p configuration is split by spin–orbit interactions into the fine-structure states $7^2P_{1/2}$ and $7^2P_{3/2}$, separated by 181 K (or $5{\cdot}43 \times 10^{12}$ Hz in frequency units) and both having a hyperfine structure. In the $7^2P_{3/2}$ state, for example, the atomic electrons (in particular the valence 7p electron) create at the nucleus an internal magnetic field and an electric field gradient $\partial^2 V/\partial z^2$. In the case of the stable isotope ^{133}Cs the nucleus has a spin quantum number $I=7/2$, and it possesses both a magnetic dipole moment and an electric quadrupole moment. The interaction energy between the magnetic dipole moment and the magnetic field depends on their relative orientations as $\boldsymbol{I.J}$, whereas the directional dependence of the electrostatic interaction between the quadrupole moment and the electric field gradient is more complicated (see below). According to the usual rule for vector addition of angular momenta, the total angular momentum $\boldsymbol{F}\,(=\boldsymbol{I}+\boldsymbol{J})$ can have the magnitudes 2, 3, 4 or 5, and since each of these hyperfine levels represents a different relative orientation of $\boldsymbol{I}$ and $\boldsymbol{J}$, each will have a different energy. The nucleus and atomic electrons can also interact with externally applied static magnetic or electric fields to cause a further splitting of the hyperfine levels F into their sublevels M_F.

The actual energies of the levels (F, M_F) in the external magnetic field $\boldsymbol{B}$ are determined by the Hamiltonian

$$H = H_{\mathrm{FS}} + a\boldsymbol{I.J} + b\,\frac{[3(\boldsymbol{I.J})^2 + \frac{3}{2}(\boldsymbol{I.J}) - \boldsymbol{I}^2.\boldsymbol{J}^2]}{2I(2I-1)J(2J-1)} + \mu_B g_J \boldsymbol{B.J} - \mu_N g_I \boldsymbol{B.I} + \ldots . \tag{5.1}$$

The first term contains the kinetic, potential and spin–orbit energies which determine the centre of gravity $W^{(\mathrm{FS})}$ of the fine-structure level (corresponding to the 455·5 nm wavelength of the $6^2S_{1/2}$–$7^2P_{3/2}$ transition). The second and third terms represent the

interactions of the nuclear magnetic dipole and electric quadrupole moments respectively with the internal fields. In the case of the ^{133}Cs isotope the constants a and b have the values $16{\cdot}610 \pm 0{\cdot}006$ MHz and $-0{\cdot}15 \pm 0{\cdot}03$ MHz respectively (Svanberg and Rydberg 1969), and the lower case letters a and b are used to indicate that the major part of the internal fields are caused by a single electron, namely the 7p valence electron, the inert core playing only a minor part. These first three terms of the Hamiltonian give the following energies, in frequency units, for the difference $W_F - W^{(FS)}$,

$$\begin{aligned}\Delta W_F &= -(27/4)a + (15/28)b = -112{\cdot}2 \text{ MHz for } F=2\\ &= -(15/4)a - (5/28)b = -62{\cdot}3 \text{ MHz for } F=3\\ &= (1/4)a - (13/28)b = 4{\cdot}2 \text{ MHz for } F=4\\ &= (21/4)a + (7/28)b = 87{\cdot}2 \text{ MHz for } F=5.\end{aligned} \tag{5.2}$$

These values are shown as the left-hand intercepts of figure 23.

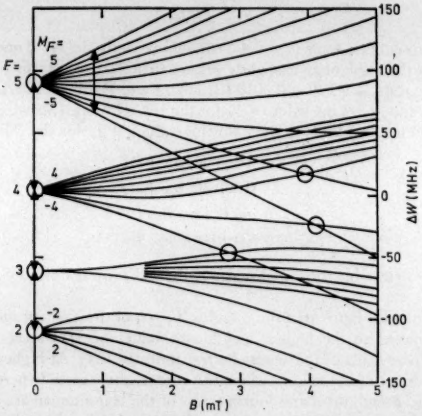

Figure 23. Hyperfine structure of the $7^2P_{3/2}$ state of the ^{133}Cs isotope of neutral caesium (after Svanberg and Rydberg 1969). The circles and arrows indicate the level-crossing, double-resonance and quantum beat effects which have been observed for this state (see text). The arrow at non-zero field represents 10 collinear arrows connecting the neighbouring sublevels of the $F=5$ level.

The fourth and fifth terms of equation (5.1) represent the interactions between the external field $\boldsymbol{B}$ and the magnetic dipole moments of the electron distribution and the nucleus respectively, the fifth term being three orders of magnitude smaller than the fourth. The quantities g_J and g_I are gyromagnetic ratios (more properly called magnetogyric ratios, since they represent the ratio of magnetic moment, in units of μ_B or μ_N, to angular momentum, in units of $\hbar$). For weak magnetic fields, for which $g_J\mu_B B \ll a$ or b, these latter two terms introduce the additional energy

$$W_{F,M_F} = g_F \mu_B \boldsymbol{F}.\boldsymbol{B} = g_F \mu_B M_F B \tag{5.3}$$

where g_F is the gyromagnetic ratio for the atom as a whole. Since $\boldsymbol{I}$ and $\boldsymbol{J}$ precess about $\boldsymbol{F}$, whilst $\boldsymbol{F}$ itself precesses more slowly about $\boldsymbol{B}$, the magnetic moment $\boldsymbol{\mu}^{(F)}$ of the atom is given by

$$\boldsymbol{\mu}^{(F)} = \boldsymbol{\mu}^{(J)} \overline{\cos(\boldsymbol{J}, \boldsymbol{F})} + \boldsymbol{\mu}^{(I)} \overline{\cos(\boldsymbol{I}, \boldsymbol{F})}$$

which gives

$$g_F = g_J \frac{F(F+1)+J(J+1)-I(I+1)}{2F(F+1)} - g_I \frac{m_e}{M_p} \frac{F(F+1)+I(I+1)-J(J+1)}{2F(F+1)}. \quad (5.4)$$

In the L–S or Russell–Saunders coupling scheme, which is a good approximation for this state of Cs, the orbital and spin momenta $\boldsymbol{L}$ and $\boldsymbol{S}$ individually precess about $\boldsymbol{J}$ and the magnetic moment of the atomic electrons is

$$\boldsymbol{\mu}^{(J)} = \boldsymbol{\mu}^{(L)} \overline{\cos(\boldsymbol{L}, \boldsymbol{J})} + \boldsymbol{\mu}^{(S)} \overline{\cos(\boldsymbol{S}, \boldsymbol{J})}$$

giving

$$g_J = 1 + \frac{J(J+1)-L(L+1)+S(S+1)}{2J(J+1)} \quad (5.5)$$

which in the present case leads to $g_J = 4/3$ (or, more exactly, 1·3341 if one takes account of the fact that the value of g_S is slightly greater than 2). In fact, the measured value for this atomic state is $1{\cdot}3349 \pm 0{\cdot}0010$ (Svanberg and Rydberg 1969). The nuclear gyromagnetic ratio g_I has the value 0·737 for the ^{133}Cs isotope (Stroke *et al* 1957) and therefore equation (5.4) leads to the following values of g_F for the $7^2P_{3/2}$ state

$$\begin{aligned} g_F &= -0{\cdot}668\,05, \text{ for } F=2 \\ &= -0{\cdot}000\,40, \text{ for } F=3 \\ &= 0{\cdot}266\,66, \text{ for } F=4 \\ &= 0{\cdot}400\,19, \text{ for } F=5. \end{aligned} \quad (5.6)$$

These g factors determine the initial slopes of the $\Delta W_{F,M_F}$ against B curves shown in figure 23.

It is clear from the figure that the energies W_{F,M_F} of the Zeeman sublevels (except those corresponding to the highest and lowest values of M_F) cease to be linearly dependent on B at fields of the order of a few times 10^{-4} T. At higher fields, and in particular for values of the field at which the energy levels cross (where by definition $g_J\mu_B B \sim a$), the second, third and fourth terms of the Hamiltonian are of comparable importance. This causes changes in the coupling of orbital, spin and nuclear angular momenta and a mixing of the zero-field wavefunctions; the resulting energies of the various levels can then only be determined by solving the appropriate secular equations. The actual dependence on B in the intermediate field region is shown in figure 23. Note that the quantum number M_F remains a good quantum number (and is, in fact, the only one to do so) and that as a consequence Zeeman levels having the same value of M_F repel each other.

In the case of an atom having a nucleus of zero spin, such as ^{198}Hg, the second, third and fifth terms of the Hamiltonian shown in equation (5.1) are all identically zero. The energies W_{F,M_F} change therefore linearly with B for much higher fields until the region in which the Zeeman sublevels of different fine-structure levels begin to approach and cross each other. This linear dependence is shown in figure 24 for the 6^3P_1 level of the ^{198}Hg atom. The nearest fine-structure level (6^3P_0) is $5{\cdot}31 \times 10^{13}$ Hz (or 1770 K) away.

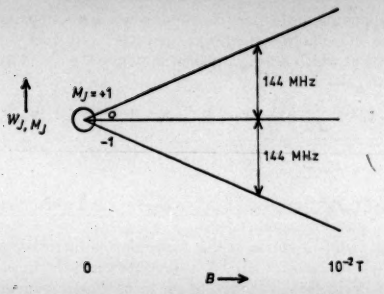

Figure 24. Splitting in a magnetic field of the fine-structure level 6^3P_1 of ^{198}Hg. The circle corresponds to a zero-field level-crossing (Hanle effect) experiment (see §5.4), and the arrows to a double-resonance experiment (see §5.8).

More complete and general accounts of fine and hyperfine structure can be found in textbooks such as those of Kuhn (1969) and Woodgate (1970) or review articles such as those of Series (1959), Budick (1967) or Kusch and Hughes (1969).

5.2. Coherence

The concept of coherence between atomic eigenstates will be mentioned frequently in the following sections and it is therefore convenient to give now a brief introduction to the topic.

It is sometimes possible to excite atoms into a definite or 'pure' eigenstate of a single Zeeman sublevel M_F. This might be achieved, for example, by irradiating with light having a frequency and polarization which will excite only one of a set of Zeeman sublevels, or by separating the sublevels with a magnetic field and using Doppler-free irradiation with narrow-band laser light. But not all excitation processes are as specific as this, either because the atomic levels are not well separated or because the exciting agent is not monoenergetic or not polarized, or for combinations of these reasons. In such cases the state of an atom at time t after the excitation event (assumed to take place at time $t=0$) is a superposition of all the accessible final states, namely (Franken 1961)

$$\Psi(t)=\sum_{\rho} f_{\rho m}\phi_{\rho}\exp\left(-i\omega_{\rho}t-\tfrac{1}{2}\gamma_{\rho}t\right) \tag{5.7}$$

where ρ represents the magnetic quantum number and any other quantum numbers necessary to specify the eigenstates ϕ_ρ of energy $\hbar\omega_\rho$ and decay constant γ_ρ, and where $f_{\rho m}$ is determined by the excitation process and is the amplitude for creating the state ρ from the initial state m (and therefore $|f_{\rho m}|^2$ is the probability of finding the atom in the state ρ). The state m of the target atom is included in this summation and for many processes one can assume that the exciting particle represents only a small perturbation to the target atom and that $|f_{mm}|^2 \approx 1$. We shall refer to the wavefunction $\Psi(t)$ as a 'superposition state'.

Suppose that the superposition state decays by photon emission with a range of wavelengths corresponding to the range of energies of the states ρ that exist in the superposition but that the detector of the emitted photons is sensitive only to a subset

of decays corresponding to the polarization direction $\boldsymbol{g}$ and to a range of wavelengths corresponding to emission from a set of excited states μ to a set of final states m. The instantaneous rate at which these particular photons are emitted by the excited atoms is proportional to

$$R(f, \boldsymbol{g}, t) = \sum_{m, m'} |\langle \phi_{m'} | \boldsymbol{g} \cdot \boldsymbol{r} | \sum_{\mu} f_{\mu m} \phi_{\mu} \exp [-(i\omega_{\mu} + \tfrac{1}{2}\gamma_{\mu})t] \rangle|^2$$

$$= \sum_{\substack{m, m' \\ \mu, \mu'}} f_{\mu m} f_{\mu' m}^{*} g_{m' \mu} g_{m' \mu'}^{*} \exp [-(i\omega_{\mu\mu'} + \bar{\gamma}_{\mu\mu'})t] \qquad (5.8)$$

where $g_{m'\mu} = \langle \phi_{m'} | \boldsymbol{g} \cdot \boldsymbol{r} | \phi_{\mu} \rangle$ etc, where $\omega_{\mu\mu'} = \omega_{\mu} - \omega_{\mu'}$ and where the summation is also over the range of possible target states m.

An important point to notice in this expression is the existence of terms which oscillate at the beat frequencies $\omega_{\mu\mu'}$. The detector can have, in principle, a response time T which is sufficiently short to respond to an oscillatory term $\omega_{\mu\mu'}$ since the detector bandwidth $\Delta\omega$ is at least $\omega_{\mu\mu'}$ and T and $\Delta\omega$ are related in general by $T\Delta\omega \sim 2\pi$. Therefore, if many atoms are excited at the same time one might be able to observe the beat frequency $\omega_{\mu\mu'}$ but only if all the excited atoms have the same value of the product $f_{\mu m} f_{\mu' m}^{*}$, or less restrictively, if the mean value of this product over all the atoms is not zero (or in other words the density matrix ρ (see appendix 2) must have a non-zero value of the off-diagonal element $\rho_{\mu\mu'}$). If this condition is satisfied the states μ and μ' are said to be excited coherently.

Note that every excitation event produces a non-zero value of $f_{\mu m} f_{\mu' m}^{*}$ if the excitation source is sufficiently broad-band to excite both the states μ and μ'. In this sense every superposition state is internally coherent, although a single detection event can give only limited information about $f_{\mu m}$ and $f_{\mu' m}$. The observation of many events is required before the presence or absence of a *consistent* coherence between these two amplitudes can be established. Note also that the time average of $\overline{R(f, \boldsymbol{g}, t)}$ contains interference terms which are non-zero if some of the mean products $\overline{f_{\mu m} f_{\mu' m}^{*}}$ are non-zero and that coherence can therefore also be established by time-averaging experiments.

Let us consider two examples, the first of which is the excitation by photon absorption of the three Zeeman sublevels shown in figure 24. Suppose that there is a magnetic field $\boldsymbol{B}$ in the same direction z as the incident light and take this direction to be the axis of quantization. A pulse of light plane polarized in the y direction will excite the two levels $M_J = \pm 1$: this can be seen by noting that the matrix elements $\langle M | y | 0 \rangle$ are non-zero for $M = \pm 1$ (see, for example, Condon and Shortley (1963) or appendix 2) or in a classical sense by noting that a linearly polarized field can be decomposed into two circularly polarized components of opposite angular momenta, corresponding to σ_+ and σ_- photons which are able to excite the $M = +1$ and -1 levels respectively. This is illustrated in figure 25. We must also assume that the exciting light contains a range $\Delta\nu_e$ of frequencies that is sufficiently broad to cover the difference $\Delta\nu$ in the frequencies of the levels $M_J = \pm 1$. This will be satisfied, for example, if the atoms of the exciting source have lifetimes shorter than $(\Delta\nu)^{-1}$ or if the incident light consists of pulses of length less than about $(\Delta\nu)^{-1}$.

The two levels $M_J = \pm 1$ start with a definite relative phase but with different energies and frequencies, so that the re-synthesis of the circular motions results in a linear oscillator which rotates at the difference frequency. This would give an oscillating intensity distribution of the emitted photons in any particular direction, an effect which is a direct consequence of the definite initial phase, and hence coherence, of the

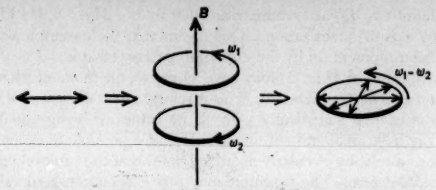

Figure 25. A plane-polarized field acting on an atom can be decomposed into two circularly polarized fields (σ_+ and σ_-) having opposite senses of rotation. If these develop with different frequencies within the atom they will recombine at time t to give emitted light having a direction of polarization which has rotated through the angle $(\omega_1-\omega_2)t$.

two sublevels. Suppose on the other hand that the incident light is unpolarized so that it can be regarded as containing linearly polarized photons with random directions of polarization. Then the excited atoms would have different relative initial phases for the sublevels $M_J=\pm 1$ and the amplitude of the oscillatory term would average out to zero. Alternatively the unpolarized light can be regarded as containing circularly polarized photons of both senses of direction, each type exciting one sublevel only and therefore precluding any interference between the sublevels within any one atom. This excitation process is clearly incoherent.

An important point for some of the level-crossing techniques to be discussed below is that an excitation process which is incoherent for one axis of quantization may be coherent for a different axis. This is illustrated by our second example which is the electron-impact excitation of atoms. If the beam axis is taken as the axis of quantization and if the beam is unpolarized then, as with unpolarized photon absorption, the excited-state sublevels M_J will be excited incoherently. Interference between them would not be observed even if their energies were separated by a magnetic field in the beam direction. The populations $a(M_J)$ $(=|f|^2$, see equation (5.7)) of the excited levels M_J are unequal, however, but always with $a(-M_J)=a(M_J)$ and usually with the smallest M_J values being most populated (see, for example, Mott and Massey 1965). Now consider one of these states, say $M_J=0$, which, in a classical sense, has an angular momentum that can be represented as a vector of length $\hbar[J(J+1)]^{1/2}$ lying anywhere in a plane perpendicular to the beam axis. With respect to an axis of quantization at right angles to the beam axis this state therefore has an angular momentum projection M_J' which can take all values from $+J$ to $-J$. More exactly, the transformation of the wavefunction $\phi(M_J)$ involves the rotation matrices $\mathscr{D}^J_{M'M}$ (see, for example, Edmonds (1957) or appendix 2) and although in fact all values of M_J' may not exist in the new frame it is clear that those that do exist are excited coherently. This means that a magnetic field at right angles to the beam axis can result in the possibility of the observation of oscillatory interference terms.

Coherences between Zeeman sublevels can also lead to variations in time-integrated intensities, as discussed below. Also the possibility of coherence is not confined to Zeeman sublevels and other examples are given in §5.9. A more general and rigorous treatment is given in appendix 2.

Two other terms which can be conveniently introduced here are those of 'alignment' and 'orientation'. In the electron-impact example just quoted, the excited-state

sublevel populations $a(M_J)$ are symmetrical (that is, $a(-M_J)=a(M_J)$) but otherwise unequal for any axis of quantization. This means that the ensemble of atoms is not given a net angular momentum by the excitation process (that is, $\langle \boldsymbol{J} \rangle = 0$) but that the population distribution of M levels may have a quadrupole moment (that is, $\langle M_J^2 \rangle \neq \frac{1}{3}\langle \boldsymbol{J}^2 \rangle$ for certain axes of quantization). This is referred to as *alignment* of the sublevels. A state which is excited statistically with all its sublevels being equally populated would necessarily have an alignment of zero. It is also possible to excite the atoms in such a way (for example, by circularly polarized light) that the sublevel populations are not symmetric about zero. The ensemble may then have a non-zero value of the net angular momentum $\langle \boldsymbol{J} \rangle$, which condition is referred to as *orientation* of the sublevels. In terms of statistical tensors (see appendix 2) orientation and alignment exist if the density tensors of rank 1 and 2 respectively have non-zero components.

5.3. Level-crossing methods

It will be noticed that certain crossing points in figures 23 and 24 are marked by circles and that some levels are connected by arrows. The arrows show the places at which double-resonance experiments have been used to determine the lifetimes of these atomic states and these are discussed in §5.8. The circles indicate the level-crossing experiments discussed in this subsection and §§5.4–5.6.

Since the lifetimes of excited atomic states are not infinite, each of the lines of figures 23 and 24 should be drawn as a fuzzy band, as shown schematically in figure 26, to indicate the uncertainty in energy. For example, the lifetime τ of the $7^2P_{3/2}$ state of caesium is known to be approximately 135 ns (see below) and therefore its energy uncertainty, when expressed as the full width at half-maximum of the corresponding

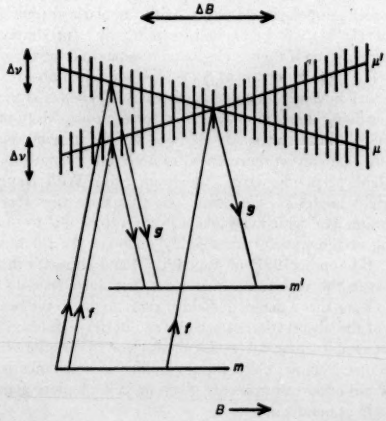

Figure 26. Schematic representation of the two routes $m \rightarrow \mu \rightarrow m'$ and $m \rightarrow \mu' \rightarrow m'$, showing the range of field B over which interference can occur between these routes.

frequency band, is

$$\Delta\nu = 1/2\pi\tau \tag{5.9}$$

which has the value 1·18 MHz (or 2·4% of the spacing between the $F=2$ and $F=3$ states). The crossings which occur between levels when the external magnetic field is varied are therefore not sharp and the crossing point is distributed over a region of field. In the simplest case involving the crossing of two levels only (such as the rightmost three circled crossings of figure 23), the width of this region is

$$\Delta B \sim \Delta\nu(\partial\nu/\partial B)^{-1} \tag{5.10}$$

where $\partial\nu/\partial B$ is the rate of change with B of the level spacing between the two levels. If the crossing of such levels produces observable changes in the yields of detected particles or photons, then these changes will take place over the range ΔB and measurements of this range can then lead to a determination of τ.

The energies of emitted or absorbed photons also have an additional width caused by the Doppler effect. In the case of caesium this amounts, at room temperature, to about 700 MHz, which is greater than the whole vertical range shown in the figure. This does not affect the level-crossing experiments, however, because it is only the *difference* in Doppler shift between two levels of the same atom which is important. Since this difference is proportional to the difference in energy of the levels, it is negligible compared with their natural widths. The Doppler shift is also negligible in the double-resonance experiments, which we shall be discussing later, since it is also proportional to the energy differences. It is in fact less than 1 kHz for the transitions shown in the figure.

The changes in observable yields at the crossing points are clearly those arising from interference effects between superposed levels. Suppose that only two states μ and μ' are excited, as indicated in figure 26, and that these are excited by photon absorption from the state m and are observed to decay by photon emission to the state m'. These labels refer to all the quantum numbers of their respective states, although as we shall see below it is primarily the magnetic quantum numbers which determine interference effects. In most of the examples discussed, the levels m and m' both belong to the ground state and the absorbed and emitted photons have essentially the same wavelength; the process is then usually referred to as resonance scattering or resonance fluorescence.

If the states μ and μ' are well separated in energy, and if a time-integrated intensity is observed, then those terms in equation (5.8) for which $\mu \neq \mu'$ will have a rapidly oscillating time behaviour which averages to zero, giving an observed rate

$$R(f,g) \propto |f_{\mu m} g_{m'\mu}|^2 + |f_{\mu' m} g_{m'\mu'}|^2. \tag{5.11}$$

If, on the other hand, the levels μ and μ' overlap completely the observed rate is

$$R(f,g) \propto |f_{\mu m} g_{m'\mu} + f_{\mu' m} g_{m'\mu'}|^2. \tag{5.12}$$

Equations (5.11) and (5.12) are, in fact, particular limits of the general expression

$$R(f,g) \propto \sum_{\substack{mm' \\ \mu\mu'}} \frac{f_{\mu m} f_{\mu' m}^* g_{m'\mu'}^* g_{m'\mu}}{1 + i(E_\mu - E_{\mu'})\Gamma^{-1}} \tag{5.13}$$

which was first derived by Breit (1933) and later re-derived by Franken (1961) and Rose and Carovillano (1961), following the level-crossing observations of Colegrove

et al (1959). An incorrect sign in the expression derived by Franken has been pointed out by Stroke *et al* (1968). In equation (5.13) the quantity $\Gamma (= \hbar/\tau)$ is the width of the excited state and the summation over the unobserved states m and m' of the initial and final states has been included. It can be seen that two levels will interfere as long as their width is comparable to their separation, as supposed in the discussion above.

The extra cross terms which are present in equations (5.12) and (5.13) but absent in equation (5.11) are responsible for the differences which may occur in the observed yield at particular scattering angles. The total yield integrated over all angles is unaffected, however, and the interference effects change only the angular distribution of the fluorescence radiation (for a particular example see Feld *et al* (1974)). The cross terms are present only when the two routes $m \rightarrow \mu \rightarrow m'$ and $m \rightarrow \mu' \rightarrow m'$ are both allowed by the relevant selection rules, the excitation and detection processes, and the experimental disposition of polarizers etc, and one may therefore say that level-crossing interference can be observed only when both routes are able to 'share' the same photons. A loose analogy exists with the Young's double-slit interference experiment in which the interference changes the distribution of light without changing the integrated intensity and for which the interference pattern exists only when the two slits are able to share the same photons, which requires that the light illuminating the slits be partially or wholly coherent across them (that is, that the slits be near together and the light source be small).

Equation (5.13) applies to excitation by broad-band or 'white' light. If the excitation is by light having a power spectrum $\rho(\omega)$ and the target atoms have velocities V_x in the direction of the incident light with a probability distribution $n(V_x)$, then each term of equation (5.13) must be multiplied by the factor (Gallagher and Lurio 1964, Norton and Gallagher 1971)

$$I(m, \mu, \mu') = \int \mathrm{d}V_x \, \mathrm{d}\omega \, n(V_x) \rho \left(\omega - \frac{\omega V_x}{c} \right) \times \left(\frac{1}{\hbar\omega - (E_\mu - E_m) + \frac{1}{2}\mathrm{i}\Gamma} - \frac{1}{\hbar\omega - (E_{\mu'} - E_m) - \frac{1}{2}\mathrm{i}\Gamma} \right). \quad (5.14)$$

5.4. The Hanle effect for atoms

The first published observations of level-crossing interference effects were made by Wood and Ellett (1923) who studied the polarization of the resonance fluorescence of the mercury 253·7 nm line. This fluorescence was already known to be polarized but Wood and Ellett established that the degree of polarization was neither large nor reproducible unless the combined magnetic field due to the Earth and laboratory sources was made zero. They found that small external fields (less than about 10^{-4} T) caused depolarization of the resonance fluorescence and measured the dependence of the degree of depolarization on the magnitude of the field for a particular relative orientation of the field, the line of observation and the direction and polarization of the incident light. They also measured the variation of the direction of fluorescence polarization as a function of these relative orientations, but for a fixed and larger magnitude of the magnetic field. These latter results were explained (Hanle 1923, Breit 1924, Pringsheim 1924) in terms of a classical (non-interfering) Zeeman effect, and although this was relevant to the development of Hanle's ideas it did not explain the depolarization results. These were later explained (Hanle 1924, Eldrige 1924) in terms of a classical precessional motion of the electron orbits of the excited atom. To

test this Hanle (1924) looked at the rotation of the plane of polarization as a function of the magnitude of the magnetic field and also made other measurements but without presenting new depolarization data. Hanle then went on to suggest (Hanle 1925) that these various experimental observations could be interpreted as an interference between overlapping Zeeman levels of the same atom.

We shall see that this depolarization is indeed caused by level-crossing interference and that its extent is directly related to the magnitude of the magnetic field and to the product $g\tau$ of the excited state. This fact has led to the measurement of many atomic and molecular lifetimes through the study of magnetic depolarization. The observed effect might properly be called the Wood–Ellett–Hanle effect, but we shall adopt the customary usage and refer to it more simply as the Hanle effect, or in some

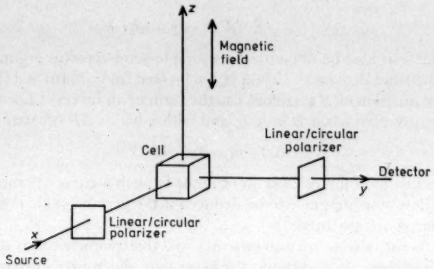

Figure 27. Geometrical arrangement for a Hanle effect experiment.

circumstances as the zero-field level-crossing effect. Previous reviews of the Hanle effect and of the associated high-field level-crossing effects discussed in §5.7 have been given by Mitchell and Zemansky (1934), Pringsheim (1949), Series (1959), Feofilov (1961), Budick (1967), de Zafra and Kirk (1967), Corney (1969), zu Putlitz (1969), Bucka (1969), Kastler (1973), Zare (1974) and Kalitejewski and Tschaika (1975), and in some cases these reviews also contain compilations of lifetimes obtained by these techniques. We first consider the Hanle effect as applied to atoms, then to molecules, and finally consider the experimental methods and systematic measurement errors in these applications.

Figure 27 shows a frequently used geometrical arrangement for a Hanle effect experiment. The polarizers are not always necessary and other orientations of the magnetic field are sometimes used, but the directions defined by the source and detector are usually at right angles to each other.

A simple transition to consider is that originally studied by Hanle, in which the mercury atom is excited from the ground state having $J=0$ to a state having $J=1$, and in which the predominant nuclear spin I (namely that of the ^{198}Hg isotope) is zero. Figure 24 shows the energy dependences of the Zeeman sublevels of this excited state and the circled crossing point represents the Hanle interference experiment. Suppose that the light and field directions are as shown in figure 27 and that the incident light is polarized in the x–y plane. The scattered light is then also polarized in the same plane and it can be shown that for this configuration and transition (see, for example, Condon and Shortley (1963) or appendix 2), the only non-zero matrix elements $f_{\mu m}$ and $g_{m'\mu}$

(where m and m' are both zero) are those having $\mu = \pm 1$, and that

$$f_{+1,0} = f_{-1,0} = i\langle r \rangle$$

and (5.15)

$$g_{0,+1} = -g_{0,-1} = \langle r \rangle.$$

$\langle r \rangle$ is real and is proportional to a reduced matrix element and the direction of quantization is that of the magnetic field. It is clear from these relationships and from equations (5.11) and (5.12) that the intensity of the resonantly scattered light is zero at the crossing point but is finite when the sublevels are well separated in energy. The more general equation (5.12) gives the field dependence

$$R \propto 1 - 1/(1 + \epsilon^2) \tag{5.16}$$

where

$$\epsilon = (E_{+1} - E_{-1})\Gamma^{-1} = 2g_J \mu_B B\tau/\hbar. \tag{5.17}$$

These equations can also be obtained by a simple semi-classical argument (see, for example, Mitchell and Zemansky 1934). It can be seen from (5.16) and (5.17) that the intensity R as a function of B therefore has the form of an inverted Lorentzian curve, with a minimum of zero when B is zero, and with a width ΔB (FWHM) given by

$$\Delta B = \hbar(\mu_B g_J \tau)^{-1}. \tag{5.18}$$

The bottom spectrum of figure 28 is an example of such a curve. A measurement of ΔB therefore allows the lifetime τ to be deduced if the gyromagnetic ratio of the state has been measured or calculated.

Hanle interference effects can also be seen with other geometrical arrangements and polarization directions. For example, suppose that the source, detector and field directions are as defined in figure 27 but that the incident light is unpolarized. This light may be resolved into two orthogonal plane-polarized components: the component polarized parallel to the y axis causes the changes $\Delta m = \pm 1$ and produces an inverted

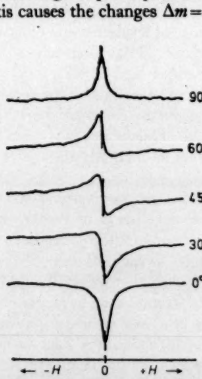

Figure 28. Hanle effect curves obtained with mercury resonance radiation, with the magnetic field directed along the x axis of figure 27. The indicated angles are those between the y axis and the direction of polarization of the incident light (from de Zafra and Kirk 1967).

Lorentzian curve, as found above, but the component parallel to the z axis produces a change $\Delta m = 0$, thus populating only one sublevel of the excited state for each initial sublevel, and this therefore gives a constant contribution to the detected light. The Hanle interference is therefore still present superimposed on a (generally undesirable) background.

The magnetic field need not have the direction shown in figure 27 and frequently it is oriented along the x direction of the incident light. If the light is linearly polarized in the y direction an inverted Lorentzian curve is again obtained, but if it is polarized in the z direction the detected light will be a maximum at zero field and the Hanle signal consists of a normal Lorentzian curve superimposed on a constant background. With an unpolarized incident beam these y and z components would add together to give a constant signal (as noted in §5.2), so with this orientation of the magnetic field a polarized incident beam is essential.

If the incident light is polarized in a direction between the y and z axes the Hanle signal has a dispersion shape or is a mixture of dispersion and Lorentzian shapes: some of these curves are shown in figure 28. The fact that only this range of shapes can be present in the Hanle signal of a single state follows directly from the form of equation (5.13), which gives

$$R \propto \alpha + \frac{\mathrm{Re}\,(\beta)}{1+\epsilon^2} + \frac{\epsilon\,\mathrm{Im}\,(\beta)}{1+\epsilon^2} \tag{5.19}$$

where the quantities α and β are independent of ϵ and α is real (and both α and β are proportional to sums of products of matrix elements f and g).

Circularly and elliptically polarized incident light may also be used in Hanle effect experiments. For example, suppose that the source, detector and field directions are again defined as in figure 27 and that the incident light is circularly polarized, then if the detector responds to only one sense of rotation of circular polarization or if it measures the difference between the intensities of the two senses, a dispersion curve such as the middle curve of figure 28 would be obtained. The essential difference between the use of linearly and circularly polarized incident light is that the former produces alignment and the latter produces orientation of the excited atoms (see §5.2). Both of these undergo precession in a magnetic field and so both produce a Hanle effect. The use of circularly polarized light would usually be an unnecessary complication except for states having $J = \frac{1}{2}$ for which it is essential (Gallagher and Lurio 1963) since these states can be oriented but not aligned. It is also essential in the study of the transfer of orientation coherence (see §5.6.1 below).

The dependence of the detected yield on the magnetic field becomes more complicated when the atom being studied has a nucleus of non-zero spin since what is then observed is a superposition of the different curves due to each of the hyperfine levels. As an example, consider the state described in §5.1 above, namely the $7^2P_{3/2}$ state of the ^{133}Cs atom. This state has four hyperfine levels and therefore four multiple crossing points exist at zero magnetic field, represented in figure 23 by the circles on the left-hand axis. Each of these crossings points has a width which depends on the gyromagnetic ratio g_F of the hyperfine level (given by equation (5.6)) and the lifetime τ, assumed to be the same for all the hyperfine levels. The width for the $F = 3$ crossing point is large, for example, since its value of g_F is very small (being determined only by the gyromagnetic ratio of the nucleus) and therefore this level contributes a broad background. The relative weights of the four contributions are determined by the statistical weights of the exciting and de-exciting transitions and that of the $F = 5$ level

is dominant. This particular Hanle effect curve has been measured by Markova *et al* (1967) and from it they were able to deduce the value $121 \pm 1{\cdot}5$ ns for the lifetime of the state.

5.4.1. Production of initial coherence for Hanle effect measurements. An essential requirement for the existence of the Hanle effect is the coherent excitation of two or more levels which cross in energy at a zero magnetic field, and in the experiments which we have described so far this coherence is produced by the absorption of suitably polarized light having the same wavelength as the detected light. Amongst other ways of producing the initial coherence are (i) stepwise excitation, (ii) electron or ion impact, (iii) foil excitation and (iv) transfer of coherence from atoms of a different species. We describe these briefly in turn.

5.4.2. Production of coherence by stepwise excitation. In the case of some excited states there are technical difficulties in exciting them by photon absorption from the ground state or the electric dipole selection rules do not allow such an absorption. It may then be more convenient to form them by photon absorption from an intermediate excited state. These intermediate states might be formed either by electron or ion impact on the ground-state atoms or by photon absorption from the ground state, but in either case the Hanle effect signal will be weak unless they are sufficiently long-lived or metastable to allow a high enough density of them to be built up. In an early experiment of this type Williams and Fry (1968) excited a beam of 2^1S metastable helium atoms by electron impact: a microwave helium discharge lamp producing light of wavelength 2·0587 μm from the 2^1S–2^1P transition in helium was used to irradiate the

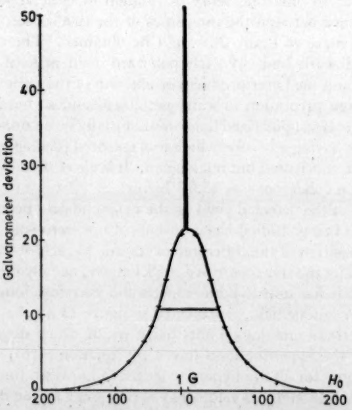

Figure 29. Hanle signal for the 6^3S_1 level of Cd excited from the metastable 5^3P_1 level (see text). A narrow spike due to the depolarization of the 5^3P_1 level is superimposed on the broader Lorentzian curve of the 6^3S_1 level (from Laniepce 1968).

beam, thus exciting some of the metastable atoms to the 2^1P state. The 1^1S–2^1P decay photons, of wavelength 58·4 nm, were detected by a channel electron multiplier, the directions of the source, detector and field being as defined in figure 27. In this way an inverted Lorentzian curve was obtained from which the lifetime of the 2^1P state could be deduced. Laniepce (1968), on the other hand, excited the intermediate metastable states, in this case the 5^3P_1 state of Cd, by photon absorption from the ground state, the excited state of interest (6^3S_1) being formed by the subsequent absorption of a photon of the relevant wavelength. The intermediate and final states both exhibit Hanle magnetic depolarization, but it can be seen from figure 29 that the very different lifetimes of the two states causes the two effects to be easily separable.

In another variation of this method (see, for example, Chang *et al* (1971) or Tai *et al* (1975)) the state of interest (b) is formed by an unobserved decay from a higher lying state (e), which in turn is created by absorption of polarized light by the ground state. Some of the coherence in the state (e) is transferred to (b) and therefore magnetic depolarization of the fluorescence from (b) can be observed. In this way Tai *et al* (1975) were able to measure the lifetimes of the $5D_{3/2}$ state of ^{87}Rb and the $6D_{3/2}$ state of ^{133}Cs.

5.4.3. Production of coherence by electron or ion impact. Alternatively the Zeeman sublevels can be excited coherently by electron or ion impact (or even by impact with fast neutral atoms or molecules, see §5.4.4). As discussed in §5.2 and appendix 2, the coherence of the sublevels M defined with respect to an axis of quantization at right angles to the beam is the result of an unequal population of the sublevels M with respect to an axis of quantization along the beam. The excited-state atoms are then aligned and the emitted light is partially linearly polarized either parallel or perpendicular to the beam direction (Mott and Massey 1965). The mechanisms by which the population inequalities are produced depend on the type and energy of the bombarding particles. For example, in the case of near-threshold electron-impact excitation, the incident beam carries no angular momentum about its own axis and therefore has $m=0$ and the slowly moving outgoing electron can carry away very little angular momentum (at least in the absence of special mechanisms such as resonant excitation) and therefore it also has $m=0$. This means that the change ΔM of the target atom is zero, which can cause a non-uniform population of the excited-state sublevels. In the opposite case of very fast incident electrons or ions one can regard the excitation as being caused by the virtual photons that are present in the time-varying field of the incident particles: these photons have various multipolarities and polarizations and can again cause a non-uniform population of the sublevels.

Whatever the mechanism for the production of the initial alignment coherence, the intensity and polarization of the emitted light cannot be altered by a magnetic field along the beam axis since this is an axis of cylindrical symmetry for the system and precessions about the field can have no effect (see also the discussion of §5.2). To observe depolarization effects with this direction of field it would be necessary to spoil the cylindrical symmetry by using a polarized particle beam or by observing the decay photons in coincidence with particles scattered in particular directions. The more usual solution is to have the magnetic field at right angles to the beam direction, although this can cause some difficulties in the use of slow electron beams because their direction is altered by the field.

This technique was first used by Faure *et al* (1963) who measured the lifetimes of various levels of helium by slow electron impact. One advantage of the method is that

charged-particle excitation is not restricted by the parity spin and angular momentum selection rules which apply to photon excitation and therefore a much wider range of excited states is accessible for study.

Charged-particle excitation, and also foil excitation (discussed in the next section), can result in the excitation of states lying above the state of interest and this therefore gives rise to the possibility of cascading from the higher states. The widths of Hanle signals then depend on the relative populations and lifetimes of all the participating levels which must be taken into account if reliable lifetimes are to be deduced from the measured widths (Wangsness 1971).

5.4.4. Production of coherence by foil excitation. Foil excitation (which is discussed more fully in §4) provides yet another way of creating coherence between excited-state sublevels. It is directly analogous to excitation by electron or ion impact, the essential difference being that in foil excitation the atoms under study are moving while the exciting agent (that is, the foil) is at rest. The excited atoms are again aligned with respect to the beam direction and the emitted light may be partially polarized parallel or perpendicular to this direction. If there is cylindrical symmetry about the beam (that is, if the plane of the foil is perpendicular to the beam and the incident atoms are not spin-polarized) then for the reasons discussed previously changes of polarization can be observed only if the magnetic field is not parallel to this direction. In the first experiment of this type Liu *et al* (1971) passed Ne^+ ions of energy 425 keV through a thin carbon foil and observed the polarization of the 640·2 nm photons ($2p_9 \rightarrow 1s_5$) from Ne I and the 422·0 nm photons ($4f\ ^4D^o \rightarrow 3d\ ^4D$) from Ne II as a function of the magnitude of a magnetic field at right angles to the axis. The excited atoms or ions passed through the field of view of their spectrometer in a time of the order of one lifetime instead of the infinite time assumed in deriving the usual Hanle response (as in equation (5.18) for example), but they were still easily able to deduce the lifetimes from the measured response functions.

When the foil is tilted (that is, when it is not perpendicular to the beam direction), the emerging atoms may be oriented (see appendix 2) as well as aligned. The emitted light may then be partially circularly polarized as well as partially linearly polarized, the direction of maximum polarization not necessarily being parallel or perpendicular to the beam or foil axes. These effects were first observed by Berry *et al* (1974) in the excitation by a carbon foil of the $2s\ ^1S$–$3p\ ^1P$ transition in ^{4}He I. Their measured polarization fractions were expressed in terms of the succinct Stokes parameters although descriptions in terms of alignment and orientation parameters or in terms of density matrix elements would be equally valid (see appendix 2). In physical terms, they found that the direction of maximum linear polarization was always between the beam direction $\boldsymbol{z}$ and the direction $\boldsymbol{n}$ of the normal to the foil and that the circular polarization was in the direction $\boldsymbol{n} \wedge \boldsymbol{z}$ as though the emerging atoms were 'rolling' off the surface of the foil. This was partially explained by Eck (1974) in terms of an electrostatic interaction between each beam particle and the tilted foil as a whole, but the subject is still developing quickly both experimentally (Church *et al* 1974, Liu *et al* 1974, Berry *et al* 1975) and theoretically (Lewis and Silver 1975, Herman 1975). Although tilted foils have not yet been used in lifetime measurements it is clear that the different forms of coherence which they produce, and in particular the creation of orientation as well as alignment, can be useful in certain cases such as the measurement of the lifetime of states having $J = \frac{1}{2}$.

5.4.5. Production of coherence by collisional transfer from atoms of a different species. The process termed 'sensitized fluorescence' occurs when a mixture of atoms A and B is irradiated with resonant light for the atoms A and when subsequent collisions of the second kind (that is, $A^* + B \rightarrow A + B^*$) lead to excited atoms B^* and hence to the emission of fluorescent radiation by these atoms. The early work in this field has been reviewed by Mitchell and Zemansky (1934). Gough (1967) studied the fluorescence from the 5^3P_1 level of cadmium atoms when a mixture of cadmium and mercury vapours was illuminated by light which excited the 6^3P_1 level of mercury and he found that if this incident light is linearly polarized then so is the sensitized cadmium fluorescence. He also found that the degree of polarization varies with magnetic field, the form of the variation being that of the Hanle effect, as though the cadmium fluorescence had been excited by polarized cadmium light.

One of the selection rules for collisions of the second kind is that ΣM_J is conserved along the collision axis in the system of the two colliding atoms (Franzen 1959). There is no such conservation rule for axes at right angles to the collision axis and it therefore follows that if the collision axis is taken as the axis of quantization the final populations of the states M_J are fully determined by the initial populations and the details of the collision, but any coherence between these M_J states is completely destroyed (that is, the diagonal elements of the density matrix are determined by the collision but the off-diagonal elements are all made zero). Series (1967) pointed out, however, that Gough's observations show nevertheless that coherence is transferred in collisions of the second kind between different atomic species and Chéron and Barrat (1968) substantiated this theoretically using a statistical tensor (see appendix 2) approach. The reason for the transfer of coherence can be most easily understood for the case in which the initial atoms A^* are oriented in such a way that they have a net mean angular momentum in some direction x since some memory of this orientation will be retained in all collisions for which the collision axis is not at right angles to x, the transfer efficiency being greatest when the collision axis is in the direction x. On averaging over all directions of the collision axis the atoms B^* therefore possess some orientation along the direction x. In the case of Gough's sensitized fluorescence experiments the mercury atoms are initially aligned rather than oriented, but this latter type of coherence is also partially transferred by the collisions.

Other types of inelastic collisions can also be used to transfer coherence between atoms of different species. For example, Schearer (1969) used Penning ionization collisions (that is, $A^* + B \rightarrow A + B^{+*} + e$) to transfer orientation coherence from optically pumped metastable (2^3S) helium atoms to excited states ($^2D_{5/2}$ and $^2P_{3/2}$) of Cd^+. The obvious difficulty in using this technique to measure ionic lifetimes is that the magnetic field causes precessions of both the ions B^{+*} and the initially excited atoms A^*. Hamel *et al* (1974) have, however, been able to measure the lifetimes of the $(4d^95s^2)$ $^2D_{3/2}$ and $^2D_{5/2}$ levels of Cd^+ by modulating the 2^3S He levels with a radio-frequency field and observing the variation with frequency of the amplitude of modulation of the resulting polarized cadmium light. This and other methods of creating coherence by collisional transfer will probably not be widely used in lifetime measurements, although there may be particular cases for which they are the most convenient.

5.5. The Hanle effect for molecules

Observations of the Hanle effect in molecules have usually been made using incident polarized light derived from either (i) atomic emission lines or laser lines

which are coincident with the molecular absorption line, or (ii) the emission spectra of the same molecular species. Other possible methods of producing the initial alignment or coherence, such as electron impact or excitation in discharge tubes (see, for example, Van der Linde and Dalby 1972), have been used infrequently. Before describing the techniques it will be useful to start by considering what is known about the gyromagnetic ratios of rotational states of simple molecules.

The internal electronic magnetic moment $\boldsymbol{\mu}$ of a molecule is of the same order of magnitude as for atoms, being dependent in both cases on the spin and angular momentum of the valence electrons and on the way in which these electrons couple to form a total electronic angular momentum $\hbar\boldsymbol{J}_e$. In the case of atoms, and neglecting hyperfine-structure effects, the gyromagnetic ratio g is proportional (see §5.1) to the ratio of the average value of $\boldsymbol{\mu}$ in the direction $\boldsymbol{J}_e$ to the magnitude of J_e itself and is of the order of unity. In the case of molecules $\hbar\boldsymbol{J}_e$ is coupled to the usually much larger nuclear rotational angular momentum $\hbar\boldsymbol{R}$† to form the total angular momentum $\hbar\boldsymbol{J}$ of the molecule (again neglecting nuclear spins and hyperfine interactions) and because the magnitude of J is usually so much larger than that for atoms and because also $\boldsymbol{\mu}$ is often approximately perpendicular to $\boldsymbol{J}$ (in those cases in which $\boldsymbol{\mu}$ lies along the internuclear axis), molecular g values tend to be much smaller than unity. For example, in the case of a molecular diatomic $^1\Pi$ state obeying Hund's coupling case a, $\boldsymbol{J}_e$ has a mean value Λ equal to 1 along the internuclear axis and this combines with the perpendicular $\boldsymbol{N}$ to give the total angular momentum quantum number J. Therefore

$$\overline{\boldsymbol{\mu}.\boldsymbol{J}} \propto \overline{\cos(\boldsymbol{\Lambda}.\boldsymbol{J})} = \Lambda[J(J+1)]^{-1/2} \tag{5.20}$$

and this divided by the magnitude $[J(J+1)]^{1/2}$ of the total angular momentum leads to the gyromagnetic ratio (see, for example, McClintock *et al* 1969)

$$g_J = [J(J+1)]^{-1}. \tag{5.21}$$

On the other hand, for a $^2\Sigma$ state obeying Hund's coupling case b, in which the electronic orbital angular momentum has no component along the internuclear axis but the electronic spin $\hbar\boldsymbol{S}$ adds to $\hbar\boldsymbol{N}$ to form $\hbar\boldsymbol{J}$, one has

$$\overline{\boldsymbol{\mu}.\boldsymbol{J}} \propto \overline{\cos(\boldsymbol{S}.\boldsymbol{J})} = \frac{J(J+1)+S(S+1)-N(N+1)}{2[J(J+1)S(S+1)]^{1/2}} \tag{5.22}$$

which, when combined with the gyromagnetic ratio g_s ($=2$) appropriate to the spin of a single electron, leads to a g value for the molecule given by (see, for example, de Zafra *et al* 1971)

$$g_{J=N\pm\frac{1}{2}} = \pm(N+\tfrac{1}{2})^{-1}. \tag{5.23}$$

In practice, the coupling schemes are not always simple and are often only inexactly known. As a further complication nuclear spins and hyperfine structures must be taken into account as well as the effects of ρ or Λ-type doubling, if these are present. These various structures are not usually resolvable and the observed Hanle signal is therefore composed of several signals of varying widths and amplitudes. In one case, that of the $A\,^2\Sigma^+$ state of OH and OD, the effective g value for the composite Hanle curve has been shown (de Zafra *et al* 1971) to be almost the same as the g value in the absence of hyperfine structure, namely that given by equation (5.22), but it is not

† We use the notation recommended by the Joint Commission for Spectroscopy, see 1953 *J. Opt. Soc. Am.* **43** 410–26.

known if this neglect of hyperfine effects has any wider validity. As well as being difficult to calculate accurately, molecular excited-state g values are also difficult to determine experimentally, both because their magnitudes are small and because molecular emission and absorption spectra typically contain a multitude of closely spaced rotational lines. The uncertainty in g values is clearly a major limitation in the use of the Hanle effect for accurate lifetime measurements in molecules.

5.5.1. Excitation by nearly coincident atomic or laser lines. A few cases have been found in which an atomic emission line is nearly coincident in wavelength with a molecular absorption line. For example, German and Zare (1969a) used the Zn I 307·206 nm line to excite the R_{12} (1) line of the (0, 0) band in the OH A $^2\Sigma^+$–X $^2\Pi$ ultraviolet system and were thus able to make a Hanle effect measurement on the $K=2$, $J=\frac{3}{2}$ rotational level of the A $^2\Sigma^+$ state. Other accidental coincidences have been used to measure lifetimes in NO (German *et al* 1971, Weinstock *et al* 1972), CS (Silvers and Chiu 1972), OH and OD (German *et al* 1973), S_2 (Meyer and Crosley 1973) and I_2 (Broyer and Vigué 1974, Broyer *et al* 1975).

For such isolated molecular transitions the fluorescence scattering intensity is given, as for atoms, by equation (5.13) which for molecules is more conveniently written as

$$R_{J,J',J''} \propto \sum_{mm'\mu\mu'} \frac{\langle J'm'|\boldsymbol{f}.\boldsymbol{r}|J\mu\rangle\langle J\mu'|\boldsymbol{f}.\boldsymbol{r}|J'm'\rangle\langle J''m''|\boldsymbol{g}.\boldsymbol{r}|J\mu'\rangle\langle J\mu'|\boldsymbol{g}.\boldsymbol{r}|J''m''\rangle}{1+\mathrm{i}(\mu-\mu')g_J\mu_B B\tau_J\hbar^{-1}} \qquad (5.24)$$

where J', J and J'' are the rotational quantum numbers of the initial, intermediate and final states respectively. With the appropriate disposition of source, field and detector, the line shape is again Lorentzian, with a width given by equation (5.18). Feofilov (1961) and Zare (1966) have derived and tabulated values of the matrix elements appearing in equation (5.24), as well as values of other relevant quantities.

In the work referred to above the exciting atomic emission lines are produced in a conventional source, such as a hollow-cathode lamp or electrodeless microwave discharge, but in one case (McClintock *et al* 1969) it has been possible to use an atomic laser line, namely the 476·5 nm argon ion laser line, which is coincident with the $v'=10$, $J'=12$ level of the B $^1\Pi_u$ electronic state of Na_2. The inherent narrowness of the laser line presents some difficulties (which are discussed in §5.6.1 below), in that the effective absorption profile is dependent on the magnetic field.

Tunable lasers offer a greater scope. For example, Kroll (1975) has made Hanle effect measurements in NH_2 using a tunable CW dye laser to selectively excite several rotational levels of the (0, 10, 0)Π vibronic state of the $^2A_1$ electronic state. The line shape was found to vary with laser intensity, which was attributed to optical pumping of the ground-state rotational levels. Other sources of error, which are common to all the Hanle experiments, were also present. Nevertheless, the versatility of this particular technique may make it the most suitable for molecular Hanle effect and level-crossing measurements.

5.5.2. Excitation by emission lines of the same molecular species. One way of obviating the need for tunable laser sources or nearly coincident atomic lines is to excite the molecular state of interest by resonance radiation of the same molecule. In the first experiment of this type Wells and Isler (1970) obtained a composite Hanle effect signal for all the rotational levels of $v'=2$ level of the CO A $^1\Pi$ state by excitation with the

entire A $(v'=2)\rightarrow$X $(v''=0)$ resonance band. This state is known to be closely represented by Hund's coupling case a and therefore the g values are given by equation (5.20) (hyperfine structure is absent because both nuclei have zero spin). To deduce the lifetime from the composite Hanle signal the relative intensities of the individual but unresolved rotational lines must be known, which in turn requires a knowledge of the temperature and absorption parameters of both the lamp (a 30 MHz RF discharge in a mixture of He and CO) and the scattering cell. These latter quantities were found by treating them as variable parameters and comparing the calculated intensity profiles of the lamp and fluorescence spectra with the corresponding actually observed spectra. There are many approximations in this procedure but nevertheless a value was obtained for the lifetime ($9{\cdot}0 \pm 1{\cdot}0$ ns) which agrees well with later more precise measurements. Their measured depolarization signal is shown in figure 30.

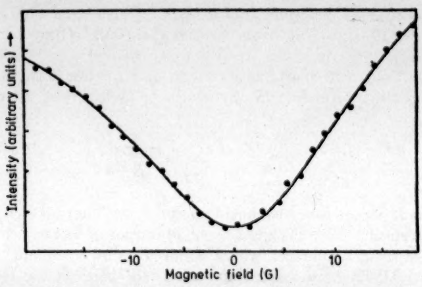

Figure 30. Hanle effect signal for the $v=2$ level of the A $^1\Pi$ state of CO (from Wells and Isler 1970).

In later versions of this technique the range of rotational levels has been limited by using a monochromator for either the incident light (Burnham *et al* (1972) who studied the $v'=1$ and 2 levels of the CO A $^1\Pi$ state) or the resonantly scattered light (de Zafra *et al* (1971) who studied the $v'=0$ level of the A $^2\Sigma^+$ state of OH and OD).

5.6. Experimental details and systematic errors

The Hanle effect is susceptible to several systematic errors which we now discuss, treating firstly those effects which may lead to a false measurement of the mean life τ and leaving the effects which might change τ itself (namely radiation trapping and collisional de-excitation) to the next section.

A schematic diagram of a typical experimental arrangement was shown in figure 27. In practice, (i) the detector is usually a photomultiplier tube, (ii) the magnetic field is usually provided by a pair of Helmholtz coils, except when molecules are being studied, when their smaller g values may necessitate much larger fields and hence the use of an electromagnet, (iii) the cell may indeed be a static gas cell but may also be an atomic or molecular beam or it may be a flowing afterglow or the site at which gases react to produce molecular radicals, (iv) the incident and scattered beams are collimated to restrict the range of scattering angles and the volume of the cell being used and either

or both of these beams contain interference filters (and sometimes narrower bandwidth monochromators) to define the state being studied and to reduce unwanted scattered light, (v) the polarizers shown in the figure may or may not be used, as discussed in §5.4 above, and finally (vi) the source is usually a suitable lamp which generates the emission spectrum of the atom or molecule being studied but may also be a tunable laser or in the case of molecules a line source which is accidentally coincident in wavelength with an absorption line of the scatterer. It is usual, particularly in the more recent work, to repeatedly sweep the magnetic field through its range, storing the detected counts in a multichannel analyser used synchronously in the multiscaling mode. An alternative way of improving the signal-to-noise ratio is to add a small modulated component to the magnetic field and to use phase-sensitive detection for the photon yield, thus effectively measuring the derivative of the fluorescence intensity. When the Hanle signal is small compared with the constant background of fluorescent light (as in molecules where the large number of initial rotational levels, only one or a few of which are resonant with the incident light, causes the signal to be only a few per cent of the background) it may be advantageous to use a rotating polarizer (Saloman *et al* 1970) or alternatively to use two detectors at different scattering angles and perhaps with different polarization directions, and to detect the difference in yield of these detectors (see, for example, German and Zare 1969a, McClintock *et al* 1969).

Apart from obvious potential sources of error in these experiments (such as modulation broadening, optical misalignments, magnetic field miscalibrations and inhomogeneities, etc) there are several less easily recognized systematic errors, many of them studied and elucidated in the careful work of Lurio, Gallagher and co-workers (for example, Gallagher and Lurio 1964, Lurio 1965, Smith and Gallagher 1966). These errors usually manifest themselves as slight divergences from the expected Lorentzian or dispersion profiles of the Hanle signal. It may be, for example, that the sensitivity of the photomultiplier or the density of target ions or radicals (Smith and Gallagher 1966, Kroll 1975), change with the magnetic field, thus changing the yield in the wings of the signal and perhaps even producing asymmetries. Unwanted (and often unrecognized) admixtures of antisymmetric dispersion profiles with the symmetrical Lorentzian profile are also an important possible source of error.

Changes in peak shape can also be caused if the exciting light does not have a uniform intensity over the Doppler-broadened absorption line of the target atoms (that is, if the excitation is not by a 'white' source), as was assumed in the derivations of §5.4. For example, the lamp might be self-reversed, in which case the separation in energy of the levels of the target atoms in a non-zero magnetic field would cause a greater probability of absorption from the higher intensity parts of the lamp's intensity profile, thus resulting in an enhancement of the wings of the Hanle signal (Lurio 1965).

A similar possible error arises when the target atoms are excited by a laser line which is narrower than the natural width of the excited states. In this case the exciting light seems far from 'white', but as Series (1966) has pointed out the important variable is the spectral distribution of the exciting light as seen by the atoms in their own moving frame of reference. Since this distribution has a Doppler width which is usually much larger than the natural width of the line the effective exciting light is approximately white, although there may be a slight diminution of yield in the wings of the Hanle signal. This diminution is more likely to be noticeable for molecules (McClintock *et al* 1969) because, although the applied magnetic fields only have to be large enough to cause energy splittings of the order of the natural width Γ itself, in the

case of a molecule the usually high value of J means that the total spread in energy of the $(2J+1)$ sublevels can be much larger than Γ.

Another effect that may accompany laser excitation is optical pumping of the target ground state, causing an unequal population of the initial magnetic sublevels and a possible consequent change in the shape of the Hanle signal (Bayliss 1968, McClintock *et al* 1969, Kroll 1975). This can always be explored by changing the focusing or intensity of the laser light and if necessary extrapolating to zero intensity. Other effects of using high-intensity laser light are discussed in §5.7.1.

5.6.1. Radiation trapping and collisional de-excitation. These two processes can cause the relaxation time τ' measured by level crossing or any other method to be longer and shorter respectively than the natural lifetime τ of an isolated atom or molecule. Another similar effect exists, namely reciprocal transfer (or collisional excitation), and this has been recently found to be important in studies of lifetimes of highly excited states (Gallagher *et al* 1975b). We start by considering the effect of radiation trapping on Hanle effect measurements.

In the case of the lifetime measurement methods discussed in §§2, 3, 4 and 6, the effect of trapping of resonance radiation is simply to increase the time delay between the emission of a photon and its eventual detection and thus to increase its apparent mean life τ_0 (the subscript 0 signifying that this is an incoherent process). This is discussed in §1.3. In the case of the Hanle effect this form of incoherent trapping could not affect the measured lifetime since each re-absorbed photon would effectively be only another source of incident radiation, and although this new source would be fairly isotropic and would therefore cause a decrease in the signal-to-background ratio, it could not cause a change in the width of the signal. But Hanle effect curves do, in fact, become narrower as the pressure is increased (in the absence of collisional de-excitation, see below), which implies that the trapping process must be partially coherent with the photons transferring coherence from atom to atom. This means, in a classical sense, that an emitted photon is able to convey information to the absorbing atom about the angle through which the emitting atom has precessed so that the precessional motion is passed on (wholly or partially) from atom to atom.

D'yakonov and Perel (1965a) have presented a simple classical argument which clarifies the process of coherent trapping and also gives the limiting rate as follows. Consider an atom emitting from an upper state having $J_1=1$ to a lower state having $J_0=0$. In the upper state the atom can be represented as a set of three mutually perpendicular dipoles and if only the z direction were excited the dipole electric field is such that its components would have the relative strengths $E_x^2 : E_y^2 : E_z^2 = 1 : 1 : 8$. The probability that an absorbing atom would be excited in the x, y or z directions is also in this ratio and therefore if I_x, I_y and I_z represent the energies of oscillation of an ensemble of atoms, and if it is assumed that all emitted photons are absorbed in the ensemble (that is, in the limit of complete trapping), then one has

$$\frac{\partial I_z}{\partial t} = -\Gamma I_z + \tfrac{1}{10}\Gamma I_x + \tfrac{1}{10}\Gamma I_y + \tfrac{4}{5}\Gamma I_z. \tag{5.25}$$

The analogous equations hold for $\mathrm{d}I_x/\mathrm{d}t$ and $\mathrm{d}I_y/\mathrm{d}t$, and by suitably combining them it can be seen that

$$\frac{\mathrm{d}I_2}{\mathrm{d}t} = -\frac{3\Gamma}{10} I_2 \tag{5.26}$$

where I_2 is the alignment parameter,

$$I_2 = I_z - \tfrac{1}{3}(I_x + I_y + I_z). \tag{5.27}$$

Therefore the limiting value $\Gamma_{2\infty}$ of the decay rate for alignment is equal to $\frac{3}{10}\Gamma$ for this particular case and the Hanle effect signal is said to be 'coherence narrowed'. For incomplete trapping the lifetime τ_2 deduced from the Hanle effect experiment would be between τ and $(10/3)\tau$. For those experiments in which the atomic orientation is measured (for example, a Hanle experiment with circular polarizers for the incident and fluorescent light) it can be shown that the limiting relaxation rate $\Gamma_{1\infty}$ is equal to $\frac{1}{2}\Gamma$ and that therefore the observed lifetime τ_1 (where the subscript 1 is used because this is the rank of the orientation tensor (see appendix 2)) would be between τ and 2τ for this particular case.

More generally D'yakonov and Perel (1965a) have shown that these various decay rates are given by equations (1.19) and (1.20), with the parameters a_t having the values:

$$\begin{aligned}
a_0 &= 1 \qquad \text{(for incoherent trapping)} \\
a_1 &= \frac{Y^2}{16J_1(J_1+1)} \qquad \text{(for orientation trapping)} \\
a_2 &= \frac{7[3Y(Y-1)-8J_1(J_1+1)]^2}{100(2J_1-1)2J_1(2J_1+2)(2J_1+3)} \qquad \text{(for alignment trapping)}
\end{aligned} \tag{5.28}$$

and

$$a_{n>2} = 0 \qquad \text{(for higher moments)}$$

where

$$Y = (J_1 - J_0)(J_1 + J_0 + 1) + 2 \tag{5.29}$$

and where J_0 and J_1 are the lower and upper J values respectively.

The dependence of the Γ_t on the gas pressure and cell dimensions have been studied by several authors. For example, Omont (1965b) has measured the dependence on pressure of the relaxation times Γ_1 and Γ_2 for the 253·7 nm line of mercury ($J_0 = 0$, $J_1 = 1$). His results are shown in figure 31 and it can be seen that the limiting values of Γ_1 and Γ_2 are approximately $0{\cdot}5\Gamma$ and $0{\cdot}3\Gamma$, as expected. He also found that the relationship,

$$\left(1 - \frac{\Gamma_1}{\Gamma}\right)\left(1 - \frac{\Gamma_2}{\Gamma}\right)^{-1} = \frac{5}{7} \tag{5.30}$$

which can be deduced from equations (1.19) and (5.28), is well followed at all pressures. It can also be noted from figure 31 that for a cell of the size used, namely a 25 mm cube, the trapping effects begin to be significant for the mercury resonance line at a density of about 10^{17} atoms m^{-3} (that is, at a pressure of 3×10^{-6} Torr). As noted in §1.3 radiation trapping, both coherent and incoherent, is usually much less important for molecules.

Another way in which the lifetime of an atom can be affected by neighbouring atoms is through collisions. Excited atoms may undergo a premature radiative decay through collisions with (i) other atoms of the same species ('like' atoms), (ii) admixed or background atoms of different species ('foreign' gas atoms) or (iii) the walls of the gas cell. Any of these processes causes the apparent lifetime to be decreased and the level-crossing signals to be 'collisionally broadened'.[5] An example from the work of Happer

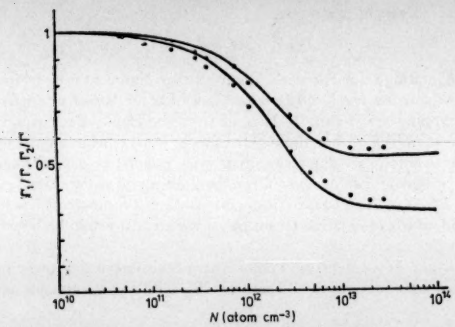

Figure 31. Orientation (Γ_1) and alignment (Γ_2) decay rates for the 6s6p $^3P_1$ state of mercury (from Omont 1965b). ○, Γ_1/Γ; ●, Γ_2/Γ; ——, theoretical curves ($L = 1{\cdot}1$ cm).

and Saloman (1965) is shown in figure 32. The earlier theoretical treatments of Byron and Foley (1964) (which was shown by D'yakonov and Perel (1965b) to contain errors), Omont (1965a) and D'yakonov and Perel (1965b) were mostly confined to resonant dipolar interactions between neutral atoms, although this has been extended more recently by several authors (for references see, for example, Gallagher and Lewis (1974)). As in the case of radiation trapping, the incoherent, orientation and alignment lifetimes (τ_0, τ_1 and τ_2 respectively) are differently affected by collisional de-excitation processes. For example, in the dipole–dipole interaction between like atoms having $J_0 = 0$ and $J_1 = 1$, D'yakonov and Perel (1965b) have shown that limiting values of the orientation and alignment rate constants are given by

$$\frac{\Gamma_1}{\Gamma} = 0{\cdot}5 + 0{\cdot}035n\lambda^3 \qquad \frac{\Gamma_2}{\Gamma} = 0{\cdot}3 + 0{\cdot}028n\lambda^3 \tag{5.31}$$

where the first terms are those for coherence narrowing alone and where n is the number density of atoms.

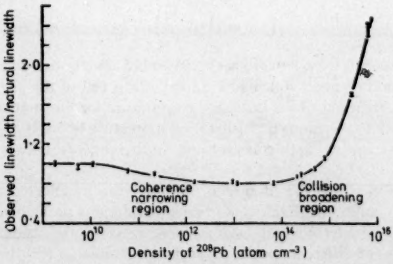

Figure 32. Linewidth of $\Delta m = 2$ Hanle effect resonances in the (6s^{2}6p7s) $^3P_1^0$ state of ^{208}Pb ($1/\tau_{a1}$). Volume of gas cell = 50 cm^3 (from Happer and Saloman 1965).

Collisional broadening almost always appears at higher pressures than does coherence narrowing (for an exception, see Gallagher and Lewis (1974)). Thus although observations of collisional broadening can give valuable information about atom–atom and atom–ion collision processes (see Gallagher (1975) for a recent review) and this information is sometimes obtained as a by-product of lifetime measurements, the subject of collisional de-excitation is not intrinsically important in the present context and therefore is not discussed in greater detail.

5.7. Level crossings at non-zero fields

To return to figure 23, there are three places within the range of magnetic field shown in the figure for which states differing in M_F by two units cross each other at a non-zero value of the magnetic field, as indicated by the three circles not lying on the left-hand axis. The topmost crossing, for example, has $M_F=-4$ and -2 and with a suitable arrangement of linear polarizers the relevant selection rules allow both these levels to be excited from, and to decay to, levels having $M_F=-3$. The two routes $-3\rightarrow(-4$ or $-2)\rightarrow-3$ interfere destructively, and as in the zero-field Hanle effect the measured yield shows a Lorentzian dip as the magnetic field is varied through the region of the crossover. This can be seen from equation (5.13) which in the present case leads to a dip having the form (Rose and Carovillano 1961, Franken 1961)

$$R\propto -\frac{\mathrm{Re}\,(D)}{1+\epsilon^2}$$

where

$$\epsilon=\frac{1}{\Gamma}(B-B_0)\frac{\partial E}{\partial B}=2\pi\tau(B-B_0)\frac{\partial \nu}{\partial B} \tag{5.32}$$

where D is a fourfold product of the matrix elements f and g and τ is the mean life of the levels. The width (FWHM) of the signal is therefore

$$\Delta B=\left(\pi\tau\frac{\partial \nu}{\partial B}\right)^{-1}. \tag{5.33}$$

The results of Svanberg and Rydberg (1969), who studied the positions and widths of the three level crossings of figure 23 and obtained the value 135 ± 1 ns for the lifetime, are shown in figure 33. Note that these are differentiated yields and the dips at the crossing points therefore appear as dispersion profiles. Note also the zero-field feature corresponding to the Hanle effect.

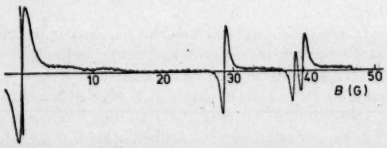

Figure 33. Differentiated level-crossing signal for the $7^3P_{3/2}$ state of ^{133}Cs (from Svanberg and Rydberg 1969). The zero-field feature (Hanle effect) corresponds to the four crossing points on the zero-field axis of figure 23, and the non-zero features to the remaining three crossing points.

The first result of this type, and the one which did much to initiate interest in the theory and applications of level-crossing experiments, was the accidental discovery by Colegrove *et al* (1959) of two crossings between Zeeman sublevels of the fine-structure levels 2^3P_1 and 2^3P_2 of helium. The zero-field splitting of these levels is sufficiently small (2292 Hz) for the level crossings to occur at easily attainable values of the magnetic field (in this case at fields less than 0·1 T) and this is also true of fine-structure crossings in hydrogen and lithium. In the more general case the required magnetic fields are too high for observations of fine-structure crossings, although they are usually amenable for crossings between hyperfine-structure levels such as those shown in figure 23.

Crossing interference effects are not confined to levels differing in M_F by two units. If the incident light is linearly polarized in a direction which is not parallel or perpendicular to the magnetic field it can excite a coherent superposition of states differing in M_F by one unit, which can thereby suffer level-crossing interference. This is also true of elliptically and circularly polarized light as in the case of zero-field level crossings. States having the same value of M_F cannot cross but repel each other because M_F is a good quantum number. Such states can still interfere with each other if they come sufficiently near together to cause their wavefunctions to mix. This was discovered by Eck *et al* (1963) who referred to the effect as level 'anticrossing'. They studied the mixing of the $(M_J=-\frac{1}{2},\ M_I=-\frac{3}{2},\ M_F=-2)$ and $(M_J=-\frac{3}{2},\ M_I=-\frac{1}{2},\ M_F=-2)$ states of the 2P levels of ^{7}Li and deduced that the interference signal has a Lorentzian shape with a width (FWHM) given by equations (5.32) and (5.33) but with the radiative width Γ replaced by

$$\Gamma' = (\Gamma^2 + |2V|^2)^{1/2} \tag{5.34}$$

where $|2V|$ is the interval between the states at their closest approach. The presence of the interaction term V means that this type of level crossing is not generally useful for lifetime determinations.

Level crossings can also be produced with combined static magnetic and electric fields (see, for example, Budick *et al* 1965) or even with electric fields alone (Khadjavi *et al* 1968, Dalby *et al* 1974). In these cases the additional terms $\alpha E^2 + (\beta E M_J)^2$ must be added to the Hamiltonian of equation (5.1), where the quantities α and β depend on the value of J and the polarizability of the atom but are independent of the electric field strength E. The first of these terms changes all levels equally and is therefore of no significance in level-crossing experiments, while the second can either bring levels into superposition (in the case of an electric field only) or can change the crossing point of already crossed levels (in the case of combined electric and magnetic fields), except in the case of levels crossed at zero magnetic fields (Hanle effect experiment), for which it has no significant effect.

As in the case of zero-field level crossing the requisite initial coherence for level crossings at non-zero fields can also be produced by the methods described in §§5.4.2–5.4.5. For example, Kaul (1967) has used bombardment by 40 keV H_2^+ ions to produce coherence between the $(J=0,\ M_J=0)$ and $(J=2,\ M_J=2)$ levels of the n^3P states of helium, where $n=3$–6, and to observe the resulting interference effects at their crossing points. The experimental errors described in §§5.6 and 5.6.1, and in particular the process of coherence narrowing, are also relevant to level crossings at non-zero fields.

Although level-crossing experiments at non-zero magnetic fields offer an accurate and powerful technique for measuring atomic lifetimes, they have not yet been widely

used for this purpose but instead have usually been aimed at obtaining information about fine-structure and hyperfine-structure splittings. The technique would seem not to be as useful for molecular lifetime measurements owing to the large numbers of crossing points and interacting levels.

The range of lifetimes covered by the zero-field and non-zero-field level-crossing techniques has usually been from 10^{-9}–10^{-6} s, with only a few experiments outside this range. At the long lifetime limit the photon absorption cross section becomes small and also wall collisions and field inhomogeneities are important. At the short lifetime limit of the Hanle measurements a high magnetic field is necessary and this can cause the frequency separation of the Zeeman sublevels to exceed the Doppler width of the source, thus changing the Hanle signal profiles (see §5.6).

5.7.1. Saturation resonances and stimulated level crossing. The monochromaticity and high field intensity of laser beams can be used in various ways to produce resonance peaks or dips having widths which are limited by the radiative widths of the levels involved. These methods therefore give information about radiative lifetimes and they will undoubtedly be exploited for this purpose in the future. Recent accounts of such methods are those of Feld *et al* (1974), Dumont (1974), Cohen-Tannoudji (1975) and Walther (1976).

An obvious example is the well known Lamb dip (Lamb 1964). Consider a single-mode laser beam of frequency Ω passing in one direction through a sample of atoms having an absorption frequency ω. The atoms which absorb the laser light are those having the requisite Doppler shift, namely those with velocity components of magnitude $(c/\omega)(\Omega-\omega)$ along the direction of the beam. Because these atoms are then no longer available (at least until they return to the lower level) to absorb further laser light, a hole is said to have been 'burnt' in the probability distribution of atomic velocities. Two laser beams of frequency Ω passing through the sample in opposite directions will be absorbed by different velocity subsets of atoms unless Ω is adjusted to be equal to ω, when the two beams will compete for the same subset, and since the absorption is non-linear this gives rise to a dip in the overall absorption. The width of the dip is the radiative width of the upper level (assuming that the lower level is the ground state) if other contributions such as pressure broadening, transit time effects, etc, can be neglected. Also the spectral width of the laser beam must be less than the width being measured and the laser must be frequency-stabilized, which in practice severely limits the range of lifetimes which can be measured by this method. A related method is that in which the opposing beams have different frequencies Ω_1 and Ω_2 and the atoms have two absorbing frequencies ω_1 and ω_2 such that $\Omega_1-\Omega_2\approx\omega_1-\omega_2$. Then the interaction of Ω_1 with ω_1 can induce narrow resonances in the interaction of Ω_2 with ω_2 and the widths of the resonances are again limited by the radiative width of the levels (Feld and Javan 1969).

Resonance peaks and dips can also be produced by a single laser beam of frequency Ω passing in one direction through a sample of atoms if the atoms have two absorbing levels ω_1 and ω_2 which can be varied by an external electric or magnetic field. Two holes are burnt in the velocity distribution, as shown in figure 34. If the levels are made to cross the two holes become superimposed and the total number of excited atoms will decrease, giving rise to a dip in the fluorescence intensity curve as shown in figure 34. This is referred to as a population effect. The width of the dip is the radiative width of the upper state, thus providing a means of measuring the upper-state lifetime. The laser need not be frequency-stabilized (unlike the Lamb dip experi-

ments), but if a multimode laser is used and the mode difference frequency equals $\omega_1 - \omega_2$ new resonance effects arise (see, for example, Dumont 1974, Kalitejewski and Tschaika 1975), some of which can also be used for measuring lifetimes.

As well as this population effect the levels 1 and 2 may also be able to interfere coherently as in the Hanle and level-crossing effects described above. These effects become more complicated in the presence of a high-intensity laser field since the possibility of saturation and of successive excitations and stimulated de-excitations can give rise to higher order effects. Ducloy *et al* (1974), for example, have studied the

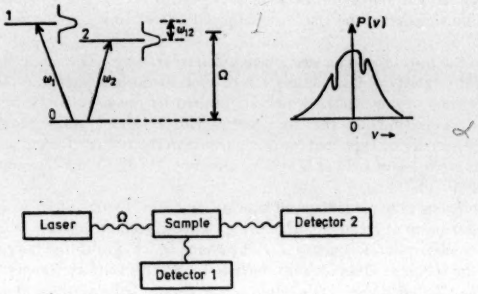

Figure 34. A saturation resonance in laser stimulated fluorescent light.

Hanle effect up to the fourth order in the laser field. In most situations these interference effects (called Zeeman coherence effects by Dumont (1974)) must be considered together with the population effect.

If the sample shown in figure 34 contains more atoms in states 1 and 2 than in state 0 (for example, if the sample is the laser medium itself) the incident light will cause stimulated emission in the sample atoms and will thus be amplified. The degree of amplification will saturate for high laser fields and will be different for separate and degenerate levels 1 and 2 (Feld *et al* 1974). Resonance behaviour, called stimulated level crossing, is therefore observed as ω_{12} is varied through zero. The widths of the features are $\Gamma_1 + \Gamma_0$ (although there are complications for multiply degenerate crossing levels), which again means that this technique could be used for lifetime measurements if the effects of pressure broadening, field broadening, laser spectral width, etc, can be made sufficiently small.

5.8. Double-resonance experiments

Other features shown in figure 23 are three arrows at zero field, connecting hyperfine levels which differ in F by one unit, and a set of ten arrows at a non-zero field (represented in the figure by a single arrow) connecting levels differing in M_F by one unit but all having $F=5$. Figure 24 also shows arrows connecting Zeeman sublevels. These various features relate to two different types of 'double-resonance' experiments, namely those in which the static magnetic fields are zero and non-zero respectively (the latter usually being labelled 'high-field' double-resonance experiments, even though the fields are sometimes less than 1 mT). The description 'double resonance' is used to indicate that the atoms are simultaneously subjected to two resonant radiations: an optical radiation to excite the atoms from the ground state and a radio-frequency radiation to induce transitions between the Zeeman sublevels. An important feature of these double-resonance experiments is that the resolution limitation of the optical Doppler width is virtually eliminated (as in the level-crossing methods already described) because the observed Doppler broadening is that associated with the radio-frequency radiation, which is usually insignificant compared with the natural widths of the lines. Previous reviews of the double-resonance technique, and in some cases including compilations of lifetimes obtained by it, have been given by Series (1959), Budick (1967), Radford (1967), Corney (1969), zu Putlitz (1969), Bucka (1969), Kastler (1973) and Zare (1974). We shall start here by discussing the high-field double-resonance experiments.

The first double-resonance experiments were those of Brossel *et al* (1950) and Brossel and Bitter (1952), following the suggestion of Brossel and Kastler (1949) and the comments of Bitter (1949) and Pryce (1950). The principle of the experiment of Brossel and Bitter can be understood by referring to figure 24. The $6s6p\ ^3P_1$ state of mercury was excited by irradiation with the intercombination line $^1S_0$–$^3P_1$ of wavelength 253·7 nm. The incident light was polarized in the π direction which ensured (in the case of the isotopes of even mass number and zero nuclear spin) that only the $M_J=0$ Zeeman sublevel could be excited. The radiation emitted by this Zeeman sublevel has an angular and polarization distribution which is different from that emitted by the $M_J=\pm 1$ sublevels. A system containing two detectors and polarizers was therefore set up to detect any changes in the relative populations of the M_J sublevels. They then induced transitions between the sublevels by means of a radio-frequency field, the magnetic dipole component of which has the correct parity (see, for example, Rose 1955) for this purpose. The frequency required, assuming that the static field B is small enough that the sublevel energies vary linearly with B, is the Larmor frequency

$$\nu_L=g\mu_B B/h. \tag{5.35}$$

In practice it was found convenient to apply an oscillating field of constant frequency (144 MHz) and to scan the static field across the Larmor resonance. Some of the results of Brossel and Bitter are reproduced in figure 35. Note that an initial population imbalance is required for this double-resonance effect but that coherence between the Zeeman sublevels is not required.

For vanishingly small values of the amplitude B_1 of the radio-frequency magnetic field, the width $\Delta\omega$ (FWHM) of the signal depends only on the natural radiative width Γ ($=1/\tau$) and has the value 2Γ (the factor of two arising because the transitions are between two levels, each having the width Γ). As B_1 is increased the effective lifetime of the levels is reduced by the induced transitions and the width has the value (for the

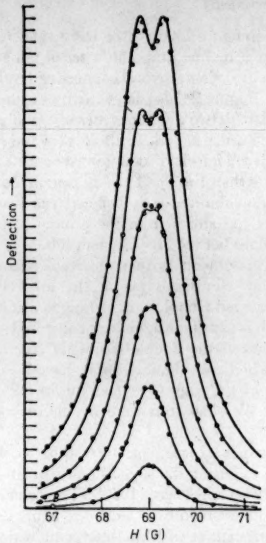

Figure 35. Radio-frequency–optical double resonance observed in isotopes of mercury having even mass number and zero nuclear spin. The RF field was of frequency 144 MHz (see also figure 24) and the optical radiation was of wavelength 253·7 nm to excite the $6s6p\ ^3P_1$ state of mercury (from Brossel and Bitter 1952).

experiment of Brossel and Bitter) given by

$$(\Delta\omega)^2=(2\Gamma)^2+23{\cdot}2\omega_1{}^2+\ldots \tag{5.36}$$

to the lowest order in ω_1, where ω_1 is the Larmor angular frequency in the frame of reference in which the inducing field $\boldsymbol{B}_1$ is non-rotating, that is

$$\omega_1=g\mu_B B_1/h. \tag{5.37}$$

This increase in $\Delta\omega$ is referred to as 'power broadening'. As B_1 is increased further, the time interval between induced transitions (which is of the order of $\omega_1{}^{-1}$ at the central resonance frequency) decreases and the strength of the resonance signal increases. When the time interval becomes comparable with the lifetimes of the levels a central dip appears in the signal shape.

Brossel and Bitter (1952) were able to deduce the lifetime of the $^3P_1$ mercury level from equation (5.36) by plotting $(\Delta\omega)^2$ against $B_1{}^2$ and measuring the intercept. The numerical coefficient (23·2) appearing in equation (5.36) has different values for other cases, but it is clear that the zero-power extrapolation of $\Delta\omega$ will always yield the natural lifetime τ, wherein lies the value of the double-resonance method for lifetime

measurements. The arrows appearing at non-zero fields in figure 23 refer to the work of Altman and Chaika (1964) who used the double-resonance technique to find a value of approximately 125 ns for the lifetime of the $7^2P_{3/2}$ state of Cs (their value has been corrected for the numerical error pointed out by Markova *et al* (1967)).

The resonance radiation in these experiments serves partly to create an initial imbalance in the population distribution of the Zeeman sublevels and partly to monitor this distribution, and although it is invariably used for the second purpose it may be replaced for the first. Pebay-Peyroula (1959a, b), for example, created the initial imbalance by electron bombardment (see also the discussion of §5.4.3) and was thus able to measure the lifetimes of three different levels in mercury. This method has since been followed by many authors of the French School. In a slightly different development Freund and Miller (see, for example, Freund and Miller 1974) have also used electron impact, but have used a microwave field to mix the Zeeman sublevels and were thus able to measure the lifetime of the d(3p) $^3\Pi_u$ state of H_2. Schearer and Holton (1970), on the other hand, created non-uniform populations in the Zeeman sublevels of the $4^2D_{5/2}$ and $4^2D_{3/2}$ states of Zn^+ and the $5^2D_{5/2}$ state of Cd^+ by Penning ionization of Zn and Cd atoms with oriented metastable 2^3S helium atoms. In another variation Hadeishi *et al* (1969) replaced not only the incident radiation, this time by foil excitation, but also the conventional radio-frequency field, using instead the high-frequency (520 MHz) electric dipole field experienced by the excited atoms as they moved through a spatially periodic static electric field. In this way they were able to mix states of opposite parity, namely Zeeman sublevels of the $3^2S_{1/2}$ and $3^2P_{1/2}$ states of atomic hydrogen.

High-field optical double-resonance experiments are clearly more difficult for molecules because of the greater complexity and narrower spacings of their energy levels. Although a few such experiments have been carried out (for example, German and Zare 1969b, de Zafra *et al* 1971, Maréchal *et al* 1972, German *et al* 1973) to determine the g values needed to deduce lifetimes from Hanle effect measurements, they have only occasionally (see, for example, Freund and Miller 1974) been used to measure lifetimes as such.

The second type of double-resonance experiment is that at a zero magnetic field as illustrated by the arrows on the zero-field axis of figure 23. If the hyperfine levels are excited from the ground state by polarized light, the population of their M_F sublevels can be non-uniform, in which case the decay photons are emitted with an anisotropic distribution of directions and polarization. In general the direction of observation and polarization would usually be arranged to give the minimum detected signal and this yield is then increased by inducing transitions between the hyperfine levels by means of a radio-frequency field.

For example, the hyperfine levels shown in figure 23 can all be excited by light of wavelength approximately 455·5 nm, and if this light is plane-polarized the minimum intensity of fluorescent light is observed in the direction of the polarization. If a radio-frequency field of 49·9 MHz (see equation (5.2)) is applied at the same time, this will

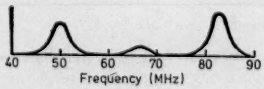

Figure 36. Double-resonance signal for the $7^2P_{3/2}$ state of ^{133}Cs (from Althoff 1955). The three peaks correspond to the three arrows on the zero-field axis of figure 23.

induce transitions between the $F=2$ and $F=3$ levels, changing the population of sublevels M_F in each, and hence changing the distribution of the emitted light. The applied radio-frequency field must be sufficiently strong for the probability of transitions between the hyperfine levels to be appreciable during the lifetime of these levels. As the frequency of the applied field is varied, the intensity of scattered light increases at each resonance frequency which connects the hyperfine levels (that is, at 49·9, 66·5 and 83·0 MHz, and their combination frequencies, for the levels of figure 23). This was observed for example by Althoff (1955) whose spectrum is shown in figure 36. The resonance peaks have widths caused partly by the natural lifetime τ of the levels, partly by the shortening of this lifetime by the induced radio-frequency transitions themselves and partly by interferences between neighbouring transitions. In the simplest case of very weak radio-frequency fields and only two connected levels the width is simply 2Γ, as in the case of the high-field double-resonance technique. Measurements of these resonance peaks can therefore lead to a determination of τ. Bucka *et al* (1959), for example, have found that the radio-frequency transitions in the $7^2P_{3/2}$ state of Cs have natural widths of approximately 2·7 MHz, implying a lifetime of approximately 118 ns.

A variation of this radio-frequency–optical double-resonance technique is the microwave–optical double-resonance method used, for example, by Solarz and Levy (1974) to measure the lifetime of a rotational level of the NO_2 molecule, the microwave (X band) frequency being necessary in this case to induce transitions between rotational levels. Optical–optical double-resonance experiments with widely separated levels are also possible in principle although the Doppler broadening, which is proportional to the energy difference of the levels, would then not be small.

Double-resonance experiments (both zero-field and high-field) are subject to the same sources of error as the level-crossing experiments (see §§5.6 and 5.6.1). An additional possible source of error arises because the radio-frequency fields must be sufficiently strong to cause transitions between the sublevels within their radiative lifetime, which inevitably produces the power broadening discussed above. The range of radio-frequencies used has usually been from about 10 kHz to about 50 MHz. The lower frequency end of the range is suitable for long lifetimes τ ($\sim 10^{-5}$ s) for which the linewidth $(\pi\tau)^{-1}$ and the frequency ν are comparable. For such long-lived states the optical excitation probability is low and wall collisions and field inhomogeneities become important. The upper frequency end of the range is used for shorter lifetimes ($\sim 10^{-9}$ s) and is limited by the fact that the RF field strengths needed to induce transitions within these lifetimes may also be strong enough to cause a discharge in the vapour.

The double-resonance technique has the advantages that (i) g values are not required, (ii) the excitation need not be coherent, and (iii) cascading from higher lying levels is not important. However, any lifetime which can be measured by this technique can also usually be measured by a level-crossing or other technique and the double-resonance method is unlikely to be extensively used for routine measurements.

5.9. Quantum beat experiments

So far we have discussed changes of time-integrated intensities resulting from level-crossing and double-resonance effects, but the coherences between sublevels which are created by these effects can also give rise to oscillatory time dependencies of the emitted light, as was mentioned in §5.2. These intensity oscillations are often referred

to as 'quantum beats' and can arise from interference between Zeeman sublevels of a hyperfine level, or between different hyperfine levels, or even between different fine-structure levels. We discuss these briefly in turn. A recent and more complete discussion of this topic has been given by Andrä (1975).

An example of quantum beats between Zeeman sublevels is provided by the work of Dodd *et al* (1964, 1967) on the decay of fluorescence following a short pulse of optical excitation. Figure 37 shows their results for the triplet resonance line in cadmium with a static magnetic field of 34·5 μT. The duration of the excitation pulse is shorter than

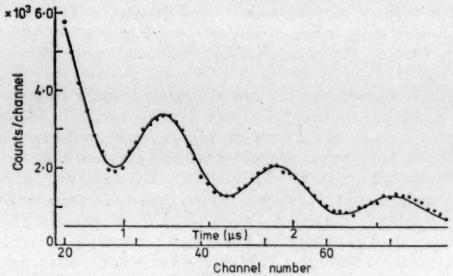

Figure 37. Modulation of the resonance fluorescence of cadmium vapour in a field of 34·5 μT, excited by pulses of length 200 ns. The full curve is an optimized theoretical fit to the experimental points (●) (from Dodd *et al* 1967).

the Larmor precessional period $2\pi\omega_L^{-1}$ and so partial coherence is established between the $M=\pm 1$ Zeeman sublevels. These then interfere (equation (5.8)) to give the observed intensity

$$I(t, \boldsymbol{B}) = [a + b\cos(2\omega_L t + \phi)]\exp(-t/\tau) \tag{5.38}$$

where a, b and ϕ are time-independent constants. The oscillatory term can also be regarded, in a classical sense, as being caused by the precessional motion of the excited atoms in the magnetic field. Other ways of producing the initial coherence are by sinusoidally modulated incident light (Aleksandrov 1963, Corney and Series 1964a, b), pulsed electron impact (Hadeishi and Nierenberg 1965) and sinusoidally modulated electron impact (Aleksandrov 1964, Hadeishi 1967). Quantum beats can also be seen in foil-excitation experiments as discussed in §4.2.1.

The quantum beats appearing in equations (5.8), (5.38) and (4.7) do not exist in the integrated intensity of the emitted light, as has been pointed out by Macek (1969, 1970). This is intuitively obvious if the beats can be viewed as being caused by precessional motion or if it is realized that the interference terms in equation (5.8) cause a redistribution of the directional intensity but without changing the net outgoing power.

The main importance of these quantum beats as far as lifetime measurements are concerned is that they can yield the g values which are needed for level-crossing experiments but they may also be useful in providing a means of suppressing cascade effects in beam–foil measurements, as described in §4.2.1.

Coherence between Zeeman sublevels can also be induced by the radio-frequency

field in double-resonance experiments, as has been shown by Dodd, Series and co-workers in an elegant series of papers (see, for example, Dodd *et al* 1959, Dodd and Series 1961). This coherence also manifests itself in modulation of the fluorescent light, but although the effect is of great intrinsic interest it has not yet been used to measure lifetimes directly. It has, however, been used to measure the g factors needed to deduce lifetimes from Hanle effect measurements (see, for example, Broyer and Vigué 1974) and it also appears in a different form in the multimode laser resonances mentioned in §5.7.1.

Quantum beats can also occur through interference of hyperfine-structure levels. Referring again to figure 23, suppose that the $7^2P_{3/2}$ state of Cs is excited from the $F=4$ hyperfine level of the $6^2S_{1/2}$ ground state by a short burst of light from a pulsed dye laser, as was done by Haroche *et al* (1973). Their pulses were of duration T approximately 2 ns and bandwidth approximately 1 GHz, and therefore the states $F=3$, 4 and 5 (for which the transitions from the ground state are optically allowed) were excited with well defined relative initial phases (since $T \ll \nu_{53}^{-1} = 6{\cdot}7$ ns). As time progresses the relative phases change at the rates given by the energy differences (see equation (5.7)) of the states. For example, the relative phase of the states $F=4$ and 5 returns to its initial value every 12·1 ns ($=1/83$ MHz). Therefore, with a suitable arrangement of polarizers the emitted light will show quantum beats of frequencies 83 MHz (ν_{54}), 66 MHz (ν_{43}) and 149 MHz (ν_{53}), as observed by Haroche *et al* (1973).

In exceptional cases quantum beats can be seen between fine-structure states. For example, Eck (1973) and Sellin *et al* (1973) have shown that the nearly degenerate s and p states of the hydrogen atom can interfere after foil excitation. The initial coherence arises in this case because the mean velocities of the proton and the electron cloud are different immediately after leaving the foil with the result that the centres of gravity become displaced from each other. This means that the wavefunction of the atom is a coherent mixture of s and p components, as in the hybrid sp orbitals which occur in the bonding of H atoms to other atoms of a molecule. This type of quantum beat phenomenon has not yet found serious application in lifetime measurements.

6. Coincidence methods

In this section we discuss methods in which a time-delayed coincidence is observed between two specific and consecutive events relating to one atom or molecule. The two main methods in this category are the photon–photon and the electron–photon delayed-coincidence methods, which we discuss in this order. Other delayed-coincidence methods, in which the first event occurs during the time of a photon or electron pulse but is otherwise not specifically observed, are treated in §§2 and 3.

6.1. The photon–photon coincidence method

The principle of this method is illustrated in figure 38. The 6D states are excited (along with other states of the atom) by bombardment with a continuous beam of 30 eV electrons and the subsequent decay photons of wavelength λ_1 and λ_2 occur in cascade and are used to respectively start and stop a timing device. The resulting spectrum of time intervals therefore gives a direct measurement of the probability distribution $\exp(-t/\tau)$ of the time interval t between the creation and decay of the intermediate state. This method, which is also known as the cascade coincidence method, is well

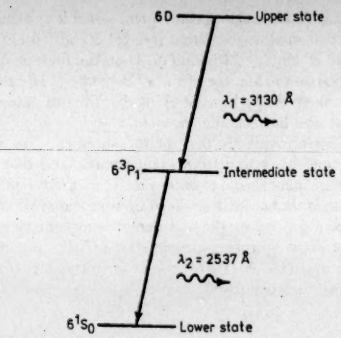

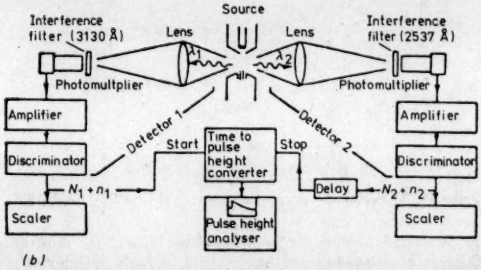

Figure 38. Principle of the photon–photon coincidence experiment. (*a*) Diagram of a cascade transition in atomic mercury. (*b*) Schematic diagram showing the detectors and coincidence electronics (from Kaul 1966).

known in the field of nuclear physics, where delayed coincidences in γ–γ cascades have been used to measure nuclear lifetimes in the range from about 10^{-11}–10^{-3} s (Bell 1965). It was proposed as a suitable method for lifetimes in atoms and molecules by Brannen *et al* (1955) and was used by them to obtain the value $11{\cdot}2 \pm 0{\cdot}2$ ns for the lifetime of the 7^3S_1 state of mercury. The method has since been used by Pardies (1968) and Camhy-Val and Dumont (1970) to measure this same lifetime in mercury, by Kaul (1966), Nussbaum and Pipkin (1967) and Popp *et al* (1970) to measure the lifetime of the 6^3P_1 level of mercury, by Camhy-Val, Dumont and co-workers (Camhy-Val and Dumont 1968b, Camhy-Val *et al* 1969b, 1970, 1975, Dumont *et al* 1970) to measure five lifetimes in Ar II, by Masterson and Stoner (1973) to measure the lifetime of the 3d′ $^2G_{7/2,9/2}$ levels in O II, and by Yamagishi and Inaba (1974) to measure the lifetimes of the $2p_8$ and $2p_9$ levels in Ne I, but these experiments (with the exception of that of Popp *et al* (1970)) have suffered from either a poor statistical accuracy or (in the case of the experiments of Camhy-Val, Dumont and co-workers) a high source

pressure (of the order of 0·1 Torr or higher) and consequent possible systematic errors from radiation trapping and collisional de-excitation (see §§1.3 and 5.6.1). It is only following the more recent work of Holt and Pipkin (1974) on the lifetime of the 7^3S_1 level of Hg, of King *et al* (1975b) on the lifetime of the a $^3\Sigma_g^+$ state of H_2, and of King *et al* (1976) on the lifetime of the 4p $^4D^o_{7/2}$ level of Ar II that the full potential of the photon–photon coincidence method has become apparent.

The main advantages of the technique are that the measurements are completely free from the effects of unwanted cascading from higher states, and that it can be applied to excited states which are inaccessible to other precise methods (such as level-crossing methods). A limitation is that at least one feeding transition (λ_1) and at least one decay transition (λ_2) must both be in the wavelength range of single-photon detectors: this range presently extends from approximately 1·7 μm (for germanium avalanche diodes, see Fichtner and Häcker (1976)) to the far ultraviolet (for channel electron multipliers and other surface detectors).

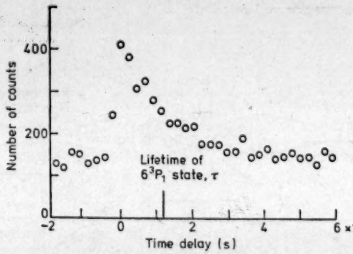

Figure 39. The delayed-coincidence spectrum obtained by Kaul (1966).

The first published photon–photon coincidence spectrum, illustrating all the important features of delayed-coincidence spectra of both the photon–photon and electron–photon coincidence methods, is shown in figure 39. The exponential decay curve can be clearly seen. Its leading edge is rounded by the finite resolving time of the coincidence detection system and the curve is brought into the range of observed delay times by means of an additional delay inserted into the stop channel (see figure 38(*b*)). As well as this decay curve of 'true coincidences', a background of 'random coincidences' can also be seen. These arise when the start or stop pulses of the timing unit originate from noise pulses or from photons emanating from different atoms: the time intervals between such pulses are completely random and therefore the resulting background is flat.

The relative counting rates of the true and random coincidences can be found as follows. Suppose that the source strength (that is, the number of transitions of wavelength λ_1 per unit time) is N and that the efficiencies with which photons of wavelength λ_1 and λ_2 are detected are ϵ_1 and ϵ_2 respectively (these efficiencies include a solid angle factor, the filter transmission, the efficiency of the photomultiplier, the probability of amplified photomultiplier pulses passing the discriminator, and in the case of λ_2 only, the branching ratio for the decay route λ_2). The start (N_1) and stop (N_2) rates are then

$$N_i = \epsilon_i N + n_i \tag{6.1}$$

where the n_i are noise counting rates caused by photomultiplier noise and in some cases by unrelated photons which have failed to be rejected by the wavelength filters. The rate of true coincidences arriving in the short interval of delay times between 0 and Δt is

$$\Delta N_T = \int_0^{\Delta t} \epsilon_1 \epsilon_2 N \frac{1}{\tau} \exp\left(-\frac{t}{\tau}\right) dt \approx \epsilon_1 \epsilon_2 N \frac{\Delta t}{\tau} \tag{6.2}$$

if the angular correlation of the cascade photons is assumed to be isotropic and if the finite resolving time of the coincidence detection system is neglected. The rate of random coincidences in the same time interval is the rate of start pulses times the probability of a stop pulse arriving in a time interval Δt, namely

$$\Delta N_R = (\epsilon_1 N + n_1)(\epsilon_2 N + n_2)\Delta t. \tag{6.3}$$

The signal-to-background ratio (also often called the true-to-random ratio) is therefore

$$\frac{S}{B} = \frac{\Delta N_T}{\Delta N_R} = \frac{1}{N\tau}\left(1 + \frac{n_1}{\epsilon_1 N}\right)^{-1}\left(1 + \frac{n_2}{\epsilon_2 N}\right)^{-1}. \tag{6.4}$$

Since the noise rates n_i can often be neglected or can be measured, a measurement of this ratio gives the absolute value of the source strength N. When combined with the measured singles rates N_i this also gives the detection efficiencies ϵ_1 and ϵ_2, from which absolute photomultiplier efficiencies can be deduced. If the effective source size is large, so that the solid-angle factors in ϵ_i vary over the source volume, then equation (6.4) (and also equation (6.5) below) must be modified by an appropriate integration over the source volume (Camhy-Val and Dumont 1968a).

If the time interval Δt represents the channel width of the pulse height analyser (see figure 38(*b*)), the noise content of each channel follows immediately from the fact that the accumulated counts follow Poissonian statistics. For a total collection time T the standard deviation is therefore $(\Delta N_T + \Delta N_R)^{1/2} T^{1/2}$ in the channel representing $t = 0$ to Δt, and therefore the signal-to-noise ratio is

$$\frac{S}{N} = \left(\frac{\epsilon_1 \epsilon_2 T \Delta t}{\tau^2}\right)^{1/2}\left(1 + \frac{n_1}{\epsilon_1 N}\right)^{-1/2}\left(1 + \frac{n_2}{\epsilon_2 N}\right)^{-1/2}\left(1 + \frac{S}{B}\right)^{-1/2}. \tag{6.5}$$

This equation shows that the signal-to-noise ratio can be increased by increasing the source strength N, leading to the conclusion that the most accurate results will be obtained with the smallest signal-to-background ratio. This analysis neglects, however, other important considerations (in particular, the differential and integral non-linearities of the system of time to pulse height converter and pulse height analyser, see §6.3), and in practice signal-to-background ratios of the order of unity or less are usually used, as in figure 39. Values of ϵ, N and N_T ($= \epsilon_1 \epsilon_2 N$) are typically of the order of 10^{-4}, 10^7 s^{-1} and 10^{-1} s^{-1} respectively, with ϵ sometimes being one or two orders of magnitude larger if very efficient mirrors and high transmission filters are used.

The type of excitation source used for photon–photon coincidence experiments has depended on the atoms being studied. In the case of mercury a simple vapour cell has been usual, the atoms being excited by electron impact with incident energies in the range from 30 eV to a few hundred eV. A similar technique was used for the measurements in Ne (Yamagishi and Inaba 1974). Masterson and Stoner (1973), on the other hand, used foil excitation (see also §4.2.1) and Camhy-Val, Dumont and co-workers used an argon glow discharge. King *et al* (1975b, 1976) have used an atomic or molecular beam crossed by an electron beam, thus limiting the volume of the excitation region and minimizing the effects of radiation trapping and collisional de-excitation.

The wavelength selective filters (see figure 38(*b*)) are usually narrow bandwidth interference filters, although in the case of the molecular studies of King *et al* (1975b), in which coincidences were measured between whole vibrational–rotational bands, it was possible to use broader-band dye filters. To minimize the probability of detecting spurious 'true' coincidences caused by extensive cosmic-ray showers it is usual to place the photomultipliers as far apart as possible, and to avoid the possibility of internal scintillations from one photomultiplier being detected by the other they are also usually placed out of sight of each other.

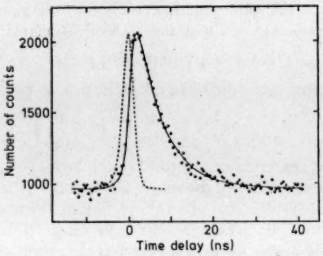

Figure 40. Delayed-coincidence spectrum for the 4p $^4D^o_{7/2}$ state of Ar II. The gas pressure was 3×10^{-4} Torr and the accumulation time was 22 h. The broken curve is the apparatus prompt response, measured with a Čerenkov source, and the full curve is the best fit obtained for the convolution of the prompt response with the decay function $\exp(-t/\tau)$. The resulting value of τ is $6{\cdot}21 \pm 0{\cdot}10$ ns (from King *et al* 1976).

The resolving time in these coincidence experiments is limited by the transit time spreads of the photomultipliers and the time jitter (spread in triggering times) in the discriminators which are used to derive timing signals from them. King *et al* (1976) measured the overall resolving time by using a 'prompt' source of photons, consisting of the Čerenkov radiation from a thallium-204 source in aqueous solution. The resulting prompt response function is shown in figure 40, together with a delayed-coincidence spectrum for the 4p $^4D^o_{7/2}$ state of Ar II. The width (FWHM) of the prompt response is 3 ns.

The measured delayed-coincidence spectrum $f(t)$ is the convolution of the prompt response $P(t)$ with the decay function $\exp(-t/\tau)$. In the work of King *et al* (1976) the lifetime τ was deduced by means of a least-squares fit of this convolution to the observed time spectrum, the variable parameters being the value of τ, the height of the background, and the height and centre position of $P(t)$. In this way the whole of the data, including the background data to the left of the decay curve, can be used to obtain an accurate value of τ. The lower limit to the magnitude of lifetimes which can be obtained with this analysis technique would be of the order of one-tenth the width of $P(t)$ (that is, about 0·3 ns). In earlier work (see also the next section) the prompt response was assumed to have a Gaussian shape, in which case the convolution of it with $\exp(-t/\tau)$ gives the function (Binder 1949)

$$f(t) = a + b\left[1 + \operatorname{erf}\left(\frac{t-t_0}{\sigma\sqrt{2}} - \frac{\sigma}{\tau\sqrt{2}}\right)\right] \exp\left(\frac{\sigma^2}{2\tau^2} - \frac{t-t_0}{\tau}\right) \qquad (6.6)$$

where σ and t_0 are the standard deviation and central position respectively of the Gaussian, erf is the normalized error function, $2b$ is the amplitude of the decay function and a is the height of the background. This function can then be used to give a least-squares fit to the experimental data points, treating τ, a, b, t_0 and σ as variable parameters. Most authors have, however, adopted the simpler approach of fitting only the right-hand tail of the observed function to a simple exponential, which is a valid procedure as long as the only data used are those for which the amplitude of the normalized prompt response function is negligible compared with the amplitude of the exponential decay function. This restriction results in a poorer statistical accuracy.

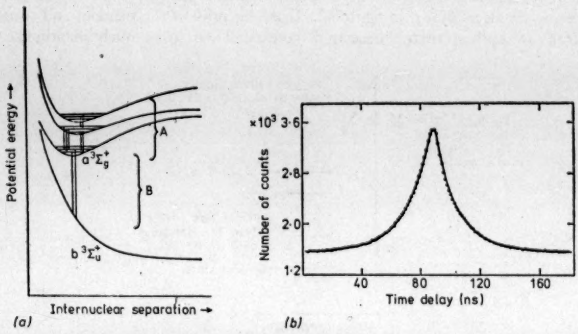

Figure 41. (*a*) Feeding (A) and decay (B) transitions for the a $^3\Sigma_g^+$ state of H_2. (*b*) Observed delayed-coincidence spectrum obtained without wavelength selection in the start and stop channels (from King *et al* 1975b).

It may sometimes happen, particularly in the case of molecular transitions, that the start and stop photons are sufficiently close in wavelength that they are not resolved by the interference filters. Figure 41 shows an example of such a case (King *et al* 1975b): the transitions (labelled A) which populate the a $^3\Sigma_g^+$ state overlap partially with the continuum (labelled B) for the decay of the state. This situation can be exploited by dispensing with wavelength selection and allowing both the feeding and decay transitions to actuate both the start and stop channels. The delayed-coincidence spectrum then becomes the superposition of two back-to-back delay curves, as shown in the figure. By appropriately analysing this spectrum King *et al* were able to obtain a second measurement of the lifetime of this state. Note that lifetimes of states which decay by continuum radiation are difficult or impossible to measure accurately by other techniques (except the electron–photon coincidence technique, see below). Note also that when the photon–photon coincidence method is used to measure lifetimes of molecular electronic states the values obtained are weighted averages over the rotational and vibrational sublevels of the state.

In general, the directions of the feeding (λ_1) and decay (λ_2) photons are partially correlated (see, for example, Devons and Goldfarb 1957, Frauenfelder and Steffen 1965, Brink and Satchler 1968). This does not affect lifetime measurements by the photon–photon coincidence technique unless a magnetic field exists in the source

region, in which case the intermediate excited state will undergo Larmor precession (see also §5) and the exponential decay function will become modulated, as observed by Popp *et al* (1970) and Dumont *et al* (1970). To avoid this the residual magnetic field must be small enough to ensure that the Larmor precessional period is much longer than the lifetime of the state.

Other possible sources of systematic error are discussed in §6.3.

6.2. The electron–photon coincidence method

The feeding transition λ_1 of figure 38(*a*) may be replaced by an inelastic electron scattering event, as shown in figure 42. If the energies of the incident and scattered electrons are both accurately measured the excited state is uniquely identified. One

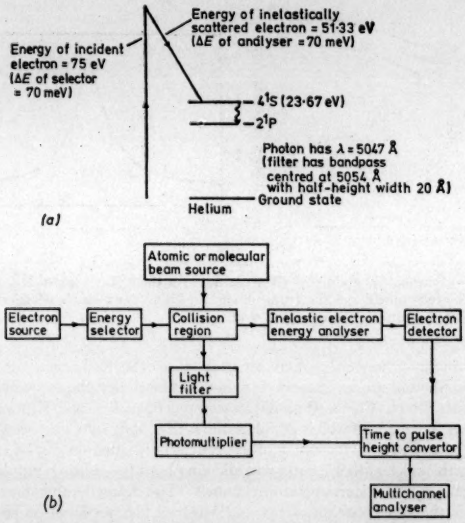
Energy of inelastically scattered electron = 51·33 eV (ΔE of analyser = 70 meV)
Energy of incident electron = 75 eV (ΔE of selector = 70 meV)
4¹S (23·67 eV)
2¹P
Photon has λ = 5047 Å (filter has bandpass centred at 5054 Å with half-height width 20 Å)
Helium
Ground state
(a)
Atomic or molecular beam source
Electron source
Energy selector
Collision region
Inelastic electron energy analyser
Electron detector
Light filter
Photomultiplier
Time to pulse height convertor
Multichannel analyser
(b)

Figure 42. (*a*) Schematic diagram of the transition used to measure the lifetime of the 4^1S level of He by the electron–photon coincidence method. (*b*) Block diagram of the apparatus used (from Imhof and Read 1969).

then has the inelastic electron–photon delayed-coincidence method. This method was first used by Imhof and Read (1969) and has since been used by these and other authors (for example, Imhof and Read 1971a, b, c, Peresse *et al* 1972, King *et al* 1975a) to measure many lifetimes in atoms and molecules, both neutral and ionic.

This method shares with the photon–photon coincidence method the advantages of being completely free from the effects of unwanted cascading from higher states and of being applicable to excited states which are often inaccessible to other precise methods.

The available incident electron currents are such that only low pressures of source gas are needed so that as in the photon–photon coincidence method the systematic errors of radiation trapping and collisional de-excitation are usually negligible (for an exception, see Smith *et al* 1973a). The efficiency ϵ_1 in the inelastic electron channel tends to be higher than that in the photon channel (see below), thus helping to improve the signal-to-noise ratio at a constant true-to-random ratio (see equation (6.5)). An advantage over the photon–photon coincidence method is that a wider range of states can be studied since the limitation that λ_1 must be in the range of single-photon detectors is removed. The electron–photon coincidence method is capable of achieving accuracies of approximately 0·5% (King and Adams 1974).

The methods of photon collection and detection are similar to those used in the photon–photon coincidence method. The energies of the incident and scattered electrons are determined by electrostatic energy selectors of either the hemispherical deflector type (for example, Imhof and Read 1971a, King and Adams 1974) or the cylindrical deflector type (Pochat *et al* 1972) and the inelastically scattered electrons are individually detected by channel electron multipliers. In both cases only electrons which have been scattered in a small angular range in the forward direction are detected, but since the scattering cross sections usually peak in this direction the efficiencies ϵ_1 tend to be high (of the order of 10^{-2}–10^{-3}) compared with efficiencies of the order of 10^{-4} for photon collection and detection. The electron energy resolution is typically 0·07 eV, which is sufficient to resolve the vibrational levels of most electronically excited states of diatomic molecules, thus enabling their separate lifetimes to be measured (Imhof and Read 1971a, b, Imhof *et al* 1972, Pochat *et al* 1973, Smith *et al* 1973a). In those cases in which two levels cannot be resolved in the electron channel (for example, the 4^1S and 4^1P states of helium) the excited state can still often be uniquely identified by the wavelength of the decay photons (see figure 42(*a*)).

The time resolution is limited by the transit time spread in the inelastic electron energy analyser (Imhof *et al* 1976) and is typically 10 ns. The apparatus prompt response function cannot be measured directly since a prompt source is not readily available and also the function is dependent on the electron and photon energies. Therefore it is necessary to assume the shape of the prompt response function (a Gaussian shape has been found to be a good approximation in practice (see §6.3)) and to analyse observed delayed-coincidence spectra by a least-squares fit to equation (6.6), treating the standard deviation of the Gaussian as one of the variable parameters. This would be a doubtful procedure for very short lifetimes of the order of one-half the width of the prompt response or less (that is, $\lesssim 5$ ns).

The electron–photon coincidence method has been extended by Smith *et al* (1975) and Shaw *et al* (1975) to measure lifetimes in ionic molecules and ionic atoms respectively. The principle of their method is illustrated in figure 43. In the reaction

$$e + M \rightarrow M^+ + e + e \tag{6.7}$$

the two outgoing electrons tend to share the available energy unequally, the most probable situation being that in which one electron (labelled the scattered electron in the figure) has nearly all the available energy while the other (the ejected electron) has much less (typically the probability that its energy is less than 1 eV is 5–10%). This unequal sharing of energy can be exploited to give a high coincidence yield by having a broad transmission window (of width about 1–3 eV) for the energy analyser at the position suitable for the higher energy scattered electrons, as shown in figure 43. The analyser then passes a high proportion of the electrons leading to the ionic excited state

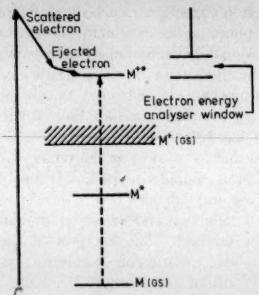

Figure 43. Measurement of ionic lifetimes by the electron–photon coincidence method (from Smith *et al* 1975).

of interest while rejecting those electrons leading to excited states of the neutral atom or molecule, or leading to higher lying ionic excited states (because these electrons have energies which are too high and too low respectively). The only electrons which are not rejected are those which have excited any lower lying ionic states, and if these exist they must be discriminated against in the photon channel. A typical coincidence delay spectrum is shown in figure 44.

A variant of this method is that of Backx *et al* (1973) who excited the B $^2\Sigma$ state of CO^+ by collisions with 10 keV electrons and used a triple coincidence technique to observe the inelastically scattered electrons, the decay photon and the molecular ion. They achieved an accuracy of 10% (50 ± 5 ns). Another recent variation of the electron–photon coincidence method is that of Bloch and Turner (1975) who have irradiated various diatomic and triatomic molecules with He I resonance radiation and have used the ejected photoelectrons to provide the timing start pulse. In this way they have measured five lifetimes with an accuracy of approximately 5–10%. In principle, scattered atoms or ions can also be used to provide the start pulse, but the energies of

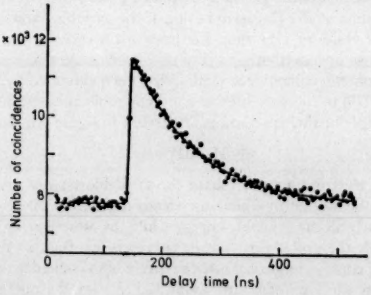

Figure 44. Delayed-coincidence spectrum for the A $^3\Pi_u$ state of CO_2^+. The full curve shows the best least-squares fit to equation (6.6) (from Smith *et al* 1975).

such particles would have to be less than about 1 keV in order to be able to distinguish different energy groups, and therefore the particle velocities would be low and the consequent timing variations would be large. Vassilev *et al* (1971), for example, have excited helium atoms by collision with helium ions and have looked at coincidences between de-excitation photons and scattered ions but the time resolution was insufficient for a lifetime measurement.

6.3. Experimental errors

The photon–photon and electron–photon coincidence methods are sufficiently accurate and free of the systematic errors which afflict many other methods that careful attention to further possible sources of error is warranted.

Although the start and stop counting rates are usually low ($\lesssim 10^4$ Hz) there is some possibility of pile-up distortion of the time spectrum caused by stop pulses being unrecorded due to the prior arrival of another stop pulse and resulting in a loss of coincidence counts at higher delay times. It may be possible to avoid this distortion, if the stop rate is much higher than the start rate, by simply interchanging the start and stop channels. Alternatively an electronic rejection device may be used to sense when two stop pulses arrive within the time range of the time to pulse height converter, and in this case to reject both pulses. Analytic correction can also be applied to spectra distorted by pile-up but it must be remembered that the probability of losing a 'true' stop pulse due to the prior arrival of a 'random' stop pulse is different from the probability of losing a random stop pulse due to the prior arrival of either a true or random stop pulse: a simple and accurate correction procedure has been described by Smith *et al* (1975).

Another distortion in the time delay occurs when excited atoms or molecules drift out of the field of view of the photon detector before they have decayed. This has been discussed by Dumont (1968) and Imhof and Read (1971a). The loss factor tends to be large for glow discharges having a high effective temperature and small size, but for atomic or molecular beams at room temperature the thermal drift effect is important only for light atoms and for times, T, longer than about 100 ns and correction factors can be easily computed for particular cases. The effect places an upper limit of the order of a few times 10^{-6} s on the lifetimes that can be measured by the photon–photon and electron–photon coincidence methods (the lower limits, as discussed above, are approximately 3×10^{-10} s and 5×10^{-9} s respectively).

Other sources of potential error lie in the differential and integral non-linearities of the timing system consisting of the time to pulse height converter and pulse height analyser. The differential non-linearities result in neighbouring channels having effectively different time widths so that the noise level of a time delay spectrum becomes higher than that expected from statistical considerations only (see equation (6.5)). This is particularly important when the true-to-random ratio is small but a correction may be made by subtracting a spectrum taken under the same conditions but consisting of a random background only (Camhy-Val *et al* 1969a). Integral non-linearities of the time to pulse height converter manifest themselves as non-linear distortions over the whole time spectrum and they can usually be minimized by operating only in the central region of the range of the converter. An associated source of systematic error is in the absolute time calibration of the system of time to pulse height converter and pulse height analyser: accurate calibration procedures have been described by Littman (1974) and Smith *et al* (1975).

A procedure which does much to indicate the absence or otherwise of systematic errors is the chi-squared test (see, for example, Bevington 1969). Each least-squares fit of a function $f(t)$, such as that of equation (6.6), to a set of experimental points $N_i(t_i)$ yields a value of χ^2, defined by

$$\chi^2 = \sum_{i=1}^{\nu} [f(t_i) - N_i]^2 \sigma_i^{-2} \tag{6.8}$$

where σ_i is the expected standard deviation of the observed value N_i (for example, in the case of Poisson statistics, which certainly apply to the coincidence experiments, $\sigma_i^2 = f(t_i)$). In the absence of systematic errors χ^2 has a value near ν, the total number of points, with a known probability distribution about ν. The likelihood of a single observed value of χ^2 can be measured by the probability $P(\chi^2)$, called the chi-squared probability, that this same value or a higher value would be obtained in subsequent similar measurements, assuming that the experimental errors are statistical only and that the function $f(t)$ is appropriate to the data. The observed values of $P(\chi^2)$ should be uniformly distributed between 0 and 100%. Figure 45 shows an example of a

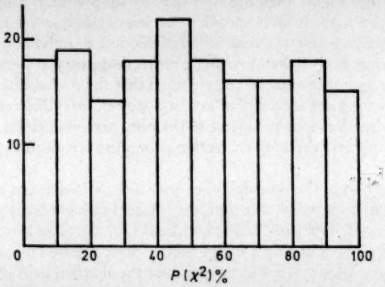

Figure 45. Histogram of frequency of observed values of the chi-squared probability $P(\chi^2)$ for a total of 174 electron–photon coincidence experiments.

histogram of $P(\chi^2)$ values taken from the early work of Imhof, Read and co-workers. Although this chi-squared test cannot reveal the presence of all systematic errors (for example, incorrect time calibrations), it is a powerful test for most systematic errors and it therefore deserves to be used more widely in the evaluation of reputedly accurate work.

Acknowledgments

We wish to thank those authors and journals who gave permission to reproduce or adapt figures, and Mr John Rowcroft for drawing the remaining figures. We thank also Miss Clara Nicholls for typing the manuscript and organizing the references, and our colleagues, in particular Dr George King, for reading and criticizing parts of the manuscript. One of us (FHR) is grateful to the Joint Institute of Laboratory Astrophysics, University of Colorado, for a Visiting Fellowship, during the tenure of which a part of this review was written.

Appendix 1. The analysis of decay curves

Most pulsed experiments, as well as foil excitation and similar experiments, yield as raw data decay curves in digital form, suitable for reduction by means of computers. Numerical data reduction techniques, therefore, form an important part of such experiments, both because by their means the best use is made of hard-won data and because a number of consistency checks can be made which help to judge the quality of the raw data or the appropriateness of the assumed decay model. Three fundamentally different approaches have been used in the analysis of decay curves: (*a*) least-squares methods, (*b*) the method of moments, and (*c*) mathematical transform methods, principally using Laplace transforms. These are briefly discussed in this appendix.

The raw data are assumed to be in the form of data points N_i such as those shown, for example, in figure 40, where N_i represents the intensity (often the number of single photons detected) in channel i, a time $t_i \pm \frac{1}{2}\Delta t$ after the instant of excitation and Δt is the width in time of the channels. The data points are assumed to be represented by a function $f(t)$ (full curve of figure 40) in the form

$$f(t)=a+bF(t) \tag{A1.1}$$

where a is the background, b is a scaling factor and $F(t)$ is the convolution (Newton 1950) of the instrumental response function $P(t)$ (broken curve of figure 40) and the probability function $g(t)$ of emission occurring a time t after excitation. Thus

$$F(t)=\int_{-\infty}^{+\infty} g(t')P(t-t')\,\mathrm{d}t'. \tag{A1.2}$$

F, g and P are assumed to be normalized probability distributions. If only a single exponential decay component is present, then

$$\begin{aligned} g(t)&=0 && (t<0)\\ g(t)&=\frac{1}{\tau}\exp(-t/\tau) && (t\geqslant 0) \end{aligned} \tag{A1.3}$$

and equation (A1.2) can be written in the form

$$F(t)=\frac{1}{\tau}\exp(-t/\tau)\int_{-\infty}^{t}\exp(u/\tau)P(u)\,\mathrm{d}u \tag{A1.4}$$

where the substitution $u=t-t'$ has been used. These are the basic relations used in the analysis of decay curves.

(*a*) *Least-squares methods*

Least-squares methods are the most widely used methods of decay curve analysis. A function $f(t)$ is assumed to represent a suitably chosen section from $i=i_1$ to $i=i_2$ of the data N_i and its parameters, including the lifetime to be determined, are chosen to minimize χ^2, the sum of the squares of the weighted residuals:

$$\chi^2=\sum_{i=i_1}^{i_2} w_i(f_i-N_i)^2 \tag{A1.5}$$

where w_i is the weight given to the ith data point and

$$f_i=a+\frac{b}{\Delta t}\int_{t_i-\frac{1}{2}\Delta t}^{t_i+\frac{1}{2}\Delta t} F(t)\,\mathrm{d}t$$

is the value of $f(t)$ in channel i. If N_i are single-photon counts then Poissonian statistics apply and (see Bevington (1969) for example)

$$w_i = f_i^{-1} \approx N_i^{-1}. \tag{A1.6}$$

The importance of using correct weights (and many other practical aspects of least-squares decay curve analysis) has been discussed by Grinvald and Steinberg (1974). The choice of the function f in equation (A1.5) depends on the experiment. The most commonly used form of analysis uses only the decaying 'tail' of the data because, as we can see by differentiating equation (A1.4) for the case when g is a single exponential decay function,

$$\frac{dF}{dt} = -\frac{1}{\tau}[F(t) - P(t)] \tag{A1.7}$$

and F satisfies the same differential equation as g for delay times long enough for P to be neglected in comparison with F. A similar conclusion applies to multi-exponential decays. The procedure is useful, therefore, for decay times that are long compared with the instrumental resolving time. Often the logarithms of the measured intensities (with the background a removed) are used because this linearizes the least-squares problem for single exponential decays and equation (A1.5) can be minimized algebraically. The semi-logarithmic representation is also useful for visually inspecting the data because deviations from exponentiality show up as deviations from linearity of the tail of the decay data. The main disadvantages are that the background must be determined separately and that the decay cannot be analysed into the region where it merges with the background because $(N_i - a)$ must be positive. The background can be determined from data well away from the influence of the decay and this can be inaccurate if the instrument suffers from integral non-linearities in the time scale. As τ and a are correlated, an error in the background will lead to an error in the lifetime. If an appreciable background is present, then it is better to fit directly to the data points N_i using a non-linear method to determine τ (see Bevington (1969), especially chap 11). The section of data used can then include the region where the decay curve merges into the background. Indeed, as $f_i = a$ at negative delay times, a section of background can be included directly in the analysis by extending the sums of equation (A1.5) over both regions. This method is much simpler than full convolution fitting (described below) and gives excellent results for lifetimes long compared with the instrumental resolving time. It cannot, of course, be used with data obtained with the foil-excitation technique where no measurements are possible at negative delay times.

For short lifetimes the full equation (A1.1) must be used in the analysis. If the prompt response function can be measured accurately, then the convolution of equation (A1.2) can be performed numerically with whatever function of g is appropriate and a non-linear least-squares method used to minimize χ^2 and thus to find the best parameters for g. This procedure has been used with a single exponential decay function to analyse the data of figure 40, for example. The source of prompt events in this case was a Čerenkov source, but other possibilities are available with other techniques. In optical-excitation experiments the excitation light pulses can be observed directly (but see end of §2.5 for a discussion of possible difficulties); in electron-impact excitation experiments, transition radiation can be used (see Mahan and Gallagher 1976). Lifetimes as short as, say, one-tenth the instrumental resolving time can be analysed in this way.

If the instrumental response function cannot be measured directly, then an approximate form can be either derived from a theoretical model or from other evidence. Although this is not as good as an accurately measured response function, it is still a more satisfactory procedure than 'tail-fitting', especially for data of low statistical accuracy. In the case of a Gaussian response function and a single exponential decay, the convolution integral can be performed analytically (see §6.1 and equation (6.6)) and this speeds up the computations. The deviations between the actual and the assumed shapes of the instrumental response function increase in importance with decreasing lifetime and the method cannot be used reliably with lifetimes that are comparable with the instrumental resolving time.

All the methods described so far can be extended to multiple exponential decays. In cases such as that of figure 9(*b*), for example, where two decays with widely different lifetimes seem to be indicated, least-squares analysis is straightforward. In general, however, the non-orthogonality of the exponential decay function leads to correlation among the parameters and no unique solution can be found, unless other information can be used to limit the ranges of the parameters. This is demonstrated, for example, in the data of figure 11 and also in several examples using synthesized data presented by Grinvald and Steinberg (1974).

(*b*) *The method of moments*

The method of moments was first proposed by Bay (1950) for the measurement of short nuclear lifetimes from delayed-coincidence spectra. It requires that the instrumental response function and the decay curve be measured under identical conditions which restricts the applicability of the method in atomic and molecular lifetime work considerably. The method is, however, relatively simple to apply even with short lifetimes and can be extended to analyse complex decays. The basis of the method is equation (A1.2), from which it can be shown that

$$M_r(F)=\sum_{k=0}^{r}\frac{r!}{k!(k-r)!}M_{r-k}(P)M_k(g) \tag{A1.8}$$

where

$$M_r(F)=\int_{-\infty}^{\infty}t^rF(t)\,\mathrm{d}t \tag{A1.9}$$

and similarly for $M_r(P)$ and $M_r(g)$ are the rth moments of F, P and g. If g is a single exponential decay of lifetime τ then, if we substitute $r=1$ into equation (A1.8),

$$\tau=M_1(F)-M_1(P) \tag{A1.10}$$

and the lifetime can be found from the first moments of F and P. These are determined from the raw data after subtraction of any background and normalization to unit area. Approximate extrapolations need to be made to extend the integrals to infinity.

Further relations among the moments, which allow analysis of multiple exponential decays, have been derived and tested with synthesized data by Isenberg and Dyson (1969) and the methods further developed by Isenberg *et al* (1973).

(*c*) *Mathematical transform methods*

The attraction of using Laplace or Fourier transforms of the data before analysis lies in the fact that the convolution of equation (A1.2) transforms in both cases into a

product. Thus

$$\mathscr{L}\{F(t)\} = \mathscr{L}\{g(t)\}\mathscr{L}\{P(t)\}$$

and

$$\mathscr{F}\{F(t)\} = \mathscr{F}\{g(t)\}\mathscr{F}\{P(t)\} \tag{A1.11}$$

where $\mathscr{L}$ and $\mathscr{F}$ have been used to represent Laplace and Fourier transformation respectively. A measured decay curve can therefore be deconvoluted using a measured instrumental response function. With Laplace transforms, for example, the single exponential decay function of equation (A1.3) transforms to

$$\mathscr{L}\left\{\frac{1}{\tau}\exp\left(-\frac{t}{\tau}\right)\right\} = \frac{1}{1+s\tau} \tag{A1.12}$$

where s is the variable in transform space. From equation (A1.11), therefore,

$$\frac{\mathscr{L}\{P(t)\}}{\mathscr{L}\{F(t)\}} = 1 + s\tau \tag{A1.13}$$

which is the basic equation used in this method (Helman 1971). The quotient of equation (A1.13) is evaluated for several different values of s by numerical integration, taking care to include extrapolations of the data to infinite delay times in some approximate way. The upper useful limit of s (corresponding to short-time behaviour at times of the order $1/s$) is determined by high-frequency noise in the data; the lower limit is given by the errors introduced by the extrapolations to infinite delay times. Intermediate values of s may be chosen to give a straight line with slope and intercept determined with standard deviations of the order of 1% in typical cases. For a decay measured over a delay time range of 30 ns with 0·6 ns channel width, for example, a range of values of s of 0·1–0·5 ns^{-1} are normally useful (Helman 1971).

Gafni *et al* (1975) extended the analysis to multiple exponential decays and tested the method with real and synthesized data.

A deconvolution using Fourier transforms is also possible with the added attraction that the deconvoluted decay can be transformed back into the time domain for visual inspection. The main difficulty seems to be high-frequency noise in the data which makes it impossible to determine the Fourier transforms at high frequencies. The noise may be 'filtered out' by multiplying the transform with some cut-off function, but this is equivalent to introducing a convolution in the time domain, heavy filtering being equivalent to convoluting with a broad function, thus reducing the time resolution in the reconstructed decay curve. Any gain in time resolution is therefore achieved at the expense of increased noise in the reconstructed decay curve. Helman (1971) discussed these difficulties and explored the method with several filtering functions. Some improvements in time resolution seem to be achievable with this method.

To summarize the methods of decay curve analysis described in this appendix, the least-squares methods are the most widely used and, with convolution fitting when necessary, seem to be the most satisfactory for several reasons. They do not require extrapolations of integrals to infinite delay times, they are applicable to experiments where negative delay times cannot be studied, or when the instrumental response function is not known accurately. Most importantly, they have in the χ^2 test (see §6.3) a most useful method of indicating the appropriateness of the data or the decay model. The Laplace transform method also has most of these features and seems to be an attractive alternative. The other methods can nevertheless be useful in some circumstances, especially the method of moments, which requires very little computer time

and power. Combinations of these methods also have their uses. For example, the method of moments can be used to provide initial parameters for non-linear least-squares iterations or the Fourier transform method can be used to replace the actual instrumental response function with a Gaussian one of known width before using equation (6.6) for analysis.

Appendix 2. Density matrices

Density matrices, and the derived quantities called spherical tensors or statistical tensors, offer a compact and powerful means of explaining and calculating many of the level-crossing, resonance and other effects discussed in this review and are being increasingly used for this purpose. We therefore give here a brief introduction to them and an example of their use. The relevant techniques and formalism were developed mostly for use in nuclear physics, although this work was derived in turn from earlier studies in statistical mechanics and atomic physics (Tolman 1938, Racah 1942). Many accounts of the subject exist, for example in the textbooks of Dicke and Wittke (1960), Brink and Satchler (1968) and Gill (1975), the reviews of Fano (1957), Devons and Goldfarb (1957), Frauenfelder and Steffen (1965), Carver and Partridge (1966), Fano and Macek (1973) and Steffen and Alder (1975), and the works of Barrat (1959a, b), Cohen-Tannoudji (1962a, b), Nédélec and Pebay-Peyroula (1964), Omont (1965a), D'yakonov (1965), Hadeishi (1967), Dumont and Decomps (1968) and Pancharatnam (1972a, b).

We saw in §5.2 that, in general, an excitation event will leave an atom in a 'mixed' or superposition state

$$\psi(t)=\sum_m a(m)\phi_m \tag{A2.1}$$

where $|a(m)|^2$ is the probability of finding the atom in the 'pure' eigenstate ϕ_m, and where we have ignored the radiative decay modes of the atom and its interaction with other atoms or external fields (but we will come back to these later). The mean value of any observable E is, for this particular atom,

$$\bar{E}=\langle\psi|E|\psi\rangle=\sum_{m,n} a(m)^* a(n)E_{mn} \tag{A2.2}$$

where

$$E_{mn}=\langle\phi_m|E|\phi_n\rangle. \tag{A2.3}$$

For an ensemble of N such atoms the mean value (now denoted by a double bar) of E is therefore

$$\bar{\bar{E}}=(1/N)\sum_{\alpha=1}^{N}\bar{E}_\alpha=\sum_{m,n}\rho_{nm}E_{mn}=\mathrm{Tr}\,(\rho E) \tag{A2.4}$$

where

$$\rho_{nm}=(1/N)\sum_{\alpha=1}^{N} a_\alpha(m)^* a_\alpha(n) \tag{A2.5}$$

which defines the density matrix ρ for this ensemble. The utility of this density matrix is that it contains all the information about all the observables of the system, but without containing sufficient information (about phases, etc) to allow detailed wave-functions to be reconstructed. Associated quantities, which are being increasingly used in atomic level-crossing and resonance studies, are the spherical tensors or

statistical tensors, defined by

$$\rho_q^k(J, J') = \sum_M (-1)^{J'+M'}(2k+1)^{1/2} \begin{pmatrix} J & J' & k \\ M & -M' & q \end{pmatrix} \rho_{Jm, J'M'}. \quad \text{(A2.6)}$$

If the atoms are subjected to external fields represented by the operator $\mathscr{H}$ the time development of the density matrix is given by

$$\dot{\rho} = -\frac{\mathrm{i}}{\hbar}[\mathscr{H}, \rho]. \quad \text{(A2.7)}$$

If in addition the atomic states are decaying at the rate Γ and are also being excited at the rate γ into states described by the density matrix ρ^0, the overall time dependence of ρ is given by

$$\dot{\rho} = -\frac{\mathrm{i}}{\hbar}[\mathscr{H}, \rho] - \frac{\Gamma}{\hbar}\rho + \frac{\gamma}{\hbar}\rho^0. \quad \text{(A2.8)}$$

After solving this equation the rate at which decay photons are detected can be obtained from equation (A2.4), where the matrix element $E_{J'M', JM}$ appropriate to the emission of photons of polarization $\boldsymbol{e}_i$ from the excited state to final states $J_f M_f$ is given by

$$E_{J'M', JM} \propto \sum_{M_f} \langle J'M'|\boldsymbol{e}_i.\boldsymbol{D}|J_f M_f\rangle\langle JM|\boldsymbol{e}_i.\boldsymbol{D}|J_f M_f\rangle^* \quad \text{(A2.9)}$$

where $\boldsymbol{D}$ is the vector electric dipole operator. One further fact that we need to know is that ρ transforms under a rotation $\mathscr{R}$ of the coordinate axes according to

$$\rho' = \mathscr{D}^J(\mathscr{R})\rho D^{J\dagger}(\mathscr{R}) \quad \text{(A2.10)}$$

for a single J of the excited state, where $\mathscr{D}^J$ is the rotation matrix of order J.

As an elementary example of the use of these formulae consider the beam–foil excitation of atoms from a state $J_i = 0$ to a state $J_f = 1$ and their subsequent decay in a transverse magnetic field $\boldsymbol{B}$. The superposition state of the excited atoms at the moment of excitation is

$$\psi(t) = a_{-1}|1, -1\rangle + a_0|1, 0\rangle + a_1|1, 1\rangle \quad \text{(A2.11)}$$

where

$$\sigma_0 = |a_0|^2$$

and $\quad \text{(A2.12)}$

$$\sigma_1 = |a_{-1}|^2 = |a_1|^2$$

are proportional to the cross sections for exciting the $M = 0$ and $M = \pm 1$ sublevels respectively. If the axis of quantization is taken along the beam direction (z) the average values of $a_{-1}a_0$, $a_{-1}a_1$ and a_0a_1 taken over an ensemble of atoms are zero, as pointed out in §5.2. Therefore the initial density matrix is given by

$$\rho^0 = \begin{pmatrix} \sigma_1 & 0 & 0 \\ 0 & \sigma_0 & 0 \\ 0 & 0 & \sigma_1 \end{pmatrix} \frac{1}{\sigma_0 + 2\sigma_1}. \quad \text{(A2.13)}$$

If $\mathscr{R}$ transforms the beam axis to the direction (y) of the magnetic field the rotation operator $\mathscr{D}^1(\mathscr{R})$ has the matrix representation (Edmonds 1957)

$$\mathscr{D}^1(0, \tfrac{1}{2}\pi, 0) = \tfrac{1}{2}\begin{pmatrix} 1 & \sqrt{2} & 1 \\ -\sqrt{2} & 0 & \sqrt{2} \\ 1 & -\sqrt{2} & 1 \end{pmatrix} \quad \text{(A2.14)}$$

and in this new frame the initial density matrix becomes

$$\rho^0 = \begin{pmatrix} \sigma_1+\sigma_0 & 0 & \sigma_1-\sigma_0 \\ 0 & 2\sigma_1 & 0 \\ \sigma_1-\sigma_0 & 0 & \sigma_1+\sigma_0 \end{pmatrix} \frac{1}{4\sigma_1+2\sigma_0}. \tag{A2.15}$$

Note that the non-zero off-diagonal elements $\rho_{11}{}^0$ and $\rho_{-1-1}{}^0$ imply coherence between the $M=\pm 1$ levels in this new frame if $\sigma_1 \neq \sigma_0$. The magnetic field $\boldsymbol{B}$, which is along the axis of quantization in the new frame, gives rise to the energy operator $g_J\mu_B \boldsymbol{B}.\boldsymbol{J}$ (see equation (5.1)) and therefore equation (A2.8) gives

$$\begin{aligned} \dot{\rho}_{MM'} &= -\frac{\mathrm{i}}{\hbar}\langle M|\mathscr{H}\rho - \rho\mathscr{H}|M'\rangle - \frac{\Gamma}{\hbar}\rho_{MM'} \\ &= -\frac{\mathrm{i}}{\hbar} g_J\mu_B \langle M|BM\rho - \rho BM'|M'\rangle - \frac{\Gamma}{\hbar}\rho_{MM'} \\ &= \left(-\mathrm{i}\omega_L(M-M') - \frac{\Gamma}{\hbar}\right)\rho_{MM'} \end{aligned} \tag{A2.16}$$

where ω_L is the Larmor angular frequency and the frame of reference is taken to be moving with the atoms. The solution of this equation, if the initial value of ρ is given by equation (A2.15), is

$$\rho(t) = \begin{pmatrix} (\sigma_1+\sigma_0) & 0 & (\sigma_1-\sigma_0)\exp(-2\mathrm{i}\omega_L t) \\ 0 & 2\sigma_1 & 0 \\ (\sigma_1-\sigma_0)\exp(2\mathrm{i}\omega_L t) & 0 & (\sigma_1+\sigma_0) \end{pmatrix} \frac{\exp(-\Gamma t/\hbar)}{4\sigma_1+2\sigma_0}. \tag{A2.17}$$

The matrix elements relevant to the detection of the emitted radiation are (Condon and Shortley 1963)

$$\langle 0, 0|\boldsymbol{D}|1, \pm 1\rangle = \mp k\sqrt{2}(\boldsymbol{e}_x \pm \mathrm{i}\boldsymbol{e}_y)$$

and (A2.18)

$$\langle 0, 0|\boldsymbol{D}|1, 0\rangle = k\boldsymbol{e}_z$$

where k is a constant and the $\boldsymbol{e}$ are unit vectors. Therefore, if light polarized along the beam direction (the new y direction) is detected the matrix E, called the efficiency matrix or the monitoring matrix, has the value

$$E = 2k^2 \begin{pmatrix} 1 & 0 & 1 \\ 0 & 0 & 0 \\ 1 & 0 & 1 \end{pmatrix} \tag{A2.19}$$

and hence equation (A2.4) gives for the detected intensity

$$I(t) \propto [(\sigma_1+\sigma_0) + (\sigma_1-\sigma_0)\cos 2\omega_L t]\exp(-\Gamma t/\hbar) \tag{A2.20}$$

showing quantum beats at twice the Larmor frequency. There is no oscillatory component in the light polarized along $\boldsymbol{B}$ (which agrees with the fact that any precessional motion is about $\boldsymbol{B}$) nor in the total emitted light (as proved more generally by Macek (1969, 1970)). The time average of the intensity is

$$\bar{I} \propto (\sigma_1+\sigma_0) + \frac{\sigma_1-\sigma_0}{1+(2\hbar\omega_L/\Gamma)^2} \tag{A2.21}$$

which is the expected Hanle signal (see §5.4).

This same example could also have been worked out in terms of spherical tensors. The initial spherical tensor, for example, can be obtained from equations (A2.6) and (A2.15) and has the non-zero components

$$\begin{aligned}
\rho_0{}^0 &= \frac{1}{\sqrt{3}}(\rho_{-1-1}+\rho_{00}+\rho_{11}) = (1/\sqrt{3}) \\
\rho_{-2}{}^2 &= \rho_{1-1} = \frac{\sigma_1-\sigma_0}{2(2\sigma_1+\sigma_0)} \\
\rho_0{}^2 &= \frac{1}{\sqrt{6}}(\rho_{-1-1}-2\rho_{00}+\rho_{11}) = \frac{\sigma_0-\sigma_1}{\sqrt{6}(2\sigma_1+\sigma_0)} \\
\rho_2{}^2 &= \rho_{-11} = \frac{\sigma_1-\sigma_0}{2(2\sigma_1+\sigma_0)}.
\end{aligned} \tag{A2.22}$$

The analogue of equation (A2.16) is the equation of motion

$$\dot{\rho}_q{}^k = iq\omega_L\rho_q{}^k - \Gamma_k\rho_q{}^k \tag{A2.23}$$

where we have now allowed the possibility that the multipole components k may have different relaxation rates Γ_k (see §5.6.1). For the initial density matrix $\rho(0)$ the solution of (A2.23) is

$$\rho_q{}^k = \rho_q{}^k(0)\exp(iq\omega_L t)\exp(-\Gamma_k t). \tag{A2.24}$$

An efficiency tensor E can be defined in terms of the efficiency matrix E (equation (A2.9)) in analogy with equation (A2.6), namely

$$E_q{}^k(J,J') = \sum_M (-1)^{J'+M'}(2k+1)^{1/2}\begin{pmatrix} J & J' & k \\ M & -M' & q\end{pmatrix} E_{JM,J'M'}. \tag{A2.25}$$

For the particular E defined by equation (A2.19), this gives

$$E_0{}^0 = \frac{4k^2}{\sqrt{3}} \qquad E_{-2}{}^2 = E_2{}^2 = 2k^2 \qquad E_0{}^2 = \frac{4k^2}{\sqrt{6}}. \tag{A2.26}$$

The analogue of equation (A2.4) is

$$\bar{E} = \mathrm{Tr}(\rho E) = \sum_{kq} \rho_q{}^k E_q{}^{k*} \tag{A2.27}$$

which reproduces the intensity given by equation (A2.20) if the Γ_k are taken to be equal.

It can be shown (by performing the summations over M and M_f in equations (A2.9) and (A2.25)) that the efficiency tensors are independent of the values of J and J_f (apart from a polarization-independent normalization) and depend only on the polarization direction $\boldsymbol{e}_i$, namely

$$E_q{}^k = \sum_{\mu=-1}^{+1} \epsilon_\mu(\epsilon_{\mu-q})^*(-1)^{\mu-1}(2k+1)^{1/2}\begin{pmatrix} 1 & 1 & k \\ \mu & (q-\mu) & -q\end{pmatrix} \tag{A2.28}$$

where the ϵ_μ are the polarization components of the light in terms of the spherical tensors of rank 1, with the z axis in the direction of the field, and are given by

$$\epsilon_0 \propto (\boldsymbol{e}_i)_z \qquad \epsilon_{\pm 1} \propto \mp\frac{1}{\sqrt{2}}[(\boldsymbol{e}_i)_x \pm i(\boldsymbol{e}_i)_y]. \tag{A2.29}$$

This property of the efficiency tensors is one of the advantages possessed by the statistical tensor approach. For the situation defined above (namely $(e_i)_y \neq 0$), $\epsilon_{\pm 1} \propto i$ and the values of $E_q{}^k$ are as given by equation (A2.26).

It follows from equation (A2.28) that the $E_q{}^k$ can only be of rank 0, 1 or 2 (this is essentially because electric dipole radiation has unit angular momentum). This means that photon detectors can be used to monitor the quantities $\rho_0{}^0$, $\rho_q{}^1$ and $\rho_q{}^2$, but that higher moments cannot be observed in this way. It is clear from equations (A2.22) that $\rho_0{}^0$ is proportional to the total number of excited atoms and that the $\rho_q{}^1$ represent the three components of the macroscopic dipole moment $\langle \boldsymbol{J} \rangle$ or in other words the 'orientation' of the ensemble of atoms. The quantity $\rho_0{}^2$ is a quadrupole moment of the population of M values and more generally the $\rho_q{}^2$ are the five quadrupole components of the distribution of M values, or in other words the $\rho_q{}^2$ specify the 'alignment' of the ensemble.

References

Abramson A S, Spears K J and Rice S A 1972 *J. Chem. Phys.* **56** 2291–308

Adler R 1967 *IEEE Spectrum* May 42–54

Aleksandrov E B 1963 *Opt. Spectrosc.* **14** 233–4

—— 1964 *Opt. Spectrosc.* **16** 209–11

Allen L, Jones D G C and Schofield D G 1969 *J. Opt. Soc. Am.* **59** 842–7

Althoff K 1955 *Z. Phys.* **141** 33–42

Altman E L and Chaika M P 1964 *Opt. Spectrosc.* **19** 538–41

Andersen T 1973 *Nucl. Instrum. Meth.* **110** 35–42

Andersen T, Jessen K A and Sørensen G 1970 *Nucl. Instrum. Meth.* **90** 35–9

Anderson R 1971 *Atomic Data* **3** 227–40

Andrä H J 1975 *Atomic Physics* **4** 635–49

Andrä H J, Gaupp A, Tillmann K and Wittmann W 1973a *Nucl. Instrum. Meth.* **110** 453–7

Andrä H J, Gaupp A and Wittmann W 1973b *Phys. Rev. Lett.* **31** 501–4

Backx C, Klewer M and Van der Wiel M J 1973 *Chem. Phys. Lett.* **20** 100–2

Barrat J P 1959a *J. Physique* **20** 541–8

—— 1959b *J. Physique* **20** 633–46

—— 1959c *J. Physique* **20** 657–68

Barton R D and King M E 1971 *Nucl. Instrum. Meth.* **97** 359–70

Bashkin S 1974 *Progress in Optics* vol XII (Amsterdam: North Holland) pp289–344

Bashkin S, Malmberg P R, Meinel A B and Tilford S G 1964 *Phys. Lett.* **10** 63–4

Bashkin S and Meinel A B 1964 *Astrophys. J.* **139** 413–6

Bästlein C, Baumgartner G and Brosa B 1969 *Z. Phys.* **218** 319–26

Baumgartner G, Demtröder W and Stock M 1970 *Z. Phys.* **232** 462–72

Bay Z 1950 *Phys. Rev.* **77** 419

Bayliss W E 1968 *Phys. Lett.* **26** A414–5

Becker K H, Capelle G A, Haaks D and Tatarczyk T 1974a *Berichte der BunsenGesellschaft* **78** 1157–60

Becker K H, Haaks D and Tatarczyk T 1974b *Chem. Phys. Lett.* **25** 564–7

Bell R E 1965 *Alpha, Beta and Gamma Ray Spectroscopy* ed K Siegbahn (Amsterdam: North Holland) pp997–1198

Bennett W R Jr 1961 *Advances in Quantum Electronics* ed J Singer (New York: Columbia University Press) pp28–43

Bennett W R Jr and Kindlmann P J 1966 *Phys. Rev.* **149** 38–51

Bennett W R Jr, Kindlmann P J and Mercer G N 1965 *Appl. Opt. Suppl. 2, Chemical Lasers* 34–57

Berry H G, Curtis L J, Ellis D G and Schectman R M 1974 *Phys. Rev. Lett.* **32** 751–4

Berry H G, Curtis L J and Schectman R M 1975 *Phys. Rev. Lett.* **34** 509–12

Berry H G, Curtis L J and Subtil J L 1972 *J. Opt. Soc. Am.* **62** 771–3

BEVINGTON P R 1969 *Data Reduction and Error Analysis for the Physical Sciences* (New York: McGraw-Hill)
BEYER R A and LINEBERGER W C 1973 *Chem. Phys. Lett.* **20** 600–4
—— 1975 *J. Chem. Phys.* **62** 4024–31
BEYER R A, ZITTEL P F and LINEBERGER W C 1975 *J. Chem. Phys.* **62** 4016–23
BICKEL W S, BERGSTRÖM I, BUCHTA R, LUNDIN L and MARTINSON I 1969 *Phys. Rev.* **178** 118–21
BICKEL W S and BUCHTA R 1974 *Phys. Scr.* **9** 148–50
BINDER D 1949 *Phys. Rev.* **76** 856–7
BITTER F 1949 *Phys. Rev.* **76** 833–5
BLOCH M and TURNER D W 1975 *Chem. Phys. Lett.* **30** 344–6
BOESL U, NEUSSER H J and SCHLAG E W 1975a *Chem. Phys. Lett.* **31** 1–6
—— 1975b *Chem. Phys. Lett.* **31** 7–11
BRANNEN E, HUNT F R, ADLINGTON R H and NICHOLLS R W 1955 *Nature* **175** 810–1
BREHM B, DEMTRÖDER W and OSBERGHAUS O 1961 *Z. Naturf.* **16a** 843
BREIT G 1924 *Phil. Mag.* **47** 832–42
—— 1933 *Rev. Mod. Phys.* **5** 91–140
BREWER L, JAMES C G, BREWER R G, STAFFORD F E, BERG R A and ROSENBLATT G M 1962 *Rev. Sci. Instrum.* **33** 1450–5
BRIDGETT K A and KING T A 1967 *Proc. Phys. Soc.* **92** 75–8
BRINK D M and SATCHLER G R 1968 *Angular Momentum* (Oxford: Clarendon Press)
BROMANDER J 1973 *Nucl. Instrum. Meth.* **110** 11–7
BROPHY J H, SILVER J A and KINSEY J L 1974 *Chem. Phys. Lett.* **28** 418–21
BROSSEL J and BITTER F 1952 *Phys. Rev.* **86** 308–16
BROSSEL J and KASTLER A 1949 *C.R. Acad. Sci., Paris* **229** 1213–5
BROSSEL J, SAGALYN P and BITTER F 1950 *Phys. Rev.* **79** 225–6
BROYER M, LEHMANN J-C and VIGUÉ J 1975 *J. Physique* **36** 235–41
BROYER M and VIGUÉ J 1974 *Méthodes de Spectroscopie sans Largeur Doppler* (Paris: CNRS) pp185–94
BRUS L E and MCDONALD J R 1974 *J. Chem. Phys.* **61** 97–105
BRZOZOWSKI J, ELANDER N and ERMAN P 1974a *Phys. Scr.* **9** 99–103
BRZOZOWSKI J, ELANDER N, ERMAN P and LYYRA M 1974b *Phys. Scr.* **10** 241–3
BUCKA H 1969 *J. Physique* **30** C1 3–9
BUCKA H, KOPFERMANN H and OTTEN E W 1959 *Ann. Phys., NY* **4** 39–49
BUDICK B 1967 *Adv. Atom. Molec. Phys.* **3** 73–118
BUDICK B, MARCUS S and NOVICK R 1965 *Phys. Rev.* **140** A1041–3
BURNHAM R L, ISLER R C and WELLS W C 1972 *Phys. Rev.* A **6** 1327–40
BYRON F W and FOLEY H M 1964 *Phys. Rev.* **134** A625–37
CAMHY-VAL C, DREUX M, DUMONT A M and MARCHAL J 1969a *Nucl. Instrum. Meth.* **70** 5–8
CAMHY-VAL C and DUMONT A M 1968a *Nucl. Instrum. Meth.* **64** 211–3
—— 1968b *C.R. Acad. Sci., Paris* **267** 689–91
—— 1970 *Astron. Astrophys.* **6** 27–50
CAMHY-VAL C, DUMONT A M, DREUX M, PERRET L and VANDERRIEST C 1975 *J. Quant. Spectrosc. Radiat. Transfer* **15** 527–30
CAMHY-VAL C, DUMONT A M, DREUX M and VITRY R 1969b *C.R. Acad. Sci., Paris* **268** 1017–9
—— 1970 *Phys. Lett.* **32A** 233–4
CAMPOS J 1971 *Anal. Fis.* **67** 439–48
CAMPOS J and ZURRO B 1973 *Anal. Fis.* **69** 299–302
CAPELLE G A and BROIDA H P 1973 *J. Chem. Phys.* **58** 4212–22
CAPELLE G A, JOHNSON S E and BROIDA H P 1972 *J. Chem. Phys.* **56** 6264–5
CAPELLE G A, SAKURAI K and BROIDA H P 1971 *J. Chem. Phys.* **54** 1728–30
CARVER T R and PARTRIDGE R B 1966 *Am. J. Phys.* **34** 339–50
CHANG S, GUPTA R and HAPPER W 1971 *Phys. Rev. Lett.* **27** 1036–9
CHÉRON B and BARRAT J-P 1968 *C.R. Acad. Sci., Paris, Séries B* **266** 1324–7
CHURCH D A, KOLBE W, MICHEL M C and HADEISHI T 1974 *Phys. Rev. Lett.* **33** 565–8
CHURCH D A and LIU C H 1973 *Nucl. Instrum. Meth.* **110** 147–9
CHUTJIAN A, LINK J K and BREWER L 1967 *J. Chem. Phys.* **46** 2666–75
COATES P B 1972 *J. Phys. E: Sci. Instrum.* **5** 148–50
CODLING K 1974 *Phys. Scr.* **9** 247–56
COHEN-TANNOUDJI C 1962a *Ann. Phys., NY* **7** 423–61

COHEN-TANNOUDJI C 1962b *Ann. Phys., NY* **7** 469–504
—— 1975 *Atomic Physics* **4** 589–614
COLEGROVE F D, FRANKEN P A, LEWIS R R and SANDS R H 1959 *Phys. Rev. Lett.* **3** 420–2
CONDON E U and SHORTLEY G H 1963 *The Theory of Atomic Spectra* (Cambridge: Cambridge University Press)
COPELAND J E 1972 *J. Chem. Phys.* **56** 689–91
COPELAND J E and FOWLER R G 1970 *Rev. Sci. Instrum.* **41** 1422–5
COPLEY J, KIBBLE B P and KRAUSE L 1967 *Phys. Rev.* **163** 34–5
CORNEY A 1969 *Adv. Electron. Electron Phys.* **29** 115–231
CORNEY A and SERIES G W 1964a *Proc. Phys. Soc.* **83** 207–12
—— 1964b *Proc. Phys. Soc.* **83** 213–6
CUNNINGHAM P T 1968 *J. Opt. Soc. Am.* **58** 1507–9
CUNNINGHAM P T and LINK J K 1967 *J. Opt. Soc. Am.* **57** 1000–7
CURTIS L J and SMITH W H 1974 *Phys. Rev.* A **9** 1537–42
DAGDIGIAN P J, CRUSE H W and ZARE R N 1974 *J. Chem. Phys.* **60** 2330–9
—— 1975 *J. Chem. Phys.* **62** 1824–33
DALBY F W, BROYER M and LEHMANN J-C 1974 *Méthodes de Spectroscopie sans Largeur Doppler* (Paris: CNRS) pp227–30
DAVIS C C and KING T A 1972 *J. Phys. E: Sci. Instrum.* **5** 1072–4
DEECH J S, LUYPAERT R and SERIES G W 1975 *J. Phys. B: Atom. Molec. Phys.* **8** 1406–14
DELGADO A, CAMPOS J and SÁNCHEZ DEL RIO 1972 *Z. Phys.* **257** 9–13
DEMTRÖDER W 1962 *Z. Phys.* **166** 42–55
DEVONS S and GOLDFARB L J B 1957 *Handb. Phys.* **42** 362–554
DICKE R H and WITTKE J P 1960 *Introduction to Quantum Mechanics* (Reading, Massachusetts: Addison-Wesley)
DODD J N, ENEMARK E A and GALLAGHER A 1969 *J. Chem. Phys.* **50** 4838–42
DODD J N, FOX W N, SERIES G W and TAYLOR M J 1959 *Proc. Phys. Soc.* **74** 789–91
DODD J N, KAUL R D and WARRINGTON D M 1964 *Proc. Phys. Soc.* **84** 176–8
DODD J N, SANDLE W J and ZISSERMANN D 1967 *Proc. Phys. Soc.* **92** 497–504
DODD J N and SERIES G W 1961 *Proc. R. Soc.* A **263** 353–70
DONOVAN J W and DUNCAN A B F 1961 *J. Chem. Phys.* **35** 1389–91
DOUGLAS A E 1966 *J. Chem. Phys.* **45** 1007–15
DUCLOY M, VIGUÉ J and BROYER M 1974 *Méthodes de Spectroscopie sans Largeur Doppler* (Paris: CNRS) pp241–6
DUFAY M 1970 *Nucl. Instrum. Meth.* **90** 15–23
—— 1973 *Nucl. Instrum. Meth.* **110** 79–87
DUMONT A M 1968 *J. Quant. Spectrosc. Radiat. Transfer* **8** 1551–4
DUMONT A M, CAMHY-VAL C, DREUX M and VITRY R 1970 *C.R. Acad. Sci., Paris* **271** 1021–4
DUMONT M 1974 *Méthodes de Spectroscopie sans Largeur Doppler* (Paris: CNRS) pp235–40
DUMONT M and DECOMPS B 1968 *J. Physique* **29** 181–95
D'YAKONOV M I 1965 *Opt. Spectrosc.* **19** 372–5
D'YAKONOV M I and PEREL V I 1965a *Sov. Phys.–JETP* **20** 997–1004
—— 1965b *Sov. Phys.–JETP* **21** 227–31
ECK T G 1973 *Phys. Rev. Lett.* **31** 270–3
—— 1974 *Phys. Rev. Lett.* **33** 1055–7
ECK T G, FOLDY L L and WIEDER H 1963 *Phys. Rev. Lett.* **10** 239–42
EDMONDS A R 1957 *Angular Momentum in Quantum Mechanics* (Princeton, NJ: Princeton University Press)
ELDRIGE J A 1924 *Phys. Rev.* **23** 772–3
ENEMARK E A and GALLAGHER A 1969 *Rev. Sci. Instrum.* **40** 40–1
ERDMANN T A, FIGGER H and WALTHER H 1972 *Opt. Commun.* **6** 166–8
ERMAN P 1972 *Research Institute for Physics, Annual Report, Stockholm* pp117–32
—— 1975 *Phys. Scr.* **11** 65–78
ERMAN P and BERRY H G 1971 *Phys. Lett.* **34A** 1–2
ERMAN P, BERRY H G, LUNDIN L and SIGFRIDSSON B 1972 *FOA Report* **6** No 3, 1–9
ERMAN P and BRZOZOWSKI J 1973 *Phys. Lett.* **46A** 79–80
ERMAN P, LYYRA M and MARTINSON I 1974 *Phys. Lett.* **49A** 41–2
ERMAN P and MARTINSON I 1973 *Phys. Scr.* **8** 269–73
FANO U 1957 *Rev. Mod. Phys* **29** 74–93

FANO U and MACEK J H 1973 *Rev. Mod. Phys.* **45** 553–73
FAURE A, NÉDÉLEC O and PEBAY-PEYROULA J-C 1963 *C.R. Acad. Sci., Paris* **156** 5088–90
FELD M S and JAVAN A 1969 *Phys. Rev.* **177** 540–62
FELD M S, SANCHEZ A, JAVAN A and FELDMAN B J 1974 *Méthodes de Spectroscopie sans Largeur Doppler* (Paris: CNRS) pp87–104
FEOFILOV P P 1961 *The Physical Basis of Polarized Emission* (New York: Consultants Bureau)
FICHTNER W and HÄCKER W 1976 *Rev. Sci. Instrum.* **47** 374–7
FIGGER H, HELDT J, SIOMOS K and WALTHER H 1975 *Astron. Astrophys.* **43** 389–94
FIGGER H, SIOMOS K and WALTHER H 1974 *Z. Phys.* **270** 371–6
FINK U 1968 *J. Opt. Soc. Am.* **58** 937–40
FOSTER E W 1964 *Rep. Prog. Phys.* **27** 469–551
FOWLER R G, HOLZBERLEIN T M, JACKOBSON C H and CORRIGAN S J B 1964 *Proc. Phys. Soc.* **84** 539–43
FRANKEN P A 1961 *Phys. Rev.* **121** 508–12
FRANZEN W 1959 *Phys. Rev.* **115** 850–6
FRAUENFELDER H and STEFFEN R M 1965 *Alpha, Beta and Gamma Ray Spectroscopy* ed K Siegbahn (Amsterdam: North Holland) pp905–30
FREUND R S and MILLER T A 1974 *Méthodes de Spectroscopie sans Largeur Doppler* (Paris: CNRS) pp201–20
GAFNI A, MODLIN R L and BRAND L 1975 *Biophys. J.* **15** 263–80
GALLAGHER A 1967 *Phys. Rev.* **157** 24–30
—— 1975 *Atomic Physics* **4** 559–74
GALLAGHER A and LEWIS E L 1974 *Phys. Rev.* A **10** 231–41
GALLAGHER A and LURIO A 1963 *Phys. Rev. Lett.* **10** 25–6
—— 1964 *Phys. Rev.* **136** A87–105
GALLAGHER T F, EDELSTEIN S A and HILL R M 1975a *Phys. Rev.* A **11** 1504–6
—— 1975b *Phys. Rev. Lett.* **35** 644–7
GERMAN K R 1975a *J. Chem. Phys.* **62** 2584–7
—— 1975b *J. Chem. Phys.* **63** 5252–5
GERMAN K R, BERGEMAN T H, WEINSTOCK E M and ZARE R N 1973 *J. Chem. Phys.* **58** 4304–18
GERMAN K R and ZARE R N 1969a *Phys. Rev.* **186** 9–13
—— 1969b *Phys. Rev. Lett.* **23** 1207–9
GERMAN K R, ZARE R N and CROSLEY D R 1971 *J. Chem. Phys.* **54** 4039–44
GILL R D 1975 *Gamma-Ray Angular Correlations* (London: Academic Press)
GORNIK W, KAISER D, LANGE W, LUTHER J, MEIER K, RADLOFF H H and SCHULZ H H 1973a *Phys. Lett.* **45A** 219–20
GORNIK W, KAISER D, LANGE W, LUTHER J, RADLOFF H H and SCHULZ H H 1973b *Appl. Phys.* **1** 285–6
GORNIK W, KAISER D, LANGE W, LUTHER J and SCHULZ H H 1972 *Opt. Commun.* **6** 327–8
GOUGH W 1967 *Proc. Phys. Soc.* **90** 287–96
GRAF P 1972 *Alta Frequenza* **41** 726–43
GRINVALD A and STEINBERG I Z 1974 *Analyt. Biochem.* **59** 583–98
GUTTMAN C and RICE S A 1974a *J. Chem. Phys.* **61** 651–60
—— 1974b *J. Chem. Phys.* **61** 661–5
HABIB E E, KIBBLE B P and COPLEY G 1968 *Appl. Opt.* **7** 673–5
HADEISHI T 1967 *Phys. Rev.* **162** 16–22
HADEISHI T, BICKEL W S, GARCIA J D and BERRY H G 1969 *Phys. Rev. Lett.* **23** 65–7
HADEISHI T and NIERENBERG W A 1965 *Phys. Rev. Lett.* **14** 891–2
HALPERN A M and WARE W R 1971 *J. Chem. Phys.* **54** 1271–6
HAMEL J, MARGERIE J and BARRAT J-P 1974 *Opt. Commun.* **12** 409–13
HANLE W 1923 *Naturw.* **11** 690–1
—— 1924 *Z. Phys.* **30** 93–105
—— 1925 *Egebn. Exakt Naturw.* **4** 214–32
HÄNSCH T W 1972 *Appl. Opt.* **11** 895–8
—— 1973 *Topics in Applied Physics. Vol 1 Dye Lasers* (Berlin: Springer Verlag) pp194–259
HAPPER W and SALOMAN E B 1965 *Phys. Rev. Lett.* **15** 441–3
HARDE H and GUTHÖHRLEIN G 1974 *Phys. Rev.* A **10** 1488–93
HAROCHE S, PAISNER J A and SCHAWLOW A L 1973 *Phys. Rev. Lett.* **30** 948–51
HEAPS W S, HAMILTON W D and YEN W M 1973 *Opt. Commun.* **9** 304–5

HELDT J, FIGGER H, SIOMOS K and WALTHER H 1975 *Astron. Astrophys.* **39** 371–5
HELMAN WP 1971 *Int. J. Radiat. Phys. Chem.* **3** 283–94
HERMAN RM 1975 *Phys. Rev. Lett.* **35** 1626–9
HERON S, MCWHIRTER RWP and RHODERICK EH 1954 *Nature* **174** 564–5
—— 1956 *Proc. R. Soc.* A **234** 565–83
HESS H 1975 *J. Phys. D: Appl. Phys.* **8** 685–9
HESSER JE 1968 *J. Chem. Phys.* **48** 2518–35
HOGAN P and DAVIS DD 1974 *Chem. Phys. Lett.* **29** 555–7
HOLLEMAN GW and STEINFELD JI 1971 *Chem. Phys. Lett.* **12** 431–3
HOLSTEIN T 1947 *Phys. Rev.* **72** 1212–33
HOLT RA and PIPKIN FM 1974 *Phys. Rev.* A **9** 581–4
HOLZBERLEIN TM 1964 *Rev. Sci. Instrum.* **35** 1041–6
HULPKE E, PAUL E and PAUL W 1964 *Z. Phys.* **177** 257–68
HUI M and RICE SA 1972 *Chem. Phys. Lett.* **17** 474–7
—— 1974 *J. Chem. Phys.* **61** 833–42
IMHOF RE, ADAMS A and KING GC 1976 *J. Phys. E: Sci. Instrum.* **9** 138–42
IMHOF RE and READ FH 1969 *Chem. Phys. Lett.* **3** 652–4
—— 1971a *J. Phys. B: Atom. Molec. Phys.* **4** 450–60
—— 1971b *J. Phys. B: Atom. Molec. Phys.* **4** 1063–9
—— 1971c *Chem. Phys. Lett.* **11** 326–8
IMHOF RE, READ FH and BECKETT ST 1972 *J. Phys. B: Atom. Molec. Phys.* **5** 896–902
ISENBERG I and DYSON RD 1969 *Biophys. J.* **9** 1337–50
ISENBERG I, DYSON RD and HANSON R 1973 *Biophys. J.* **13** 1090–115
JACKSON WM 1974 *J. Chem. Phys.* **61** 4177–82
JEUNEHOMME M and DUNCAN ABF 1964 *J. Chem. Phys.* **41** 1692–9
JIMÉNEZ E, CAMPOS J and SÁNCHEZ DEL RIO C 1974 *J. Opt. Soc. Am.* **64** 1009–10
JOHNSON AW and FOWLER RG 1970 *J. Chem. Phys.* **53** 65–72
JOHNSON SE 1972 *J. Chem. Phys.* **56** 149–54
JOHNSON SE, CAPELLE G and BROIDA HP 1972 *J. Chem. Phys.* **56** 663–5
JONES OC 1964 *J. Sci. Instrum.* **41** 653–61
JOURDAN A, NEGRE JM, DUFAYARD J and NÉDÉLEC O 1976 *J. Physique Lett.* **37** L29–31
KAISER D 1975 *Phys. Lett.* **51A** 375–6
KALITEJEWSKI NI and TSCHAIKA M 1975 *Atomic Physics* **4** 19–45
KASTLER A 1973 *Nucl. Instrum. Meth.* **110** 259–65
KAUL RD 1966 *J. Opt. Soc. Am.* **56** 1262–3
—— 1967 *J. Opt. Soc. Am.* **57** 1156–7
KAY L 1963 *Phys. Lett.* **5** 36–7
—— 1965 *Proc. Phys. Soc.* **85** 163–6
KAY L and LIGHTFOOT B 1970 *Nucl. Instrum. Meth.* **90** 289–94
KEYSER LF, LEVINE SZ and KAUFMAN F 1971 *J. Chem. Phys.* **54** 355–63
KHADJAVI A, LURIO A and HAPPER W 1968 *Phys. Rev.* **167** 128–35
KIBBLE BP, COPLEY G and KRAUSE L 1967a *Phys. Rev.* **153** 9–12
—— 1967b *Phys. Rev.* **159** 11–3
KINDLMANN PJ and SUNDERLAND J 1966 *Rev. Sci. Instrum.* **37** 445–51
KING GC and ADAMS A 1974 *J. Phys. B: Atom. Molec. Phys.* **7** 1712–8
KING GC, ADAMS A and CVEJANOVIĆ D 1975a *J. Phys. B: Atom. Molec. Phys.* **8** 365–71
KING GC, MOHAMED KA, READ FH and IMHOF RE 1976 *J. Phys. B: Atom. Molec. Phys.* **9** 1247–50
KING GC, READ FH and IMHOF RE 1975b *J. Phys. B: Atom. Molec. Phys.* **8** 665–73
KLOSE JZ 1966 *Phys. Rev.* **141** 181–6
KNIGHT AEW and SELINGER BK 1973a *Aust. J. Chem.* **26** 1–27
—— 1973b *Aust. J. Chem.* **26** 499–504
KNIGHT AEW, SELINGER BK and ROSS IG 1973 *Aust. J. Chem.* **26** 1159–72
KROLL M 1975 *J. Chem. Phys.* **63** 1803–9
KUHN HG 1969 *Atomic Spectra* (London: Longmans)
KURZWEG L, EGBERT GT and BURNS DJ 1973 *J. Chem. Phys.* **59** 2641–5
KUSCH P and HUGHES VW 1969 *Handb. Phys.* **37/1** 1–172
KUZNETSOVA LA, KUZ'MENKO NE, KUZYAKOV YU YA and PLASTININ YU A 1974 *Sov. Phys.–Usp.* **17** 405–23

LAMB W E 1964 *Phys. Rev.* **134** A1429–49
LANIEPCE B 1968 *J. Physique* **29** 427–33
LAOR U and LUDWIG P K 1971 *J. Chem. Phys.* **54** 1054–7
LAWRENCE G M 1965 *J. Quant. Spectrosc. Energy Transfer* **5** 359–67
—— 1966 *Colloq. Int. CNRS* 239–45
—— 1969 *Douglas Advanced Research Laboratories Research Communication* 93
LEWIS C and WARE W R 1973 *Rev. Sci. Instrum.* **44** 107–14
LEWIS E L and SILVER J D 1975 *J. Phys. B: Atom. Molec. Phys.* **8** 2697–707
LINDQVIST L, LOPEZ-DELGADO R, MARTIN M M and TRAMER A 1974 *Opt. Commun.* **10** 283–7
LINK J K 1966 *J. Opt. Soc. Am.* **56** 1195–9
LITTMAN M G 1974 *Rev. Sci. Instrum.* **45** 1608–9
LIU C H, BASHKIN S, BICKEL W S and HADEISHI T 1971 *Phys. Rev. Lett.* **26** 222–4
LIU C H, BASHKIN S and CHURCH D A 1974 *Phys. Rev. Lett.* **33** 993
LIU C H and CHURCH D A 1972 *Phys. Rev. Lett.* **29** 1208–11
LOPER J L and LEE E K C 1972 *Chem. Phys. Lett.* **13** 140–3
LOPEZ-DELGADO R, TRAMER A and MUNRO I H 1974 *Chem. Phys.* **5** 72–83
LURIO A 1965 *Phys. Rev.* **140** A1505–8
MCCLELLAND G M and YARDLEY J T 1973 *J. Chem. Phys.* **58** 4368–73
MCCLINTOCK M, DEMTRÖDER W and ZARE R N 1969 *J. Chem. Phys.* **51** 5509–21
MACEK J 1969 *Phys. Rev. Lett.* **23** 1–2
—— 1970 *Phys. Rev.* A **1** 618–27
MAHAN A H and GALLAGHER A 1976 *Rev. Sci. Instrum.* **47** 81–3
MALMBERG P R, BASHKIN S and TILFORD S G 1965 *Phys. Rev. Lett.* **15** 98–100
MARÉCHAL M A, JOST R and LOMBARDI M 1972 *Phys. Rev.* A **5** 732–40
MARKOVA G, KHVOSTENKO G and CHAIKA M 1967 *Opt. Spectrosc.* **23** 456–7
MARTINSON I 1974 *Phys. Scr.* **9** 281–96
MASTERSON K D and STONER J O JR 1973 *Nucl. Instrum. Meth.* **110** 441–4
MEYER K A and CROSLEY D R 1973 *J. Chem. Phys.* **59** 1933–41
MITCHELL A C G and ZEMANSKY M W 1934 *Resonance Radiation and Excited Atoms* (Cambridge: Cambridge University Press)
MÖHLMANN G R, BHUTANI K K, DE HEER F J and TSURUBUCHI S 1976 *Preprint*
MOORE C B 1971 *Ann. Rev. Phys. Chem.* **22** 387–428
MOTT N F and MASSEY H S W 1965 *The Theory of Atomic Collisions* (Oxford: Clarendon Press) 3rd edn
NÉDÉLEC O and PEBAY-PEYROULA J-C 1964 *C.R. Acad. Sci., Paris* **259** 3729–32
NEW G H C 1972 *Alta Frequenza* **41** 706–17
NEWTON T D 1950 *Phys. Rev.* **78** 490
NICHOLS L L and WILSON W E 1968 *Appl. Opt.* **7** 167–70
NORTON M and GALLAGHER A 1971 *Phys. Rev.* A **3** 915–27
NUSSBAUM G H and PIPKIN F M 1967 *Phys. Rev. Lett.* **19** 1089–92
OMONT A 1965a *J. Physique* **26** 26–40
—— 1965b *C.R. Acad. Sci., Paris* **260** 3331–4
OONA H and BICKEL W S 1970 *Nucl. Instrum. Meth.* **90** 223–8
OSBERGHAUS O and ZIOCK K 1956 *Z. Naturf.* **11a** 762–3
OTTINGER C and ZIOCK K 1961 *Z. Naturf.* **16a** 720
PACE P W and ATKINSON J B 1975 *Can. J. Phys.* **53** 937–41
PAECH F, SCHMIEDL R and DEMTRÖDER W 1975 *J. Chem. Phys.* **63** 4369–78
PAISNER J A and WALLENSTEIN R 1974 *J. Chem. Phys.* **61** 4317–20
PANCHARATNAM S 1972a *Proc. R. Soc.* A **330** 265–70
—— 1972b *Proc. R. Soc.* A **330** 271–81
PARDIES J 1968 *C.R. Acad. Sci., Paris* **266** 1586–8
PEBAY-PEYROULA J C 1959a *J. Physique* **20** 669–79
—— 1959b *J. Physique* **20** 721–9
PERESSE J, POCHAT A and LE NADAN A 1972 *C.R. Acad. Sci., Paris* **274** 791–4
PETTIFER R E W and HEALEY P G 1974 *J. Phys. E: Sci. Instrum.* **7** 617–20
PIESTRUP M A, POWELL R A, ROTHBARD G B, CHEN C K and PANTELL R H 1976 *Appl. Phys. Lett.* **28** 92–4
POCHAT A, DORITCH M and PERESSE J 1973 *J. Chim. Physique* **6** 936–40
POCHAT A, GELEBART F, DORITCH M and PERESSE J 1972 *Analusis* **1** 368–73

Popp M, Schäfer G and Bodenstedt E 1970 *Z. Phys.* **240** 71–92
Pringsheim P 1924 *Z. Phys.* **23** 324–32
—— 1949 *Fluorescence and Phosphorescence* (New York, London: Interscience)
Pryce MHL 1950 *Phys. Rev.* **77** 136–7
zu Putlitz G 1969 *Atomic Physics* **1** 227–64
Racah G 1942 *Phys. Rev.* **62** 438–62
Radford HE 1967 *Methods of Experimental Physics* **4B** 105–214
Rose ME 1955 *Multipole Fields* (New York: Wiley)
Rose ME and Carovillano RL 1961 *Phys. Rev.* **122** 1185–9
Sackett PB and Yardley JT 1970 *Chem. Phys. Lett.* **6** 323–5
—— 1971 *Chem. Phys. Lett.* **9** 612–4
—— 1972 *J. Chem. Phys.* **57** 152–67
Sakurai K, Capelle JA and Broida HP 1971 *J. Chem. Phys.* **54** 1220–3
Saloman EB, Baghdadi A and Halpern JB 1970 *Rev. Sci. Instrum.* **41** 1148–53
Saloman EB and Happer W 1966 *Phys. Rev.* **144** 7–22
Schäfer FP 1973 *Topics in Applied Physics. Vol 1 Dye Lasers* (Berlin: Springer Verlag) pp1–85
Schearer LD 1969 *Phys. Rev. Lett.* **22** 629–31
Schearer LD and Holton WC 1970 *Phys. Rev. Lett.* **24** 1214–7
Scheps R, Florida D and Rice SA 1974 *J. Chem. Phys.* **61** 1730–47
Schlag EW, Schneider S and Chandler DW 1971 *Chem. Phys. Lett.* **11** 474–7
Schlag EW, Selzle HL, Schneider S and Larsen JG 1974 *Rev. Sci. Instrum.* **45** 364–7
Schlag EW and von Weyssenhoff H 1969 *J. Chem. Phys.* **51** 2508–14
Schwartz SE and Johnston HS 1969 *J. Chem. Phys.* **51** 1286–302
Schlectman RM, Curtis LJ, Strecker C and Kormanyos K 1970 *Nucl. Instrum. Meth.* **90** 197–201
Selinger BK and Ware WR 1970 *J. Chem. Phys.* **53** 3160–8
Sellin IA, Mowat JR, Peterson RS, Griffin PM, Lambert R and Haselton HH 1973 *Phys. Rev. Lett.* **31** 1335–7
Series GW 1959 *Rep. Prog. Phys.* **22** 280–328
—— 1966 *Proc. Phys. Soc.* **89** 1017–20
—— 1967 *Proc. Phys. Soc.* **90** 1179–80
Shaw DA, Adams A and King GC 1975 *J. Phys. B: Atom. Molec. Phys.* **8** 2456–60
Silvers SJ and Chiu C-L 1972 *J. Chem. Phys.* **56** 5663–7
Simpson JA and Kuyatt CE 1963 *Rev. Sci. Instrum.* **34** 265–8
Siomos K, Figger H and Walther H 1975 *Z. Phys.* A **272** 355–8
Sipp B, Miehe JA and Lopez-Delgado R 1976 *Opt. Commun.* **16** 202–4
Smalley RE, Ramakrishna BL, Levy DH and Wharton L 1974 *J. Chem. Phys.* **61** 4363–4
Smith AJ, Imhof RE and Read FH 1973a *J. Phys. B: Atom. Molec. Phys.* **6** 1333–8
Smith AJ, Read FH and Imhof RE 1975 *J. Phys. B: Atom. Molec. Phys.* **8** 2869–79
Smith MW, Martin GA and Wiese WL 1973b *Nucl. Instrum. Meth.* **110** 219–26
Smith PL 1973 *Nucl. Instrum. Meth.* **110** 395–403
Smith WH 1970 *Nucl. Instrum. Meth.* **90** 115–9
Smith WH, Brzozowski J and Erman P 1976 *J. Chem. Phys.* **64** 4628–33
Smith WW and Gallagher A 1966 *Phys. Rev.* **145** 26–35
Solarz R and Levy DH 1974 *J. Chem. Phys.* **60** 842–5
Spears KJ and Rice SA 1971 *J. Chem. Phys.* **55** 5561–81
Steffen RM and Alder K 1975 *The Electromagnetic Interaction in Nuclear Spectroscopy* ed WD Hamilton (Amsterdam: North Holland) pp505–644
Stoner JO Jr and Leavitt JA 1971a *Appl. Phys. Lett.* **18** 477–9
—— 1971b *Appl. Phys. Lett.* **18** 368–9
—— 1973 *Optica Acta* **20** 435–48
Stoner JO Jr and Radziemski LJ Jr 1972 *Appl. Phys. Lett.* **21** 165–6
Stroke HH, Fulop G, Klepner S and Redi O 1968 *Phys. Rev. Lett.* **21** 61–4
Stroke HH, Jaccarino V, Edmonds DS and Weiss R 1957 *Phys. Rev.* **105** 590–603
Sutherland RA and Anderson RA 1973 *J. Chem. Phys.* **58** 1226–34
Svanberg S and Rydberg S 1969 *Z. Phys.* **227** 216–33
Tai C, Happer W and Gupta R 1975 *Phys. Rev.* A **12** 736–47
Tango WJ and Zare RN 1970 *J. Chem. Phys.* **53** 3094–100
Tatum JB 1967 *Astrophys. J. Suppl.* **14** 21–56

THAYER C A, POCIUS A V and YARDLEY J T 1975 *J. Chem. Phys.* **62** 3712–25
THAYER C A and YARDLEY J T 1972 *J. Chem. Phys.* **57** 3992–4001
TOLMAN R C 1938 *The Principles of Statistical Mechanics* (Oxford: Oxford University Press)
TURNER W H 1973 *Appl. Opt.* **12** 480–6
VAN DER LINDE J and DALBY F W 1972 *Can. J. Phys.* **50** 287–97
VAN DER WERF R, ZEVENHUIJZEN D and KOMMANDEUR J 1974 *Chem. Phys. Lett.* **27** 325–31
VASSILEV G, BANDON J, RAHMAT G and BARAT M 1971 *Rev. Sci. Instrum.* **42** 1222–7
VEROLAINEN Y F and OSHEROVICH A L 1966 *Opt. Spectrosc.* **20** 517–20
WAHL P, AUCHET J C and DONZEL B 1974 *Rev. Sci. Instrum.* **45** 28–32
WALTHER H 1974 *Phys. Scr.* **9** 297–305
—— 1976 *Topics in Applied Physics* vol 2 (Berlin: Springer Verlag) pp1–124
WALTHER H and HALL J L 1970 *Appl. Phys. Lett.* **17** 239–42
WANGSNESS R K 1971 *Phys. Rev.* A **3** 1275–8
WARE W R 1971 *Creation and Detection of the Excited State* vol 1, ed A Lamola (New York: Marcel Dekker) pp213–302
WEINSTOCK E M, ZARE R N and MELTON L A 1972 *J. Chem. Phys.* **56** 3456–62
WELLS W C and ISLER R C 1970 *Phys. Rev. Lett.* **24** 705–8
WIESE W L 1970 *Nucl. Instrum. Meth.* **90** 25–33
WILLIAMS W L and FRY E S 1968 *Phys. Rev. Lett.* **20** 1335–6
WOOD R W and ELLETT A 1923 *Proc. R. Soc.* A **103** 396–403
WOODGATE G K 1970 *Elementary Atomic Structure* (London, New York: McGraw-Hill)
YAMAGISHI A and INABA H 1974 *Opt. Commun.* **12** 213–5
YARDLEY J T, HOLLEMAN G W and STEINFELD J I 1971 *Chem. Phys. Lett.* **10** 266–8
YEUNG E S and MOORE C B 1971 *J. Am. Chem. Soc.* **93** 2059–60
—— 1973a *Fundamental and Applied Laser Physics* ed M S Feld, A Javan and N A Kurnit (New York: Wiley-Interscience)
—— 1973b *J. Chem. Phys.* **58** 3988–98
DE ZAFRA R L and KIRK W 1967 *Am. J. Phys.* **35** 573–82
DE ZAFRA R L, MARSHALL A and METCALF H 1971 *Phys. Rev.* A **3** 1557–67
ZARE R N 1966 *J. Chem. Phys.* **45** 4510–8
—— 1974 *Méthodes de Spectroscopie sans Largeur Doppler* (Paris: CNRS) pp29–40
ZIOCK K 1957 *Z. Phys.* **147** 99–112

Forthcoming articles

R H Garstang
JILA, Boulder, Colorado
Atoms in high magnetic fields

H G Berry
The University of Chicago
Beam–foil spectroscopy

J Reinhardt and W Greiner
Institut für Theoretische Physik,
Frankfurt am Main
Quantum electrodynamics of strong fields

H W Kugel and D E Murnick
The State University of New Jersey and
Bell Laboratories
The Lamb shift in hydrogenic ions